NTNU – Trondheim
Norwegian University of
Science and Technology

Wear of carbon cathode lining in aluminium electrolysis cell

The effect of rotation speed in laboratory test cell

Saeid Nobakhtghalati

Light Metals, Silicon and Ferroalloy Production
Submission date: August 2014
Supervisor: Tor Grande, IMTE
Co-supervisor: Arne Petter Ratvik, SINTEF

Norwegian University of Science and Technology
Department of Materials Science and Engineering

Acknowledgments

First and foremost, I would like to express my sincere gratitude to my supervisor, Professor Tor Grande for his guidance, encouragement and supports during the project. Also, my special thanks to my co-supervisor, Arne Petter Ratvik, for his key comments, advices and helps.

I would like to thank Kati Tschöpe for introducing me to this topic and helping me a lot in the beginning. My special thanks to Anne Støre for her technical supports, advices and valuable helps.

Stein Rørvik is also acknowledged for carrying out the Tomography experiments. I am also grateful to Henrik Gudbrandsen and Ove Darell for their precious assistance during the laboratory works.

Summary

The aluminium smelters are continually trying to increase their production either by designing high amperage cells or increasing the amperage on available cell designs. The service life for aluminium reduction cells is often limited by cathode carbon, due to preferential wear along the periphery of the cell. This phenomenon becomes more important when aluminium smelters increase the amperage of the cells and shifted towards graphitized cathode materials with higher electrical conductivity. The present work has focused on the cathode wear rate and its correlation with hydrodynamic conditions, cathodic current density and carbon materials.

The electrolysis experiments were performed in an inverted test cell to determine the wear arte of carbon cathodes as a function of rotation speed, cathodic current density and carbon material. In the experimental setup, carbon cathode during the electrolysis is directly exposed to the molten cryolitic bath. The fundamentals of cathode wear are still unknown. But it is generally agreed that the formation and dissolution of aluminium carbide is an important factor for cathode wear. The formation and dissolution of aluminium carbide is influenced by current density and rotation speed. The experiments show that the wear rate is increased by increasing the current density and the rotation speed. Generally, chemical wear, mechanical wear and physical abrasion are three different wear mechanisms in carbon cathodes. Chemical and electrochemical wear are relevant to this study, while the other mechanisms are not subject of discussion.

Totally fifteen samples from different types of carbon material were experimented. The rotation speed was the only variable for all tests to observe the effect of hydrodynamic conditions on the wear rate. Increasing the rotation speed leads to increase in the wear rate. The mass transport through the diffusion layer is a key factor in the wear process. Before the above experiments, a few wear tests had been performed with the same set up, to find the correlation between current density and wear rate. The experiments revealed the influence of current density on the wear rate, where wear rate increases with increasing the current density. The results show a sharp increase in wear rate at low current densities, while at the higher current densities the wear rate was less dependent on the current density. The effect of type of carbon material on the wear rate was observable. In addition the influence of initial molten aluminium and electrical current on the penetration of bath into the cathode was indicated via EPMA. It shows that for penetration of bath components at least one factor (aluminium or current) should be present, while for the cathode wear only the presence of current is enough. The samples were examined by x-ray computed tomography (CT) to observe inside the cathodes, before and after the test. All graphitized cathodes were completely penetrated. Contrary, in the large pores of the anthracite based cathodes, the bath penetration was not observed.

Table of Contents

1. Introduction

1.1 Background

The Hall-Héroult process is the only industrial and economic method to produce of primary aluminum. During the last decades increasing in demand of aluminum metal has persuaded aluminum industries to use more efficient cells. It has forced the industries to use durable materials in the cells. The carbon cathode is one of the most important parts in the cell, which determines the service life of the aluminium reduction cells.

The carbon cathode works either as an electric conductor and a container of the molten aluminium and electrolyte that when worn out the whole cell has to be stopped. Remarkable cost is related to cell shutdown in terms of delay in metal production, deconstruction of the pot and relining of a new pot. Spent pot lining (SPL) represents an environmental challenge and causes expenses for waste handling, either by storage, immobilization of fluoride or recycling [1,2]. The average service life of modern reduction cells is around 6 years [3]. Improving the cathode lifetime will decrease the annual amount of shutdowns which would be along with considerable amount of economic advantages. Wear of carbon cathode block is the main limiting factor for cell life and one of the greatest challenges for aluminum industry. The very non-uniform wear in form of W shape or WW shape becomes worse after change to cathode carbon with high electrical conductivity for modern high-amperage cells [4,5]. Since the highest local wear rate limits the cell lifetime, the great amounts of carbon cathode still remains intact in the cell. If able to reduce the highest wear rate and distribute the wear uniformly it would be along with considerable amount of economic advantages.

1.2 Hall–Héroult process

Production of aluminium from alumina (Al_2O_3) is impossibly by the electrolysis of an aqueous aluminium salt because hydronium ions readily oxidize elemental aluminium. Since the melting point of aluminium oxide is above 2000 ˚C, a molten aluminium salt can be used for electrolysis of alumina. The inventors of process, Hall and Héroult, discovered independently of each other the electrochemical process to reduce alumina to aluminium metal [6]. In the Hall- Héroult process, dissolved alumina in cryolite (Na_3AlF_6), is reduced electrochemically to pure aluminium and carbon dioxide between a carbon anode that is consumed and a carbon cathode at about

960 ˚C [7]. The overall cell reaction is given in Eq. (1.1), and a principle drawing of a cell is shown in Figure 1.1.

$$2Al_2O_3\,(\text{dissolved}) + 3C\,(s) = 4Al\,(l) + 3CO_2\,(g) \qquad (1.1)$$

Industrially, the electrolyte is a melt, based on cryolite, which contains addition of AlF_3 and some other additives (CaF_2, LiF) to modify the important properties of the bath, such as the melting point, the electrical conductivity and the aluminium solubility [8, 1]. Alumina is fed into the cell regularly during the process and aluminium is produced continuously on the cathode surface. One or several anodes are immersed into the molten electrolyte (bath) and oxygen from the alumina reacts electrochemically with the anode carbon which gradually is consumed by the formation of carbon dioxide (CO_2) [7]. Therefore the carbon anodes need to be changed regularly during the operation of the cell. In Hall- Héroult cell, molten aluminium is the acting electrochemical cathode, where the cathodic reaction occurs. However the whole assembly is called the cathode, i.e. molten aluminium, carbon blocks, baked ramming paste, refractory and insulation, collector bars and steel shell [1]. The carbon cathode does not participate in the reaction, but serves as a container and electrical connection to the aluminium pad. Although, an unwanted wear happens for the carbon block.

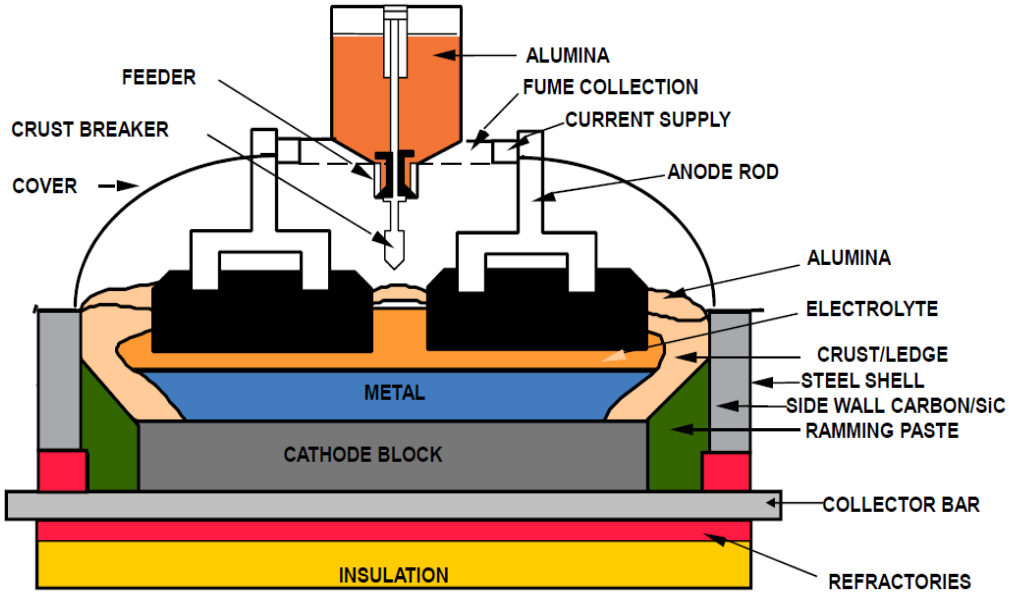

Figure 1.1. Schematic drawing of the cross section of a Hall- Héroult aluminium reduction cell.

1.3 The cathode wear phenomenon

Cathode wear is one of the important factors determining the service life of Hall- Héroult aluminium electrolysis cells. Wear is generally defined as net removal of material from a surface [9]. The main reason for the shutdown of electrochemical cells in the aluminium industry is the cathode wear. The carbon block is worn continuously during operation until the steel collector bars become exposed to the aluminium pad. Then the cell must shut down because of higher iron content in the produced aluminium [10]. Hence, the life time of electrochemical cells is usually determined by the lifetime of the carbon cathode. The strongly non-uniform cathode wear is not really understood. The phenomenon is first of all related to the cathodes with high electrical conductivity, where the current density at the surface of the carbon is also very non-uniform. Almost the entire current passes through a narrow zone located along the periphery. It seems to be generally agreed that the wear is somehow related to the current density, but still no credible mechanism has been proposed. Abrasion due to alumina particles dragged along the cathode may play a role, and thereby, the metal velocity [11]. In chemical wear the carbon block can react with the aluminium pad which leads to formation of aluminium carbide. Electrochemical formation of aluminium carbide is also likely because the bath contain aluminium species, which can be transported to the cathode due to the charge transport through the bath [10]. In industrial cells the wear rate of cathode carbon can amount to 2-6 cm per year [8]. Figures 1.2 and 1.3 show a worn cathode block after 5 years and longitudinal wear profile for 19 cathodes in an industrial cell.

Figure 1.2. A worn cathode block after 5 years [4].

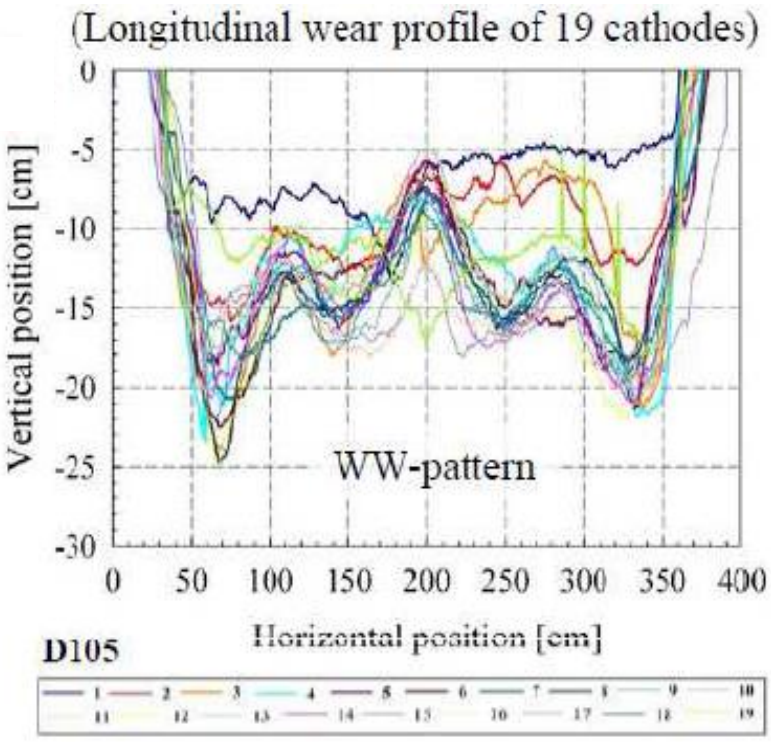

Figure 1.3. Typical double-w wear profile of an industrial cell for 19 cathodes [4].

Nowadays, aluminium smelters are increasing the amperage in the cells and graphitized cathode blocks with higher electrical conductivity have become the most common cathode materials to reduce the ohmic losses in the lining. However, graphitized cathodes have been reported to have higher wear rates and cathode wear have during the last decade become one of the main challenges in the aluminium industry [10, 12].

1.4 Aim of the work

During the past decades due to the increase in aluminium demand, the smelters have tried to enhance the productivity of the Hall- Héroult cells via increasing the amperage. Therefore a change from anthracitic carbon to graphitized materials, improved electrical and thermal conductivity which enabled higher production through higher current. Today, failure due to wear of carbon cathode blocks is one of the decisive factors for the lifetime of the cells. It is believe that the wear is caused by both physical and chemical wear. However, different opinions exist on the wear mechanism.

The present work is a part of the project “Durable Materials in primary aluminium production” (DuraMat). One of the main objectives of the DuraMat project is fundamental studies of the

cathode wear mechanism. This work was focused on the influence of hydrodynamic conditions, current density and cathode material on the wear rate. The experiments were performed in an inverted test cell which is a quick method to observe the wear rate than the industrial conditions. The effect of polarization and initial molten aluminium on the cathode wear and bath penetration were shown via EPMA. Furthermore, to visualize the depth of bath penetration into the cathode, the cathode materials were examined through the x-ray computed tomography (CT).

2. Cathode wear in aluminium electrolysis cells

2.1 Carbon materials and cathode blocks

The carbon lining in aluminium electrolysis cells is used for two purposes. It acts as a refractory container for the molten metal and electrolyte, and conducts electricity out of the cell [1]. Beside the conductivity, mechanical stability for keeping liquid metal on the cathode and resistance to chemicals in the electrolyte are the other important properties for the cathode blocks. The nature and crystallographic structure of the carbon material have a key role in the properties and behavior of the blocks. Thus the graphitic structure is an important factor for carbon cathodes. This structure is obtained naturally or through the graphitization heat treatments. Graphitization is a solid state transformation of thermodynamically unstable non-graphitic carbon into graphite by thermal energy at high temperature.

Carbon cathode as prebaked blocks is produced from different three carbon sources, anthracite, graphitic material and graphitized material. Cokes are generally poorly ordered material. They may contain impurities, and hydrogen atoms are bonded to the peripheral carbon atoms. When heat-treated, the hydrogen and volatiles are slowly removed from the structure, the layers become more and more parallel and the distance between the layers decreases. A further increase in temperature (up to 3000 ˚C) will lead to crystallite growth until the material becomes mostly graphitic [1]. Anthracite behaves somewhat differently. Its structure is more ordered then the coke, but it is a relatively weak electrical conductor. Anthracite is a natural carbonaceous material of fossil origin. It is oldest and highest rank of coal with low content of moisture and volatile. Carbon content is between 92% and 98% after calcination with simplified processing towards high density carbon. To increase the electrical conductivity, anthracite is calcined before use. Prebaked cathode block from anthracite traditionally were made by two calcination methods towards gas calcined anthracite, GCA, via rotary kiln or electrically calcined anthracite, ECA, in a shaft furnace. ECA is partly graphitized which can contain a notable amount of graphitic carbon while GCA is absolutely amorphous, without graphite. In electro calciner to obtain ECA temperature near the center is larger than 2500 °C, while the anthracite near the walls has a temperature smaller than 1000 °C. Calcination temperature for GCA in rotary kiln is about 1200 °C. Higher calcination temperature in electro calciner gives higher crystalinity, higher real density and lower electrical resistivity in ECA relative to GCA [3].

During last three decades most of producers, in addition of anthracite blocks, (ECA, GCA), also have produced graphitic blocks and graphitized blocks after forming and baking. In graphitic blocks the dry aggregates are graphite, mostly made of scraped graphite from steel furnace electrodes (2800 °C) and also graphitized petcoke (2500 °C). The dry aggregates are mixed with coal tar pitch and baked to 1100-1200 °C. The dry aggregates in graphitized blocks are needle coke and special petcoke qualities. They are mixed with coal tar pitch and baked to 800 °C. Then, baked materials are heat treated to 2300-3000 °C for graphitization [3, 1]. Figure 2.1 shows the main steps of process and flow of materials in production of cathode blocks.

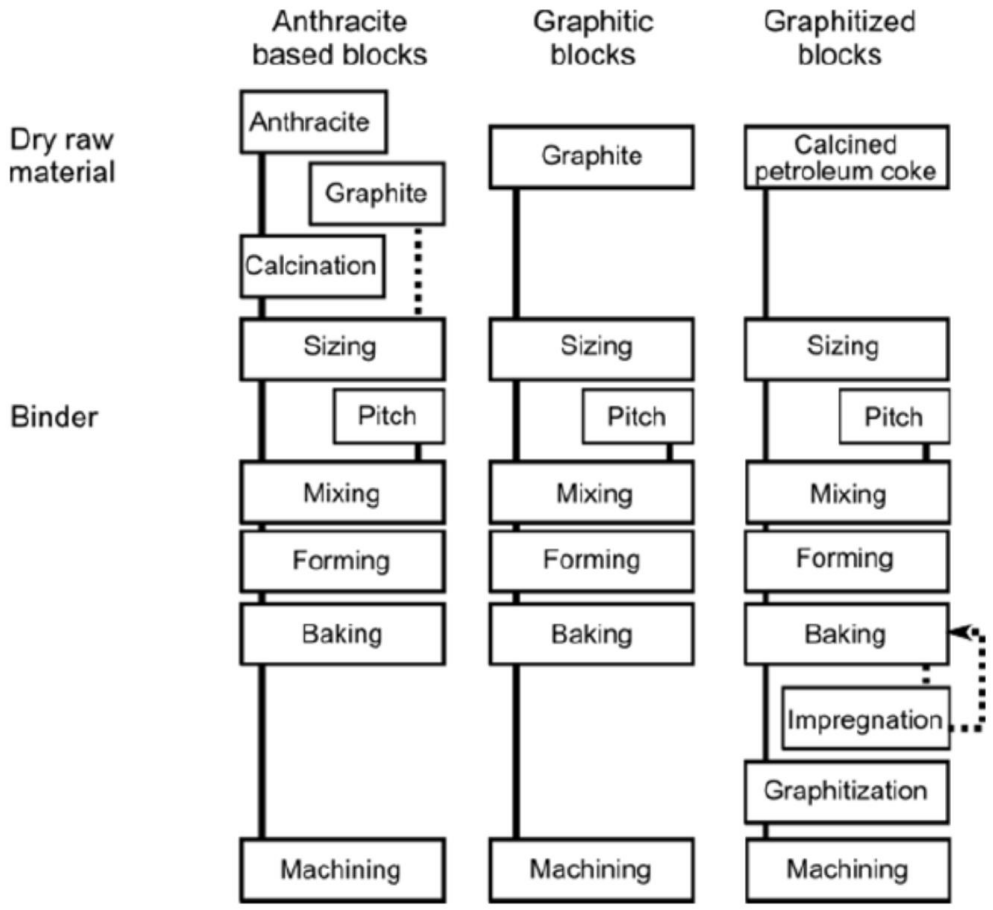

Figure 2.1. Steps in making of different types of cathode blocks [3, 10].

The four main categories of cathode blocks for aluminium reduction cells are anthracitic, semigraphitic, semigraphitized and graphitized, where in the written sequence the graphitic character is increased. They are classified as follow [1]:

- *Graphitized*: the whole block (aggregate and binder), consisting of graphitizable materials, has been heat treated, usually to above 2500 °C, giving a graphitic material.

- *Semi-graphitized*: The whole block (filler and binder), consisting of graphitizable materials, has been heat treated to about 2300 °C.

- *Semi-graphitic*: The aggregate is graphitized, but the block (binder phase) has been baked to 1200 °C.

- *Anthracitic*: The filler material is anthracite and often some graphite is added. The block has been baked up to 1200 °C.

In the past 10-20 years significant changes from using only anthracitic carbon to semigraphitic, graphitic or graphitized materials have taken place. Graphite has higher thermal and electrical conductivities and is less susceptible to sodium penetration than anthracitic carbon. Graphite also has a higher thermal shock resistance, which is advantageous during preheating and startup of new cells [8, 1, 3].

2.2 The laboratory test cell

During industrial electrolysis of aluminium the wear rate of the cathode carbon is in the range of 2-6 cm/year [8]. This equals 0.05-0.16 mm/day. Thus, it is difficult to measure the wear rate of carbon by dimensional changes during a short time laboratory experiment. On the other hand, it is believe that a bath film exist between the aluminium pad and the carbon cathode [13]. Since the solubility of carbon in cryolite is about 100 times higher than in aluminium, the wear rate is also believe to be higher in cryolite, in a magnitude that makes the wear possible to measure after a short time laboratory experiment. For these reasons, a cell design with a vertical rotating cathode exposed to molten cryolite was developed. The deposited aluminium on the cathode surface drains off and the carbon cathode will always be exposed to bath [1]. A schematic drawing of the experimental setup for an inverted cell is shown in Figure 2.2.

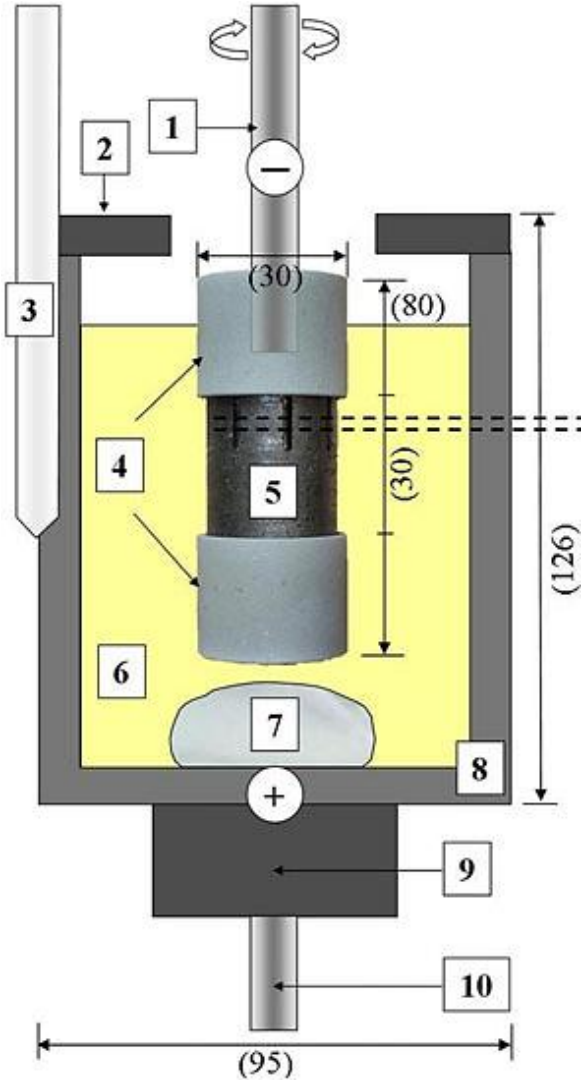

Figure 2.2. Schematic drawing of the experimental setup in an inverted test cell with a vertical rotating cathode. 1) rotating cathode connecting rod, 2) lid of sintered alumina, 3) thermocouple, 4) Si_3N_4 linings covering both ends, 5) cathode sample, 6) electrolytic bath, 7) aluminium metal, 8) graphite crucible(anode), 9) graphite support and 10) anode current lead [9].

In the rotating cathode experiments a vertical tube furnace (resistance closed furnace) is used. The experimental setup consists of a graphite crucible placed on a graphite supporter in the isothermal zone of the furnace. Nitrogen, used as inert carrier gas, is flushed from below, and the system is kept as gas-tight as possible with an outlet gas collection into a fume hood. The crucible is positively charged acting as an anode, which contains cryolitic bath and molten aluminium metal. The negatively charged cathode specimen is immersed into the electrolyte. The electrolysis temperature is set to programmed temperature (970 °C) and is kept constant during the experiment by an external temperature controller. A heat resistant steel rod is used to conduct current to the cathode. Dependent on the experimental plan, the rotation speed, the current

density and the experiment time can be changed. The cell voltage, current and temperature are recorded during the experiment [5, 9, 1].

After the experiment the furnace is turned off while maintaining the nitrogen atmosphere. The steel rod with the cathode is lifted out of the bath and is allowed to cool in the colder part of the furnace [5]. Figure 2.3 is shown a cathode sample with slots and its cross section in a laboratory test cell. Details about the preparation and dimensions of the sample are given in the next chapter.

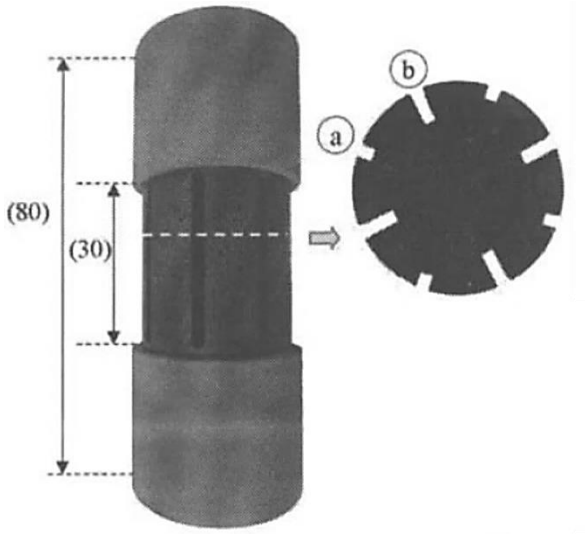

Figure 2.3. Image of the cathode sample with slots and its cross section. The dimensions in millimeters are given in brackets [5].

2.3 Cathode wear

However up to now a lot of studies have been carried out to realize the mechanism of erosion in cathode carbon and some of them are going, but the fundamentals of wear are still subject of discussion. The wear of cathode carbon due to physical abrasion caused by solid alumina particles and formation of aluminium carbide (Al_4C_3) which dissolves in aluminium and in cryolite melts [8]. It is generally agreed that the formation, dissolution and transport of aluminium carbide are the important factors for the cathode wear, however the mechanism of formation so far is based on theory [5]. Aluminium carbide is formed according to the reaction (2.1) at the carbon-liquid aluminium interface [8, 5]:

$$4Al\ (l) + 3C\ (s) \rightarrow Al_4C_3\ (s, dissolved) \qquad (2.1)$$

2.3.1 Wear mechanisms

Wear of carbon materials in linings used in aluminum reduction cells might occur by three different mechanisms [1]:

- Mechanical wear attributed to the cavity cleaner.
- Physical abrasion due to interaction with a flow of sludge or metal.
- Chemical wear due to chemical or electrochemical formation of Al_4C_3.

Mechanical wear attributed to the cavity cleaner can be put aside because the blocks are generally more erode than the neighboring small joints. Physical abrasion should be enhanced in high velocity areas. Toda and Wakasa [14] found, the abrasion resistance is 3 times higher for anthracitic blocks compared to graphitized blocks. Chemical wear has been found to increase with increased current density. This wear is caused by formation and dissolution of aluminium carbide according to reaction (2.1).

2.3.2 Formation of aluminium carbide

Aluminium production in electrolysis cell is occurred via the chemical and electrochemical reactions between electrodes (anode and cathode), liquid aluminium and molten bath. It is well known that aluminium can react directly with carbon to form aluminium carbide according to reaction (2.1). The reaction is thermodynamically favored ($\Delta G°$=-147 kJ, T=970 °C) at the temperature corresponding to the operation of the cell [10]. This reaction does not occur easily at normal aluminium melting temperature due to the aluminium oxide film that covers the liquid aluminium [2]. Therefore, lack of direct contact between liquid aluminium and the carbon cathode prevents the reaction to proceed [10, 15]. On the other hand, graphite is known to be poorly wetted by liquid aluminium (wetting angle $\theta > 90°$) [5,10,15]. When the surface of aluminium is covered by thin layer of aluminium oxide, the wetting angle becomes higher. This oxide layer works as a barrier between aluminium and carbon. The reaction of aluminium carbide formation (2.1) is controlled by slow diffusion of aluminium through the oxide film [13]. The aluminium oxide layer can be removed (evaporation) by the following reaction, (2.2) [10, 15]:

$$Al_2O_3\,(s) + 4Al(l) \rightarrow 3Al_2O\,(g) \qquad (2.2)$$

By proceeding the reaction (2.2) the wetting angle is decreased. When the oxide film is removed, the contact between aluminium and carbon is provided, so that the interaction is then characterized by the wetting angle between aluminium and carbon. The evaporation of oxide layer is occurred at higher temperature and/or lower total pressure [10]. Thus reaction (2.1) produces just small amounts of aluminium carbide and it is not possible to form detectable amounts of the carbide below 1000°C without the presence of the bath [5, 15].

2.3.3 Chemical formation of aluminium carbide

In industrial cells aluminium is transported across the cryolite layer and reacts with carbon at the graphite-cryolite interface to forms Al_4C_3 [5]. Chemical formation and dissolution of aluminium carbide is taken place in a system contain carbon, aluminium and molten cryolite at the temperature of aluminium electrolysis. Because of poor wetting of aluminium on the surface of carbon and presence of the bath layer between the cathode carbon and the aluminum, formation of Al_4C_3 via the reaction (2.1) is likely a reaction between the cathode carbon and aluminium dissolved in the bath [13]. An alternative reaction involving intercalated sodium rather than aluminium may occur [2]:

$$4AlF_3\,(diss) + 12\,Na\,(in\,C) + C\,(s) \rightarrow Al_4C_3\,(s) + 12NaF\,(l) \qquad (2.3)$$

or aluminium carbide formation due to bath penetration which can be explained by chemical means according to the reaction (2.4) [3, 5]:

$$4Na_3AlF_6\,(l) + 12Na\,(in\,C) + 3C\,(s) \rightarrow Al_4C_3\,(s) + 24NaF\,(l) \qquad (2.4)$$

By proceed the reaction (2.3) the concentration of AlF_3 is reduced and the concentration of sodium and NaF is increased at the interface in comparison with the bulk bath. The reaction rate is affected by changes in reactant concentrations. Reduction in concentration of AlF_3 reduces the rate of reaction, while increased concentration of intercalated sodium increases the rate [2].

Absorbed sodium also can react chemically with carbon and alumina to form aluminium carbide, according to the reaction (2.5) [1]:

$$8Al_2O_3\,(s) + 12Na\ (in\ C) + 3C\ (s) \rightarrow Al_4C_3\,(s) + 12NaAlO_2\,(s) \qquad (2.5)$$

The experiments show that the carbide was found in cracks, where electrolyte and aluminium metal were exist, while aluminium carbide is seldom found in cathode pores without aluminium metal [2, 5]. This indicates that presence of aluminium might be a prerequisite for aluminium carbide formation [2]. Current density is an important factor which has tremendous effect on the wetting ability of the carbon cathode and infiltration of bath [16]. According to studies the driving force of aluminium carbide formation increases with increasing current density [17]. In addition, the activities of Aluminium and sodium are linked by equilibrium reaction (2.6). If the activities of AlF_3 and sodium are very low to form Aluminium in the pores, the driving force for producing aluminium carbide is low [2].

$$3NaF\ (l) + Al\ (l) \leftrightarrow 3Na\ (diss\ in\ C) + AlF_3\,(diss) \qquad (2.6)$$

In aluminium carbide formation, the mass transfer of aluminium through the cryolite is the rate limiting step [5, 13].

2.3.4 Electrochemical formation of aluminium carbide

It has been proved that the electrochemical reactions strongly contribute to the cathode wear in Hall- Héroult cells [18]. The cathode wear rate is increased with increasing current density [2]. Electric current is passing through the cathode and a general form of electrochemical formation of aluminium carbide can be written as the reaction (2.7) [10]:

$$3C + 4Al^{3+} + 12\bar{e} \rightarrow Al_4C_3 \qquad (2.7)$$

Aluminium carbide formation via the bath penetration can be described by electrochemical means according to the reaction (2.8) [3]:

$$3C\ (s) + 4AlF_3\ (diss) + 12\bar{e} \rightarrow 3Al_4C_3\ (s) + 12F^-\ (diss) \qquad (2.8)$$

A strong correlation between local cathode wear and local current density in industrial cells indicating electrochemical formation and dissolution of aluminium carbide [2,10,18]. Another electrochemical formation of aluminium carbide may take place according to the reaction (2.9). This reaction is based on reduction of aluminium fluoride in the bath layer between the aluminium bulk and the carbon cathode [2].

$$4AlF_3\ (diss) + 3C\ (s) + 12Na^+ + 12\bar{e} \leftrightarrow Al_4C_3\ (s) + 12NaF\ (l) \qquad (2.9)$$

Figure 2.4 indicates the reaction mechanism based on steady supply of Al^{3+} ions from the metal-bath film interface [2].

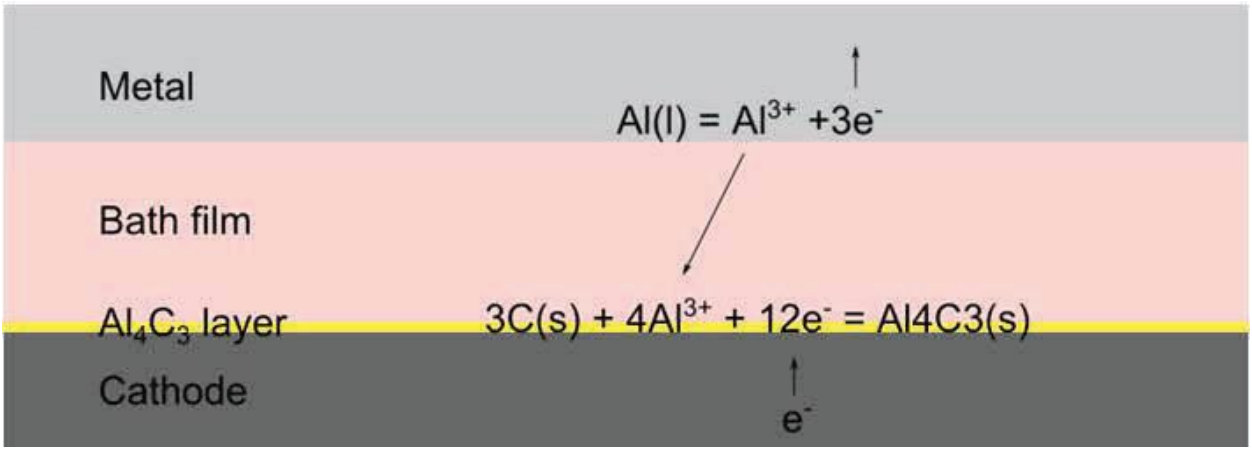

Figure 2.4. Electrochemical formation of Al_4C_3 at the cathode-bath film interface, with dissolution of aluminium at the metal-bath film interface as the anode reaction [2].

The industrial surveys show that by increasing the cell amperage the average service life of cathode and the cell is reduced from 3000 to 2000 days [10, 4]. Aluminium carbide formation makes an insulated film on the carbon cathode surface, thus carbide should dissolve in the bath to allow carbon at the interface reproduces aluminium carbide [2].

2.3.5 The effect of cryolite

The cryolite has an important effect on the reaction between carbon and aluminium. However aluminium oxide film on aluminium prevents the direct contact between carbon and metal, but formation of aluminium carbide is enhanced in presence of the molten electrolyte between liquid aluminium and carbon cathode [13]. Since on the aluminium-carbide interface there is a thin layer of cryolite, this film can act as a wetting agent which makes perfect wetting, (θ=0°) [10, 13]. Cryolite cannot wet carbon materials and the wetting angle is 115° [13]. By adding aluminium oxide to the cryolite the wetting angle will decreased to 65°, while addition of aluminium changes the wetting to near perfect, (θ=0°) [10]. Cryolite also can dissolve the aluminium oxide film which works as an obstacle for direct reaction between aluminium and carbon [19]. In addition cryolite may acts as a solvent of aluminium carbide that is formed at the aluminium-carbon interface [10].

2.3.6 Solubility of aluminium carbide

Molten cryolite can dissolves Al_4C_3 layer which is formed at the aluminium-carbon interface and works as a barrier for mass transfer [10, 20]. Solubility is increased with rising temperature and also by decreasing the alumina concentration [2, 20]. Cryolite ratio (CR) has the largest effect on the solubility of carbide [2]. The maximum solubility is 2.15 wt % and some additives like Al_2O_3 and CaF_2 are reducing the solubility of aluminium carbide in molten bath [2,10,20]. The solubility of aluminium carbide as a function of CR, at 1020 °C, is shown in Figure 2.5. As can be seen from the graph, the solubility has a maximum value at CR=1.8 [1]. The dissolution of aluminium carbide in cryolitic melt is occurred through the following reaction [2, 10]:

$$Al_4C_3\,(s) + 5AlF_3\,(diss) + 9NaF\,(l) \rightarrow 3Na_3Al_3CF_8\,(diss) \qquad (2.10)$$

The cryolite ratio for this reaction is equal to CR=1.8 that is the value of CR for obtain maximum solubility of aluminium carbide [10]. The dissolution of aluminium carbide in the bath also can be written as the following reaction [5]:

$$Al_4C_3\,(s) + 5AlF_3\,(diss) + 9NaF\,(l) \rightarrow 3Al_3CF_8^{3-} + 9Na^{+} \qquad (2.11)$$

The studies show that solubility of aluminium carbide in aluminium is two times lower than the solubility in cryolite, so that it increases with the cryolite ratio to a maximum of 2 wt% at CR=1.8 [2, 5, 20].

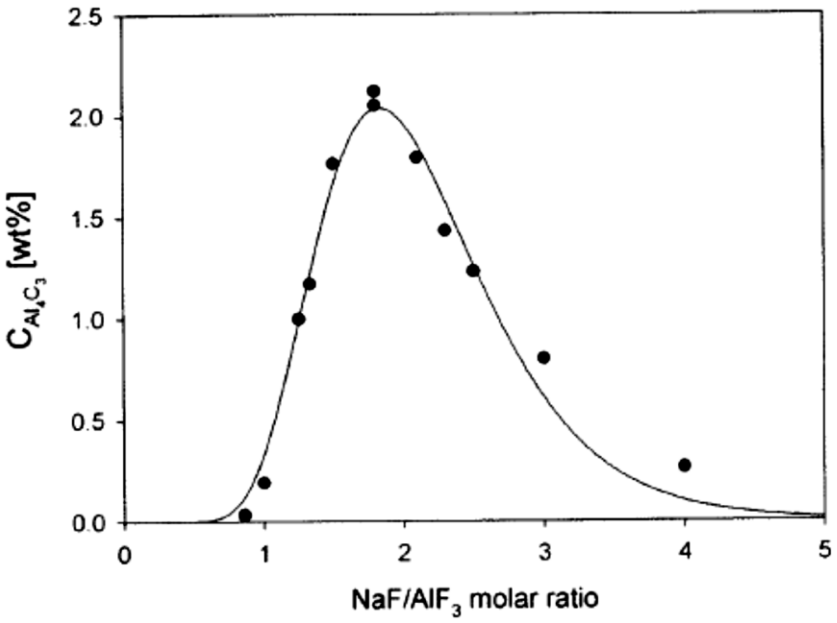

Figure 2.5. Solubility of Al_4C_3 as a function of CR in NaF-AlF_3 melts at 1020 °C [1].

2.4 The effect of sodium

It is known that the main effect of sodium is on degradation of refractory lining and also the ceramic side lining. Nevertheless, the influence of sodium on cathode carbon is not negligible, particularly that cathode carbon is the gateway for sodium entering to the lower parts of cathode and reaction with them. A qualitative understanding of the diffusion of sodium into the cathode lining including the carbon cathode, the ceramic side lining and the refractory lining is very important to improve the cathode cell design and performance [21]. As mentioned earlier carbon is not wetted by liquid aluminium and also poorly wetted by a fluoride melt. Therefore it could be expected that carbon should be impervious to infiltration. But it is clear that there is 10-26 % open porosity on cathode block materials which leads to a remarkable permeability. With adequate time the carbon cathode will be fully impregnated by the bath components [3]. According to the chemical reaction (2.12), sodium is formed at the interface between the molten bath and the liquid aluminium through the reduction of Na^+ that is the main free cation present in the cryolite-alumina mixture [3, 22]:

$$Al\ (l) + 3NaF\ (\text{in cryolite}) = 3Na\ (\text{in carbon}) + AlF_3\ (\text{in cryolite}) \qquad (2.12)$$

Also sodium is deposited via the direct reduction at the carbon cathode surface (2.14) [3, 22]. The initial aluminium deposition is [22]:

$$Al^{3+} + 3\bar{e} = Al\ (l) \tag{2.13}$$

while the direct electrochemical deposition of sodium is:

$$Na^{+}\ (\text{in electrolyte}) + \bar{e} = Na\ (\text{in carbon}) \tag{2.14}$$

Sodium penetrates into the carbon cathode materials and forms intercalation compound during the cell operation [3, 21]. Sodium in carbon block causes the cathode swelling and changes the bath chemistry [22, 21]. Also sodium changes the wetting properties of the carbon cathode with respect to the molten bath [22, 21, 23]. Sodium opens the way or makes it more likely which bath penetrates into the carbon cathode through the pores and cracks of the carbon [22].

The main source of sodium is soda ash which is added to the cell to maintain the optimal bath chemistry and to compensate for sodium loss down into the lining materials. In addition, sodium in form of Na_2O is entered to the cell as the main impurity in primary alumina. The carbon anode also contains around 25-250 ppm sodium [21].

2.5 Current density

The experiments show by increasing current density, the wear rate increases. The laboratory studies are in good agreement with industrial observations. At the periphery of the cell the high current densities are expected, so that the most intensive wear is observed in these areas. Even if current density not impressing directly the wear but, increased current density can enable the other possible wear enhancing factors such as increased convection via the electromagnetic field [2]. Therefore the current distribution is one of the most important factors for cathode wear rate. Laboratory experiments explain the effect of current density on carbon cathode wear rate. As shown in Figure 2.6, by scanning the cross section of virgin and worn sample and superimposing the images, the effect of current density and worn area visualizes.

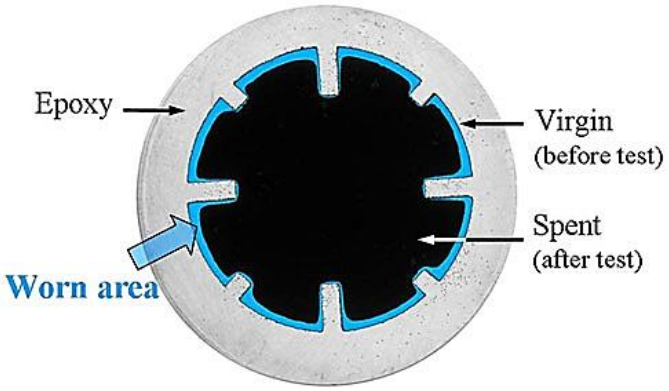

Figure 2.6. Superimposed image of the scanned cross sections of a cathode sample before and after the experiment [9].

The current density distribution has an important role on the difference of wear rate from the place to another place. Simulation of the current density distribution can specifies the effect of this factor. In the same laboratory test that mentioned above, Figure 2.7 indicates the simulated current density distribution of the bath inside the slots and at the surface of the cathode sample at stationary condition. Simulation shows the maximum current density at the edges of the slots. Therefore, due to the difference in current density, the wear rate is enhanced at the surface of the cathode compared with the bottom of the slots [5]. In industrial cells the cathodic current density is changed in the range of 0.3-1.3 A/cm^2 [8].

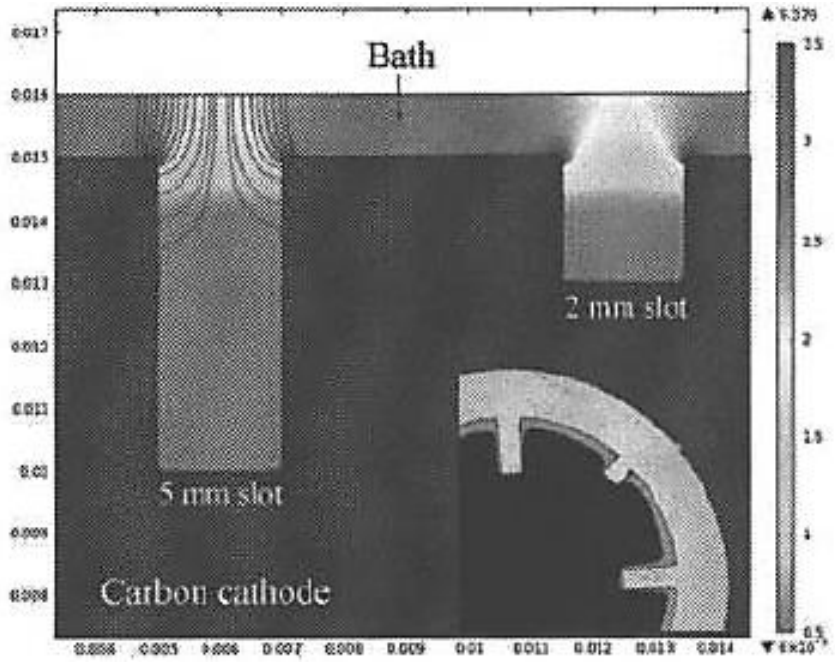

Figure 2.7. Simulation of the current density distribution of the bath inside slots of two different depths (2 and 5 mm) at stationary conditions [5].

2.6 Hydrodynamic effect

In high amperage reduction cells strong convection in the metal pad is often observed. The measured metal velocities in a number of cells suggested a very complex relationship between the metal circulation and the operation parameters. There appear to be many factors influencing the metal circulation. Among these are magnetic field strength, the current distribution and muck formation [1]. In laboratory test the cathode sample is rotated inside the molten bath. Rotation of sample provides the possibility for study about hydrodynamic effect on wear rate. Simulation is also used in order to figure out hydrodynamic consequence in laboratory scale test. The experiments indicate by increasing the rotation speed, in the test cell, from 50 rpm to 125 rpm the wear rate becomes worse at the side of the slot that faces the rotation direction. This specifies that the wear rate enhances with accelerated rotation speed and it is controlled via mass transport. Figure 2.8 shows the simulation of the velocity magnitude in m/s or motion of electrolyte relative to the cathode at stationary state in the neighborhood of two slots (2 and 5 mm depths). The rotation speeds are 50 rpm and 125 rpm. Figure 2.9 is shown the magnification of this simulation, where the velocity and thereby the rate of mass transfer at the edge 1 is larger than edge 2 [9]:

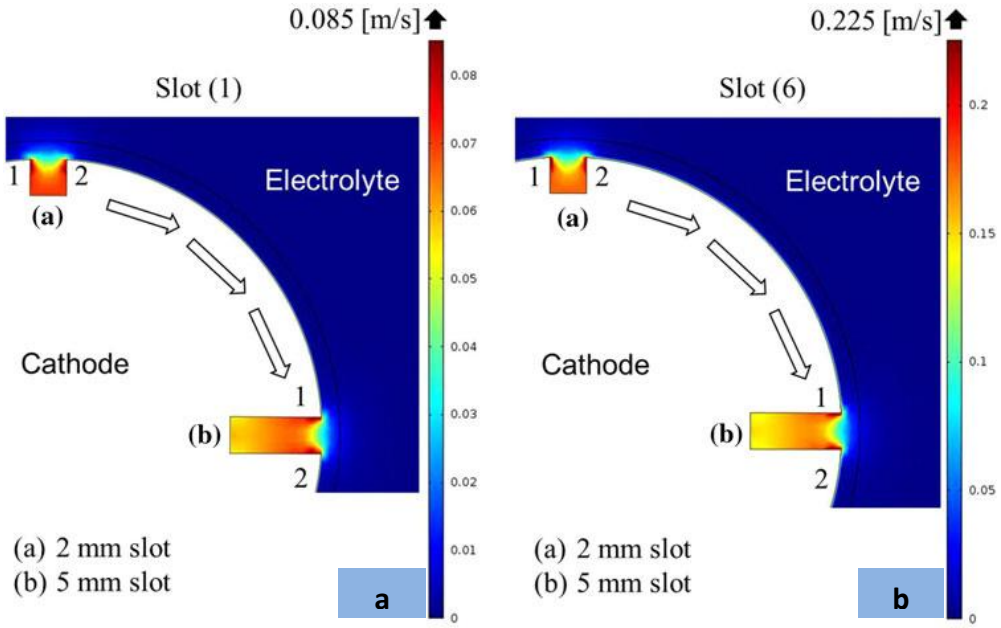

Figure 2.8. Simulation of the velocity magnitude in m/s at stationary state for two different slots (2 and 5 mm depths). Sample (a) at 50 rpm and sample (b) at 125 rpm [9].

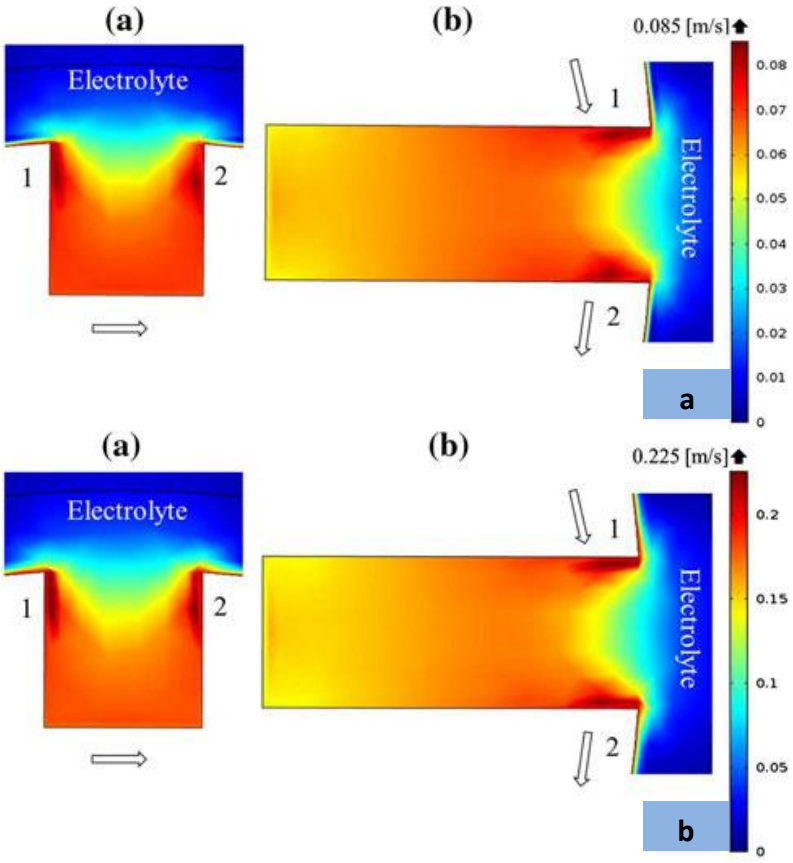

Figure 2.9. Magnification of the simulated velocity field inside the 2 mm and 5 mm deep slots for samples (a) and (b) in Figure 2.8 [9].

Increased flow and convection causes to increase abrasive forces and mass transport in the melt. Thus increased convection and metal flow leads to higher wear rate [2]. Broadly speaking, current density is the most important factor in cathode wear, while convection has a complementary and detrimental effect. Figure 2.10 displays the influence of current density and hydrodynamic effect on cathode wear in three experiments. For the experiment without polarization (slot 4) no wear is happened on the cathode surface, while in the experiment with polarization and with rotation (slot 6) the maximum wear is observable [9].

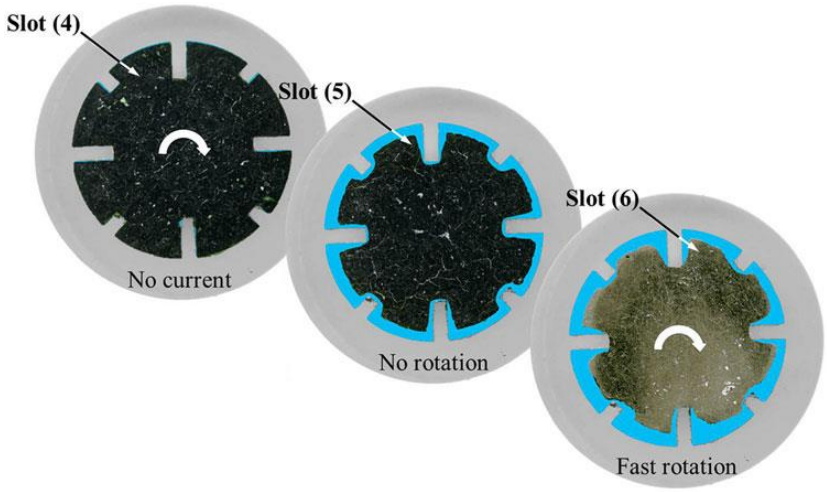

Figure 2.10. Superimposed images of the scanned cross sections of three cathode samples. Slot (4) shows the effect of polarization on cathode wear in comparison with other samples. Slots (5) and (6) illustrate the influence of rotation on wear rate in presence of current [9].

3. Experimental methods

The experimental setup of the inverted test cell was illustrated in previous chapter, Figure 2.2. In this work, fifteen cathode specimens were experimented. The experimental condition including rotation speed and carbon material for each sample is given in Table 3.1. Two types of graphitized cathode from Elkem were used, EI and EA which are respectively isotropic and anisotropic carbon materials. Before start the experiments the apparent density and open porosity of cathodes were determined by hydrostatic method (DIN 51918:1986-11). The density and porosity of specimens is given in Appendix A. The test pieces were 30 mm in diameter and 80 mm long. The cathode samples were prepared in two different types, with slots and without slots. The cathodes without slots are used for ranking of different carbon materials, while the other one is applied for studying the wear mechanism [5, 9]. The both types of specimens are shown in Figure 3.1. For the samples with slots, two types of slots were cut into the surface around the periphery as shown in Figure 3.2. In order to prevent non-uniform current distribution and wear it was considered to be important to define the exposed area accurately [5]. Each end of the cathode specimen was covered by an insulating material (Si_3N_4), defining a uniform 30 mm high cylindrical area exposed to the electrolyte, as shown in Figure 3.3. With this setup it was possible to achieve accurate data on wear, relative to the current density.

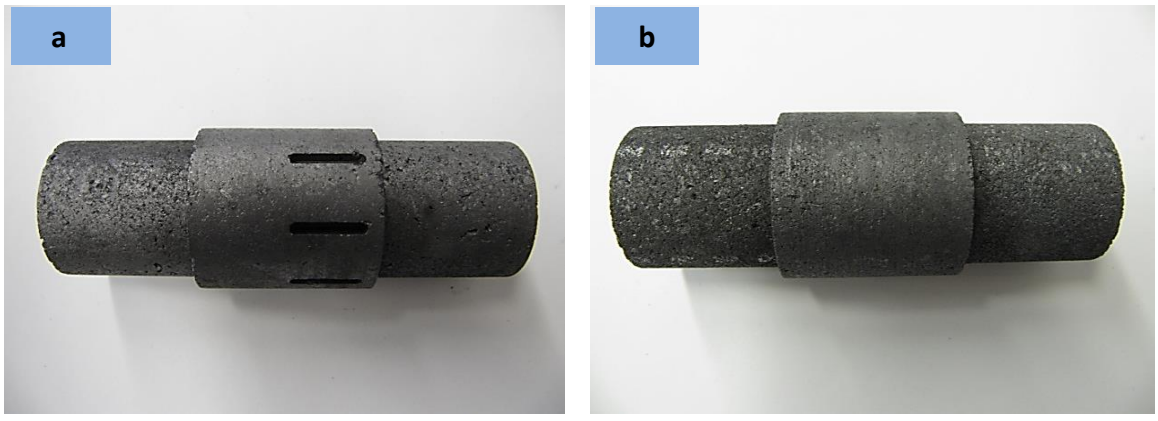

Figure 3.1. Virgin cathode samples. (a) With slots. (b) Without slots.

Table 3.1. The defined conditions for fifteen wear tests. i = 1 A/cm^2, T=970 °C and Time = 24 h.

Carbon cathode	Material	Rotation speed (rpm)
SI 13	Graphtized (slot)	0
SI 30	Graphtized (slot)	80
SI 31	Graphtized (slot)	100
EI 14	Graphtized	125
EI 30	Graphtized	125
BN 9	Graphtized	125
BN 10	Graphtized	125
5BDN 12	Anthracite base	125
5BDN 20	Anthracite base	125
EI 31	Graphtized	0
BN 21	Graphtized (slot)	125
5BDN 21	Anthracite base-(slot)	125
BN 22	Graphtized (slot)	50
EA 1	Graphtized - Anisotropic	125
EA 2	Graphtized - Anisotropic	125

The cathode wear was calculated by measuring the diameters of the specimens before and after the electrolysis. The diameters of the samples were measured with a digital caliper. For each sample the diameter was measured 10 times from top to bottom of the cathode. To obtain more accurate data, this measurement was repeated for 3 times in 3 different positions. Thus the diameter of each cathode was measured for 30 times. The diameters of virgin and worn samples, as well their averages are given in Appendix B.

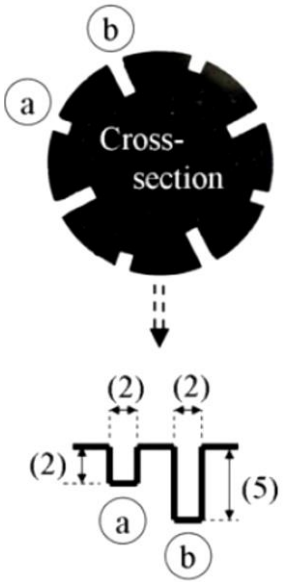

Figure3.2. The cross section of the cathode with two different depths. Eight slots evenly distributes around the periphery [9].

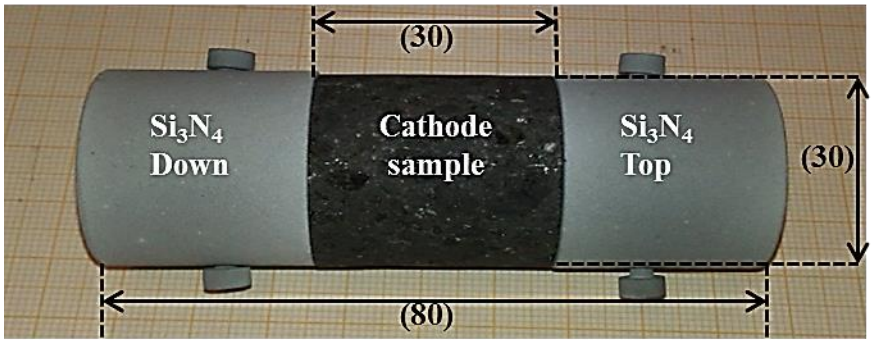

Figure 3.3. Image of the cathode sample with Si_3N_4 covered ends. The dimensions in millimeters are given.

The chemical composition of the electrolyte is given in Table 3.2, which gives the cryolite ratio equal to, CR=2.07 as a constant ratio for all tests. In addition, 100 grams pure aluminium shot (a small pool of molten aluminium during the electrolysis) was added at the bottom of the crucible, before making the bath.

Table 3.2. Chemical composition of electrolyte bath in cathode wear test.

Component	Weight (g)	percent
Synthetic cryolite	540.06	74.8
AlF_3	96.27	13.3
CaF_2	36.10	5
Al_2O_3	49.50	6.9

The electrolysis temperature was set to 970 °C and kept constant during the experiment by an external temperature controller. The cathodic current density used, was 1 A/cm^2 and the electrolysis time was 24 hours. The software Emdac (developed by Henrik Gudbrandsen, SINTEF) was used to monitor the cell voltage, the current and the temperature in the bath during the experiment. When the temperature in the melt reached to the programmed temperature, 970 °C, the cathode specimen was lowered into the melt, 25 mm from the bottom of the crucible. The test could be run in two general hydrodynamic conditions, stationary state or rotation of the cathode. At the end, the cathode was lifted out of the bath.

Besides the study of the wear rate, some cathodes were investigated to identify the sodium and bath concentration gradients in the cathode after electrolysis. The procedure involved the preparation of cathode sample cross sections and then measurements of element distributions via the electron probe microanalysis, EPMA/wavelength dispersive spectroscopy, (JXA-8500F Hyperprobe), apparatus (JEOL Ltd., Tokyo, Japan). In addition, the cathode specimens were examined through the x-ray computed tomography (CT). The CT technique enables a macroscopic observation inside the sample, in terms of penetration of bath, grain size and grain distribution.

4. Results and discussion

The result of the wear rate experiments of the cathode material is given in this section. The wear tests were done to study the effect of cathodic rotation speed on the wear rate of carbon cathode. The current work was performed by fifteen experiments on the four different types of carbon materials, listed in Table 3.1. Since the main purpose of the project is the influence of rotation speed on the wear rate of carbon cathode, identical current density equal to i=1 A/cm^2 was applied. The experiment time was 24 hours for all tests. Figure 4.1 displays a representative sample of each group of cathode material after the experiment, including their cross sections. The wear profile and also the extent of the wear are different in each case.

In electrochemical processes, many factors affect the behavior of the system, e.g. current density, conductivity of solution and electrodes, material, hydrodynamic conditions, etc. In this work the only variable factors were cathode material and rotation speed. The results of the experiments at different conditions (various carbon cathode and rotation speed) the wear profiles for each group of cathode materials were different. As an example it is shown in Figure 4.1, that the wear profile in the anthracite based cathode is less uniform than the other types of carbon materials. The surface appearance after experiment for each type of carbon material is different. Hence, the wear profile and the surface appearance after the electrolysis are strongly dependent on the carbon material. Figure 4.1 shows this diversity well, from one material to another.

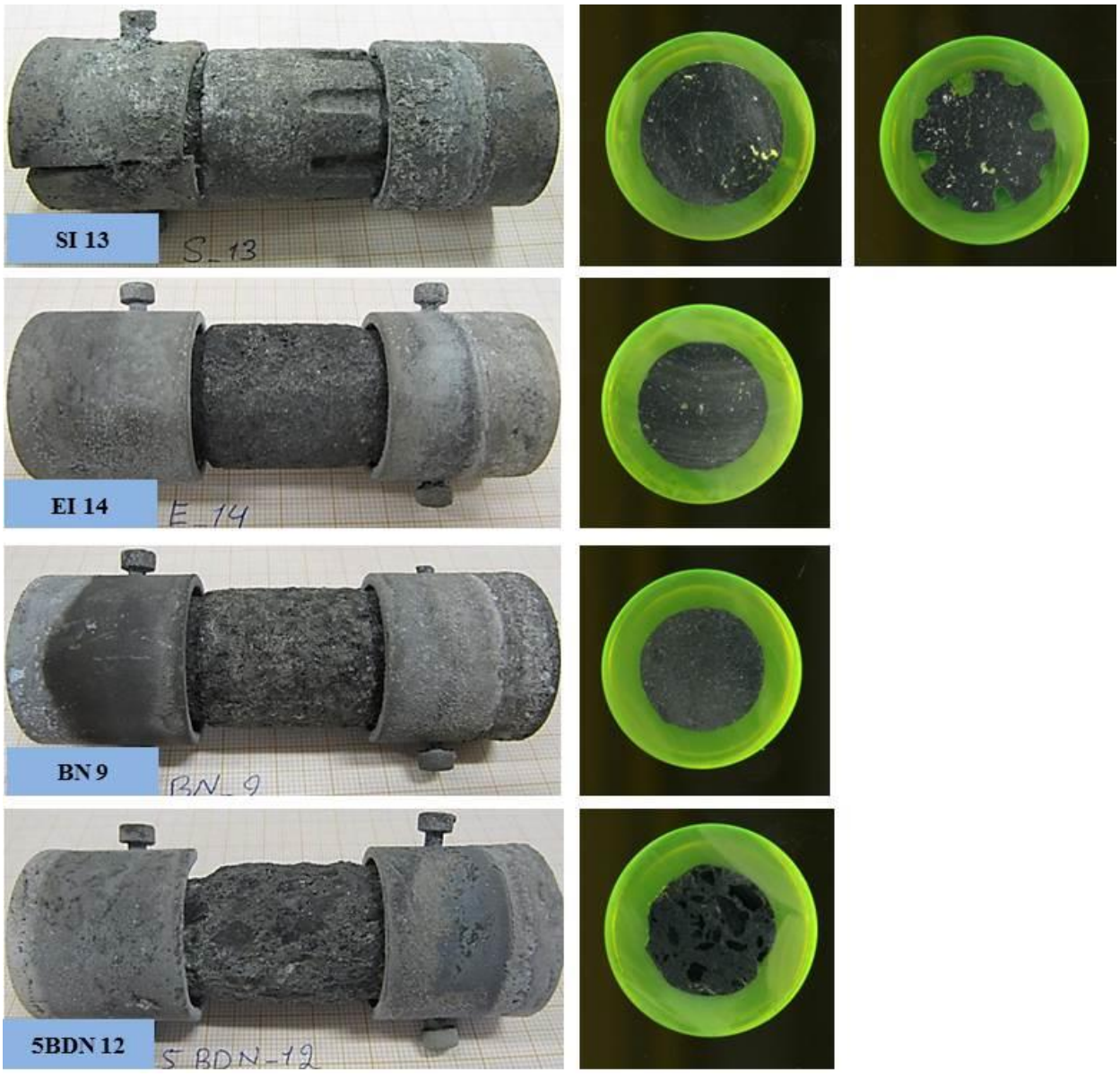

Figure 4.1. The samples after experiment (Left); their cross sections (Right).

4.1 Edge effect

What is common in all the experiments is severe wear at both sides of the samples, i.e. at the border of carbon cathode and lining material. Figure 4.2 shows a virgin cathode sample before and after installation of the linings (a, b) and the sample after electrolysis (c). The linings after experiment (c) have been removed. Experiments show the maximum wear has been occurred at the upper and lower parts of the exposed area to the bath and current, where the sample has edges.

The reason for this phenomenon is the edge effect. The conception of edge effect in every electrochemical cell is the concentration of current lines at the edges of the electrode, which results to higher current density. A schematic of the edge effect is illustrated in Figure 4.3, where the current density distribution in a simple cell with flat parallel electrodes is shown. It can be assumed that a homogenous electric field and, consequently, a uniform current distribution are present over the whole electrode surface up to the edge of the electrode. At the edge of the electrode current density increases.

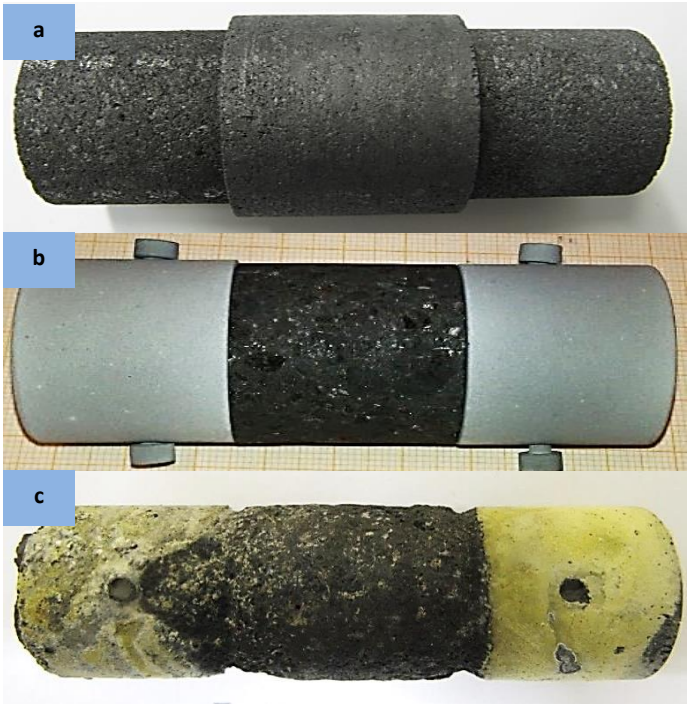

Figure 4.2. (a) Virgin carbon cathode before installation of the linings. (b) Virgin carbon cathode after installation of the linings. (c) Carbon cathode after experiment and with removed linings.

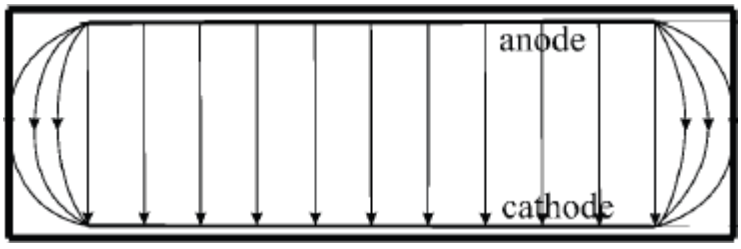

Figure 4.3. The current density distribution in a cell with flat parallel electrodes edges [24].

In a homogenous field there is only one current line between two symmetrically positioned points on the cathode and anode electrodes. Therefore current density in the homogenous field should be lower than current density at the edges. At the edges of the electrodes there is an infinitely large number of the current lines between two symmetrically placed points. Thus it can be concluded that the overall resistance between these two points is equal to an infinitely large number of resistances connected in parallel, being lower than in the homogenous field [24]. Since in the experimental setup of this project anode and cathode (graphitic crucible and cylinder sample) are parallel, thus the above condition is valid for the current work. Hence the current density at the both heads of the cylindrical cathode (the edges) is greater than the bulk area. The edges of the carbon cathode are subject to the maximum current density and apparently the highest wear occurs in these zones.

Dependent on the experimental conditions such as material, hydrodynamics of the system, current density, etc, the degree of cathode wear changes. Regardless, the wear profile for different conditions throughout the length of the sample from top to down follows the similar pattern. The minimum radius of the sample after electrolysis is observed at both heads of the cathode, where the edge effect causes highest wear. At the middle of the cathode minimum wear is observed. Thus the wear profile of all the cathodes after electrolysis is more or less barrel shaped. Figure 4.4 displays the variations of the cathode radius over the length of the samples from top to bottom for every category of cathode material.

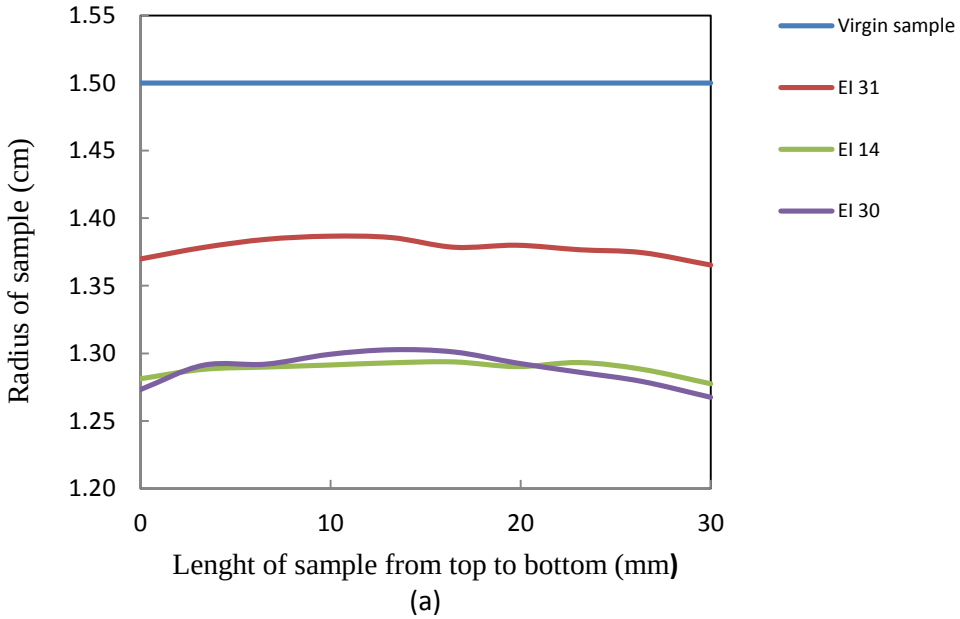

(a)

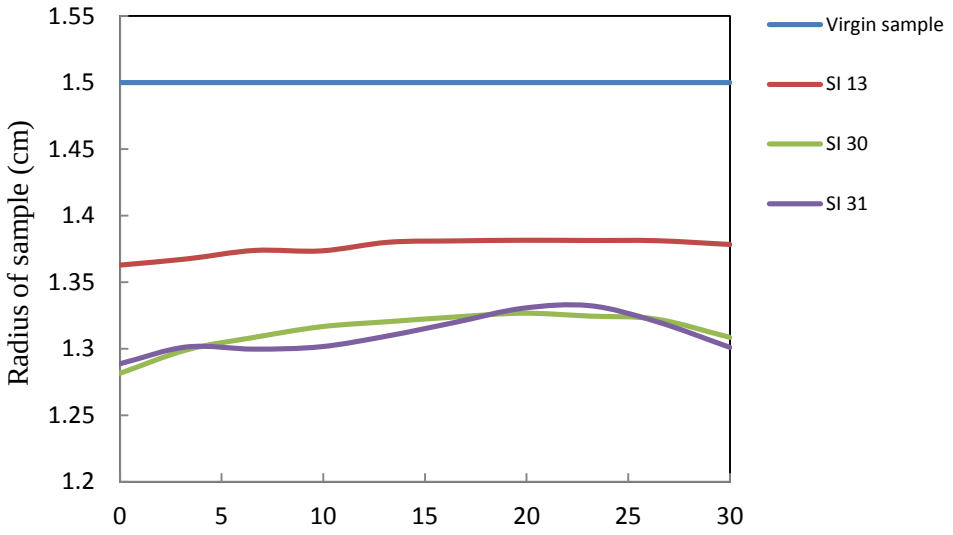
1.55
1.5
1.45
1.4
1.35
1.3
1.25
1.2
Radius of sample (cm)
0
5
10
15
20
25
30
Length of sample from top to bottom (mm)
Virgin sample
SI 13
SI 30
SI 31

(b)

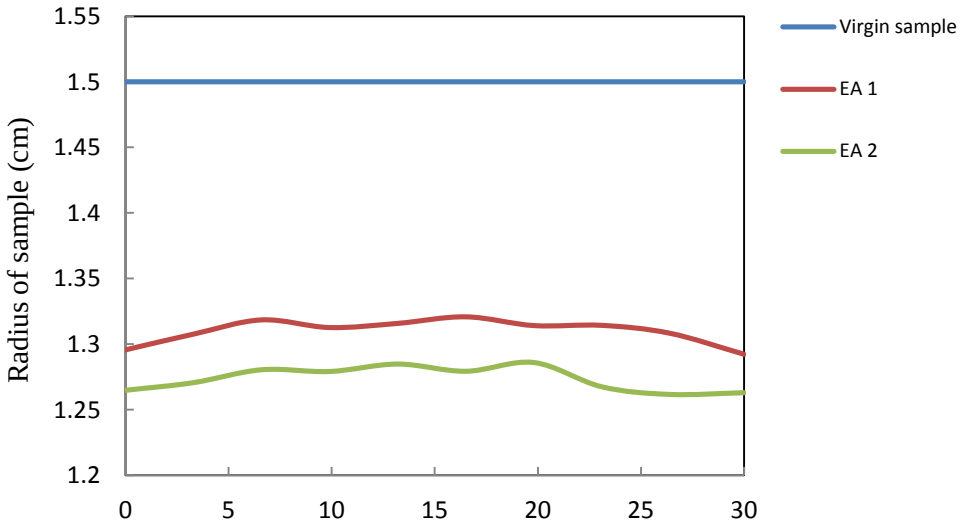
1.55
1.5
1.45
1.4
1.35
1.3
1.25
1.2
Radius of sample (cm)
0
5
10
15
20
25
30
Length of sample from top to bottom (mm)
Virgin sample
EA 1
EA 2

(c)

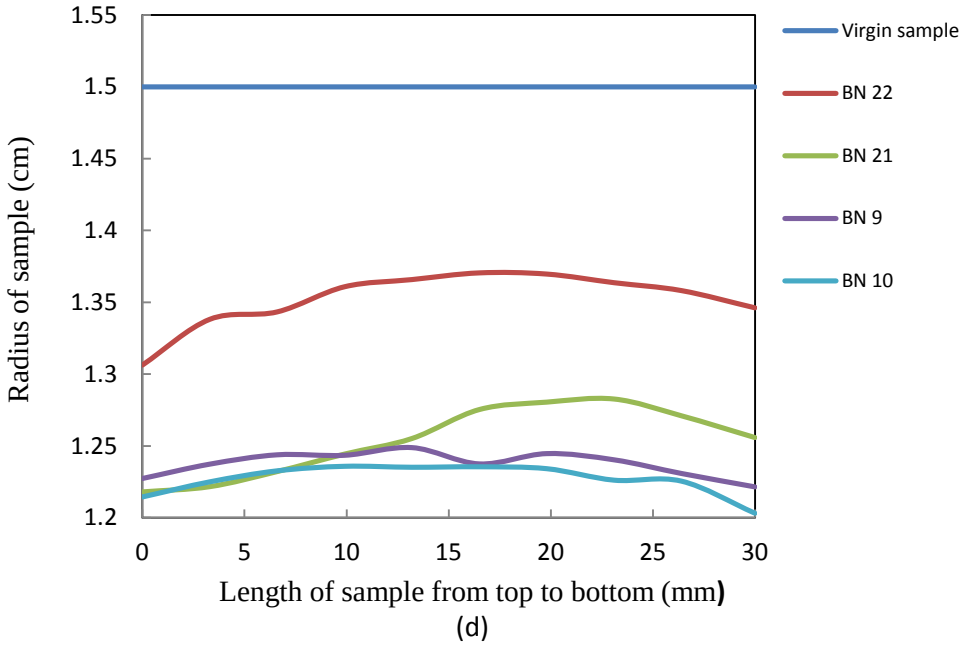

(d)

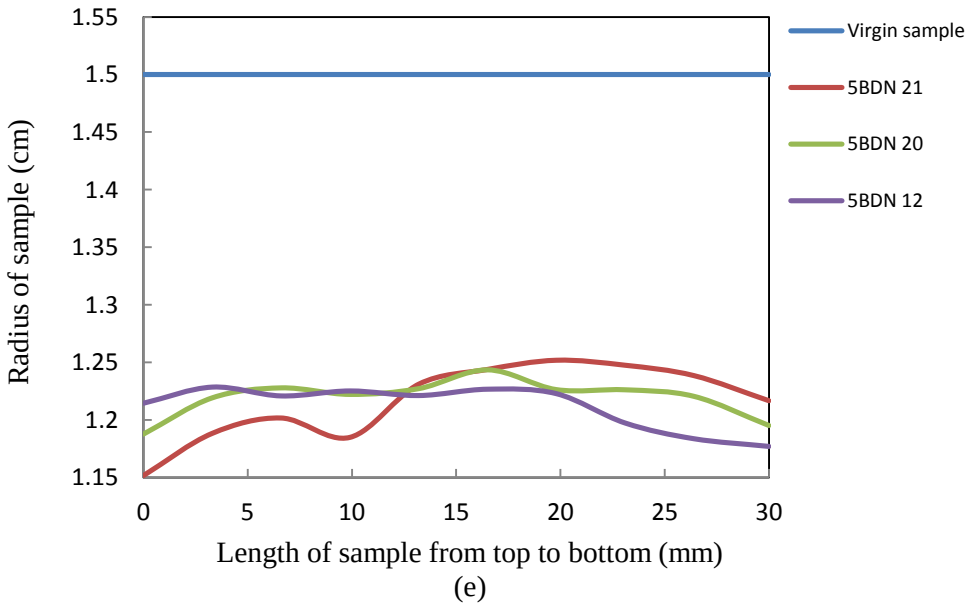

(e)

Figure 4.4. Variation of cathode radius after electrolysis throughout the length of the sample for different carbon material. (a) EI (graphitized-elkem), (b) SI (graphitized-elkem, with slot), (c) EA (graphitized-elkem, anisotropic), (d) BN (graphitized) (e) 5BDN (anthracite base).

The above curves and also the surface appearance of the samples show that the surface smoothness of carbon cathodes after experiment for different carbon materials is not similar. The anthracite base cathodes, 5BDN have a very non-uniform and uneven surface, while the graphitized cathodes, EI, EA and BN, present a more uniform and smooth surface. The above difference goes back to the crystalline structure of carbon material and consequently to their

electrical resistivity. Anthracite has not 3-dimensional long order of graphitic structure. Indeed anthracite is an amorphous form of carbon, because its carbon atoms are randomly distributed in the material. Therefore the electrical conductivity of anthracite is lower than the other forms of crystalline carbon material. Contrary to anthracite, a 3-dimensional long order of graphitic structure is dominant in graphitized carbon material, which gives higher electrical conductivity. Hence contribution of graphitized carbon in electrochemical reactions is more efficient and as a result the wear rate of this kind of carbon cathodes is greater than anthracitic cathodes. But it should be mentioned that the anthracite base cathode which is used in industry and also for this work is a combination of anthracitic carbon, graphitized carbon and pitch as binder. Because of that in anthracite base cathodes the high eroded zones are belong to graphitized carbon while the anthracite grains have less wear. This different behavior from anthracitic and graphitized carbon, simultaneously and in one sample, during the electrolysis gives a very uneven surface over the cathode. Figure 4.5 compares the surface smoothness of anthracite based and graphitized cathodes.

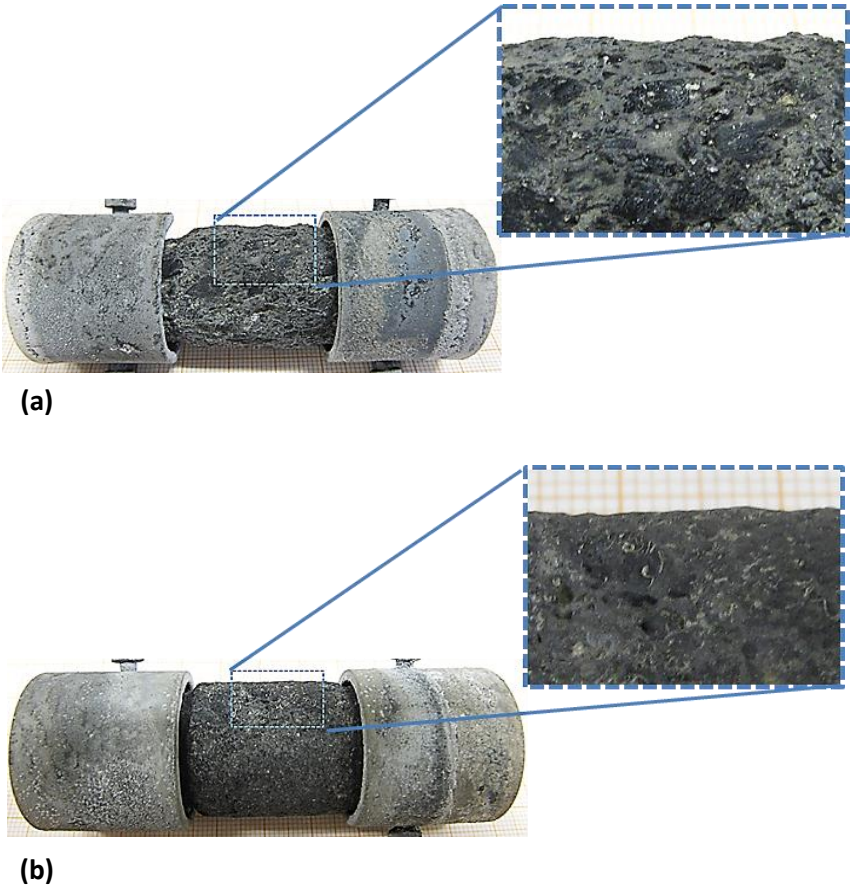

Figure 4.5. The influence of carbon material on the surface smoothness after electrolysis. (a) Anthracite based cathode with uneven surface. (b) Graphitized cathode with smooth surface.

4.2 Ranking of cathode materials

Most of the experiments during this project were performed at high rotation speed, i.e. at 125 rpm. Comparing the obtained data with the results from previous works at lower rotation speed enable us to analyze the cathode wear phenomena and find the correlation between rotation speed and wear rate. In Table 4.1 the variation of wear rate by changing the cathode material and rotation speed at constant current density, temperature and time, is shown.

Table 4.1. Calculated wear rate for various carbon cathodes at different rotation speeds.

sample	Rotation speed (rpm)	Wear rate (cm/year)
SI 13	0	37.2
SI 30	80	57.97
SI 31	100	59.1
EI 14	125	70.13
EI 30	125	71.36
BN 9	125	89.46
BN 10	125	93.08
5BDN 12	125	97.73
5BDN 20	125	94.44
EI 31	0	37.56
BN 21	125	76.69
5BDN 21	125	91.48
BN 22	50	43.6
EA 1	125	62.47
EA 2	125	75.83

Increase in wear rate by ascending the rotation speed is observed regardless of the cathode material. By calculating the difference in wear rate when the only variable is rotation speed it can be found that the hydrodynamic of the system impose a significant impact on the cathode wear. This is measurable for SI, EI and BN samples because they have been tested in different rotation speeds. For SI13 and SI31 samples when rotation speed increases from 0 to 100 rpm an increase equal to 59 % in wear rate is observed. The increase for EI31 and EI30 samples is 90 %, where

the change in rotation speed is from 0 to 125 rpm. Also for BN22 and BN21 samples by increasing the rotation speed from 50 to 125 rpm, the increase in wear rate was 76 %. For the experiments with the equal conditions (repetitive tests) the results are in good agreement, e.g. EI14=70.13 and EI30=71.36, BN9=89.46 and BN10=93.08, 5BDN12=97.73 and 5BDN20=94.44 and finally, EA1=62.47 and EA2=75.83 cm/year.

When the only variable is the slots on the surface and the other parameters are constant, a difference in wear rates is observable. As mentioned earlier the difference between SI and EI cathodes is the slots on the upper part of the SI samples. The wear rates for SI13 and EI31 respectively are 37.2 and 37.56 cm/year. These wear rates are very close, so that the wear rate of EI31 within experimental error for a minor amount is larger than SI13 at 0 rpm. The above difference is more obvious in BN and 5BDN samples. For the samples without slot, BN9 and BN10, the wear rates are 89.46 and 93.08 cm/year respectively at 125 rpm, while for BN21 which has slots, the wear rate is 76.69 cm/year at the same rotation speed. Also for 5BDN12 and 5BDN20 without slots, the wear rates are 97.73 and 94.44 cm/year respectively at 125 rpm, but in 5BDN21 which is a sample with slots the wear rate 91.48 cm/year observed at the identical rotation speed.

The mentioned difference in wear rate goes back to the surface added due to the slots which cause to change in current density. Indeed the equal size of all cathodes and also the applied current, designed to make an equal current density for all experiments. But obviously the samples with slot have more surface area. Hence, when the current is constant, the current density for the sample with slot is lower than the sample without slot. Therefore smaller current density in the sample with slot gives lower wear rate. Figure 4.4 (a,b,d,e) shows this diversity very well. However in the samples with slots, the cathode wear around the slot area is very intense due to the edge effect, but the total wear over the length of the cathode in the samples without slot is greater. To report the wear rate of the samples with slots, the dimensions related to slot area were not accounted.

For raking the cathode material in terms of wear resistance, repetitive experiments were used. All the cathodes for this purpose have been exposed to the maximum rotation speed of 125 rpm. Also the current density and experiment time for all of them were constant. Figure 4.6 shows the ranking of EI, EA, BN and 5BDN cathodes, where for each group of cathodes, two experiments were performed with the samples without slot. Figure 4.6 indicates, the wear rate of graphitized cathodes made by Elkem, EI and EA (isotropic and anisotropic) are close, in the range 62-75 cm/year. The average wear rate of the other graphitized material, BN, is about 90 cm/year which is higher than the Elkem material. The difference in wear rate between Elkem and BN material may come from the production recipe which is used for these cathodes. Finally the anthracite based cathodes, 5BDN, with the average wear rate around 96 cm/year have the maximum wear rate of the studied carbon cathodes at 125 rpm.

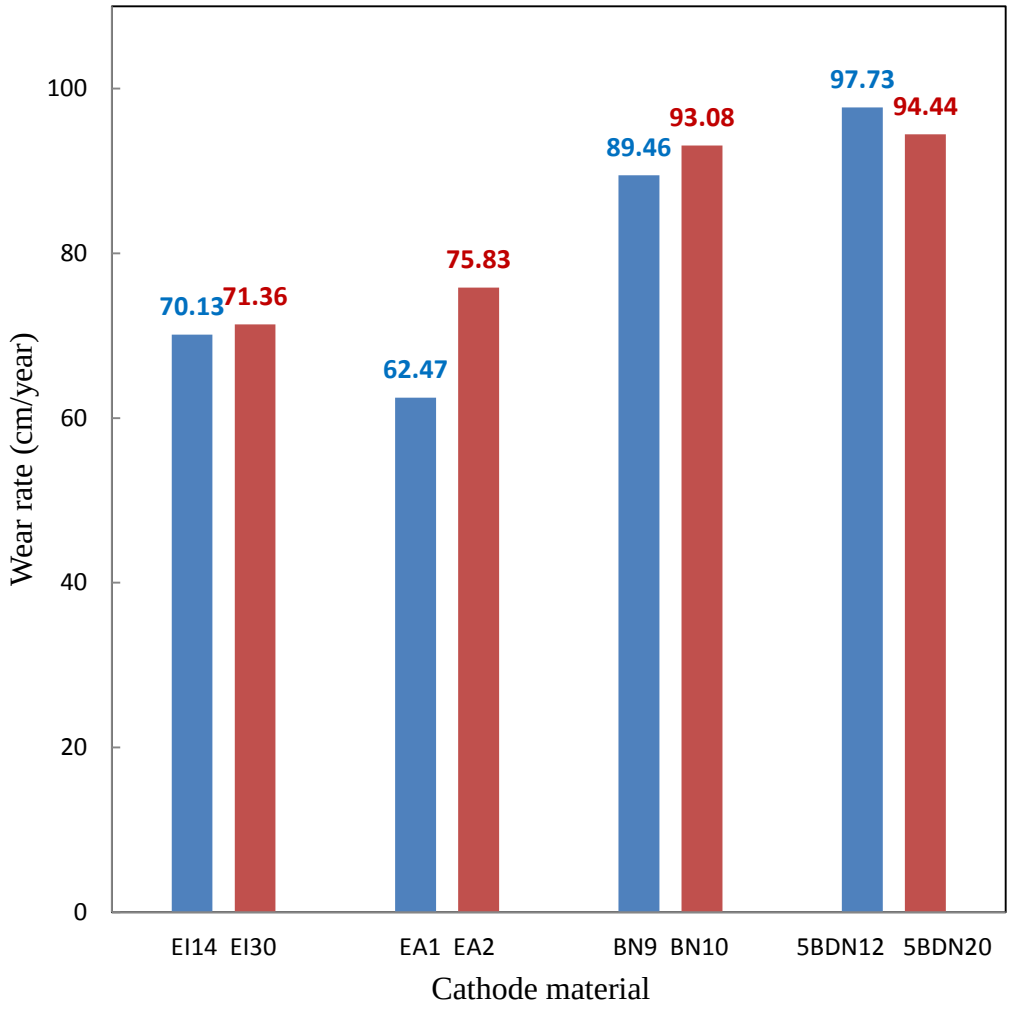

Figure 4.6. Wear rate in cm/year for four carbon cathodes at maximum rotation speed, 125 rpm. (EI)Elkem-garaphitized.isotropic,(EA)Elkem-graphitized,anisotropic, (BN)graphitized, (5BDN)anthracite based. i=1A/cm^2, Time=24h.

4.3 The effect of rotation speed

Basically, the cathode wear is influenced by hydrodynamic of the system, so the wear rate is directly correlated with rotation speed. Figure 4.7 illustrates the changes in wear rate versus the rotation speed for the cathodes listed in Table 4.1, where the wear rate increases when the rotation speed is increased. Figure 4.7 consists of different categories of carbon cathodes, including with slots and without slots. This indicates that the wear process is mass transfer controlled. The changes of the wear rate are not quite linear for various speeds. Actually, with reference to previous studies and the current work, the growing path of the wear rate at lower speeds is different with high speeds. The increasing pattern of the wear rate at slow speeds is nearly linear with a moderate slope. The increasing profile of the wear rate at high speeds is

nonlinear, where wear rate rises exponentially by increasing the rotation speed. The difference in increasing profile of the wear rate between lower and higher speeds maybe related to the pattern and degree of fluid flow which surrounds the rotating cathode.

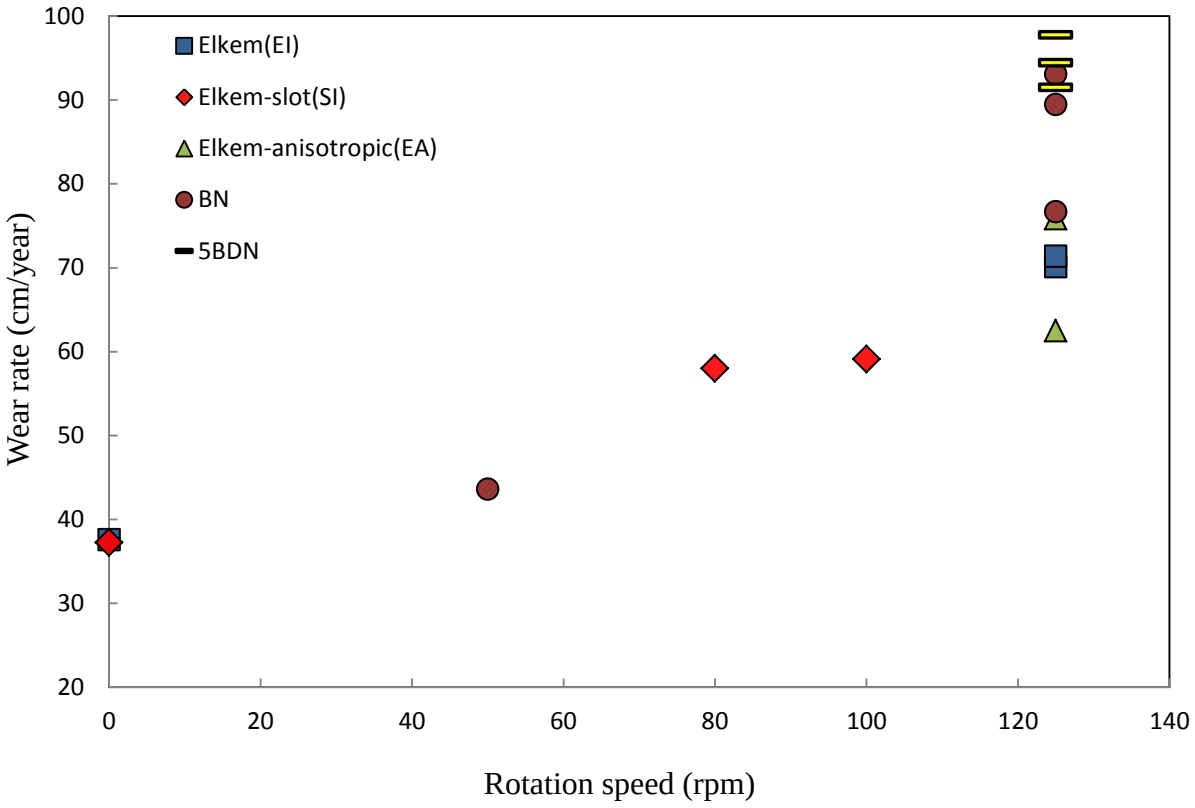

Figure 4.7. The cathode wear rate as a function of rotation speed for fifteen samples listed in Table 4.1.

As mentioned previously, cathodic current density, cryolite ratio and cathode rotation speed are influencing factors on cathode wear rate. As a matter of fact, presence of current (polarization) is a prerequisite for cathode wear because of the electrochemical reactions, while the rotation speed has a complementary effect on wear due to the fact that it enhances the mass transport. The main aim of this study is the investigation about the influence of rotation speed on the cathode wear rate. Hence, the only variable parameter was rotation speed which applied to different carbon materials. Therefore, the major part of the discussion is dedicated to the changes in wear rate due to the different hydrodynamic conditions. The cathodic current density, $i=1A/cm^2$, was constant for all the experiments. As well, the cryolite ratio, CR=2.07, throughout the project was kept invariant.

In every electrochemical process, mass transport is taken place towards/from the electrodes through the diffusion layer. Outside the diffusion layer, which is called bulk electrolyte, the electrolyte concentration is uniform, whereas inside the diffusion layer there is a concentration gradient for electrolyte. The thickness of diffusion layer as a determining factor effects the rate of mass transport. Principally, as the thickness of diffusion layer decreases, the mass transport gets faster. Dependent on the hydrodynamic condition of the system, the thickness of diffusion layer is varied. This thickness changes from a few millimeters for stagnant state to several atomic layers for turbulent flow at high rotation speeds. Indeed by transition from stationary state to laminar flow and then turbulent flow respectively, the thickness of diffusion layer gradually decreases.

The laminar and turbulent flows, as two conceptual flow patterns, are far from each other. In point of fact, these models are two extreme states. The flow pattern of the current study, even at the maximum rotation speed, 125 rpm, is neither a laminar flow nor a turbulent flow. It means that hydrodynamic of the system is a mixture of both models and the flow regime is in somewhere between laminar flow and turbulent flow. When there is no rotation, the system has only convection by thermal fluctuation, where convection determines the thickness of the stagnant diffusion layer [25]. In this case the diffusion layer is thick with large concentration gradient towards the surface. Against, any rotation in cylindrical cathode reduces the thickness of diffusion layer and consequently brings down the concentration gradient. Due to the surface tension the inner layer of diffusion layer sticks to the cathode surface. When rotating is started and the flow pattern approaches from laminar toward turbulent flow, the diffusion layer gets closer to the cathode surface and becomes thinner. In other words, the thickness of the diffusion layer is directly influenced by hydrodynamic of the system, so that by increasing the rotation speed, the thickness of the diffusion layer decreases which in turn helps to accelerate the mass transport. That is why in the Figure 4.7, the highest wear rate has been occurred at maximum rotation speed.

Fundamentally, three types of mass transport are available in an electrochemical experiment, i.e. diffusion, convection and migration. Since in this project the voltage and current density were kept constant, migration is not subject of discussion. Depending on the hydrodynamic conditions, stagnant state or stirring by rotation of cathode create respectively, natural convection or forced convection. Diffusion is common to all electrochemical experiments due to the concentration gradients set up between the bulk solution and the interfacial region. Thus, for the current electrochemical experiments (called hydrodynamic techniques) the mass transport is a combination of convection and diffusion [26].

The cryolite ratio has a considerable effect on carbon consumption as well as cathode wear rate. From previous studies it seems that decreasing cryolite ratio leads to increasing wear rate [17]. It is assumed that this is due to the increased solubility of aluminium carbide in cryolite with increasing acidity of cryolit17e. In fact the cryolite ratio decreases with increasing the acidity.

In an electrochemical cell the cryolite ratio in the bulk is constant, but there is a concentration gradient in the cathodic diffusion layer. At the cathode surface the cryolite ratio is maximum. The minimum cryolite ratio (bulk concentration) is observed at the interface of bulk and diffusion layer. For a constant thickness of diffusion layer, higher cryolite ratio gives a larger concentration gradient. Figure 4.8 illustrates the concentration profile in the cathodic diffusion layer for three different cryolite ratios at a constant current density [1].

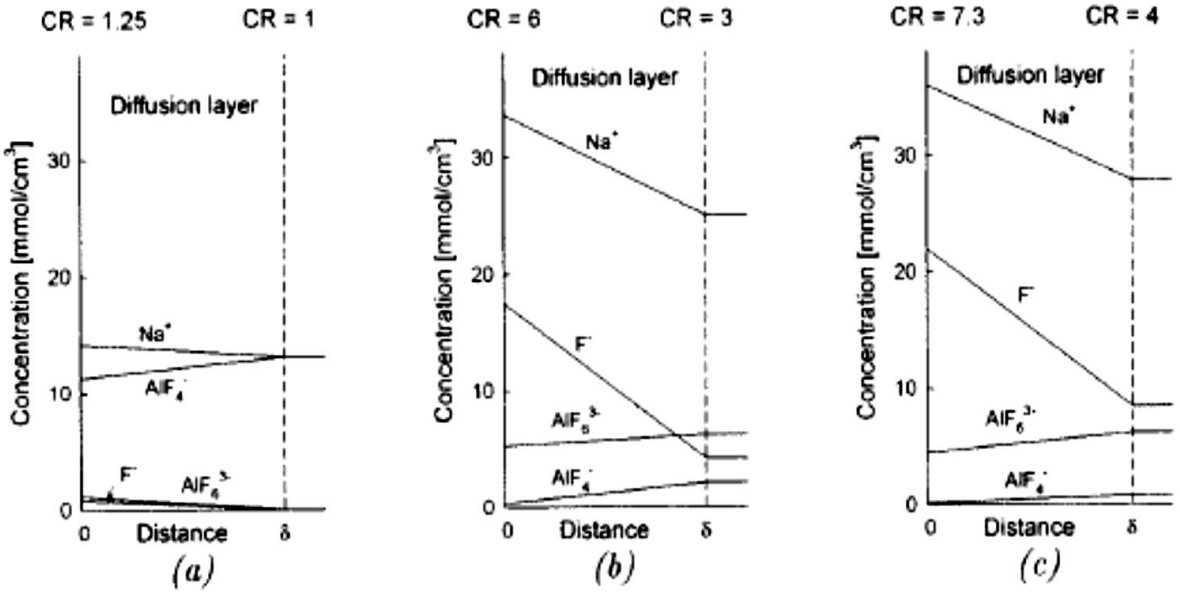

Figure 4.8. Concentration gradient in the cathodic diffusion layer by electrolysis at i = 0.6 A/ cm^2 and a)CR=1, b)CR=3 and c)CR=4 in the bulk of the melt [1, 27].

The cryolite ratio, was constant (CR=2.07) for all the experiments. But different hydrodynamic conditions create different thicknesses of diffusion layer, where with increasing rotation speed the thickness of diffusion layer is decreased. In this case there are two scenarios about the change in concentration gradient. In the first one when the thickness of diffusion layer decrease, the cryolite ratio does not change. Contrary in the second scenario, the cryolite ratio at the cathode surface is reduced by decreasing the thickness of diffusion layer. Figure 4.9 indicates the concentration gradient in the diffusion layer for stationary state, as well as both situations may happen after starting the rotation.

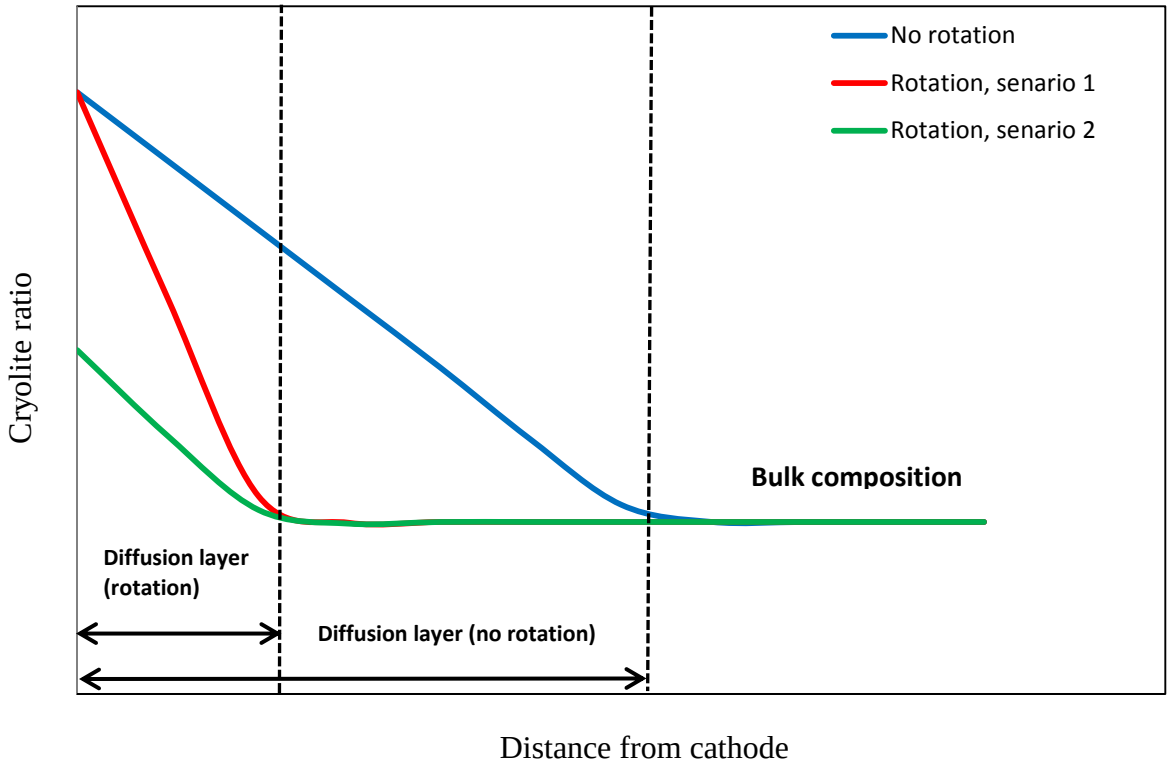

Figure 4.9. The possible scenarios for change in concentration gradient after decreasing the thickness of diffusion layer. (Blue) stagnant state, (Red) rotation-scenario 1, (Green) rotation-scenario 2.

It seems the second scenario is most likely, because it is in good agreement with previous and current results. Indeed by increasing rotation speed the concentration gradient is decreased and cryolite ratio at the cathode surface approaches to the bulk composition. It means that the acidity of cryolite increases and consequently the solubility of aluminium carbide in cryolite is enhanced which gives higher wear rate. Therefore, based on the second scenario it can be concluded that for a constant cryolite ratio, the concentration gradient decreases when the rotation speed is increased. In other words, the minimum concentration gradient and the maximum wear rate are observed at the highest rotation speed. Figure 4.10 shows the changes in cryolite ratio at the cathode surface with increasing rotation speed relying to second scenario.

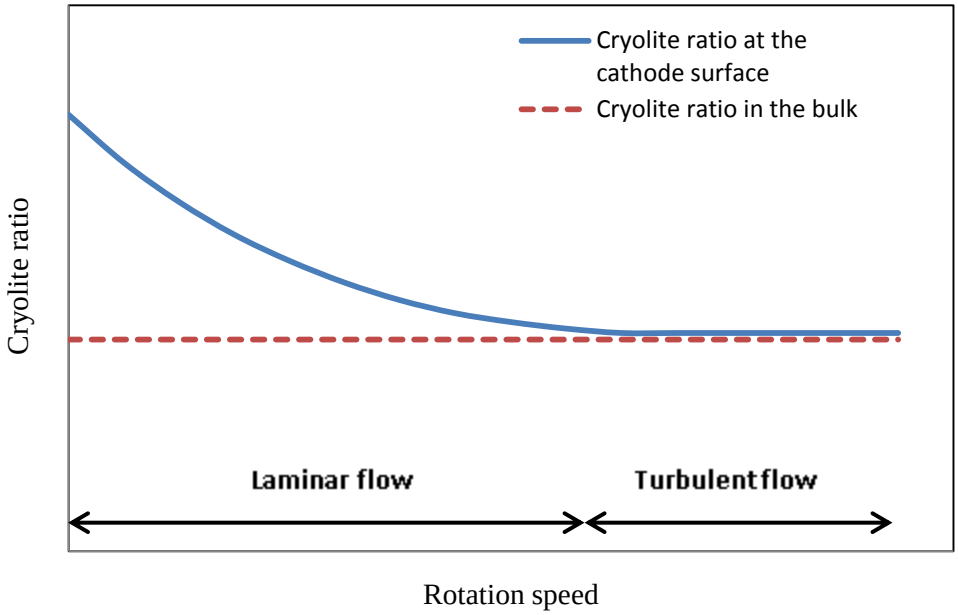

Figure 4.10. The cryolite ratio at the cathode surface as a function of rotation speed.

Figure 4.11 illustrates the results of experiments that have been accomplished before the current study. The only variable for this group of experiments was rotation speed. Among these samples, Elkem-slot (red mark) was tested at three rotation speeds, 0, 50 and 125 rpm. Thus it is a good example to show the correlation between the wear rate, the thickness of diffusion layer and the cryolite ratio. The dotted line indicates the wear rate is increasing, where the thickness of diffusion layer and the cryolite ratio are decreased with increasing the rotation speed.

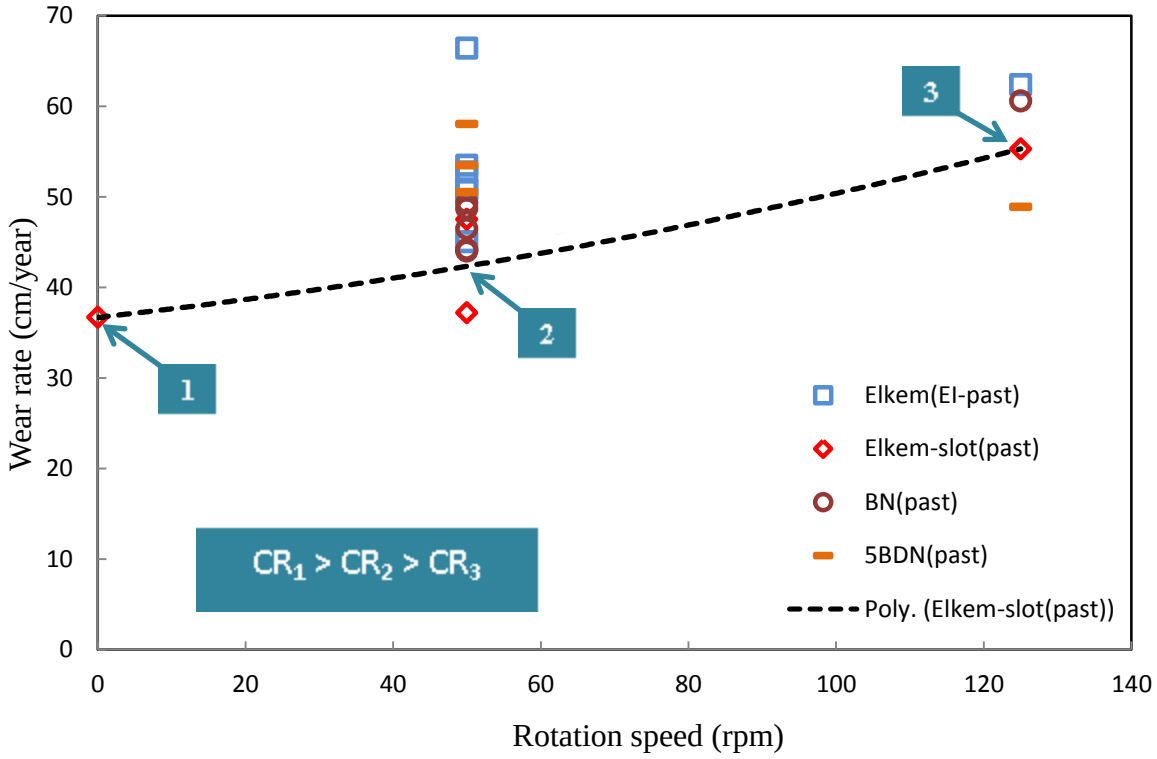

Figure 4.11. The cathode wear rate as a function of rotation speed for previous experiments at i=1 A/cm^2 and Time=24 h.

Figure 4.12 shows the results of current study and previous work, together. The effect of rotation speed on cathode wear rate was the purpose of all experiments. However, by increasing the rotation speed, the cathode wear rate increases, but distribution of results at different rotation speeds is not the same. The results at high speeds were distributed at a wider range than the lower speeds. When the experiment is performed at stagnant state or at low rotation speed, the cylindrical cathode is in vertical position. It means that the surfaces of cathode and anode are parallel. In this situation the current lines from anode to cathode are the same. Thus, the current distribution over the length of the cathode is uniform which gives similar results. On the contrary, for the experiments at high rotation speeds, the cathode is not quite vertical. In fact, at fast rotations the cathode deviates from vertical posture and starts to vibrate. In this case, the current lines are not the same which result to less uniform current distribution. Current distribution in electrochemical cells depends on cell geometry, electrolyte conductivity, the reaction kinetics at the cathode and mass transport conditions [28]. When in an experiment all the parameters are constant, the cell geometry can be a factor which effects on the current distribution. Dependent on the degree of vibration, the current distribution at different area of the cathode is varied. Hence, the distance between the results at high speeds are larger than the low speeds. This is the effect of the cell geometry on this type of electrochemical experiments.

Distribution of the results between two dotted lines indicates the effect of cell geometry as shown in Figure 4.12.

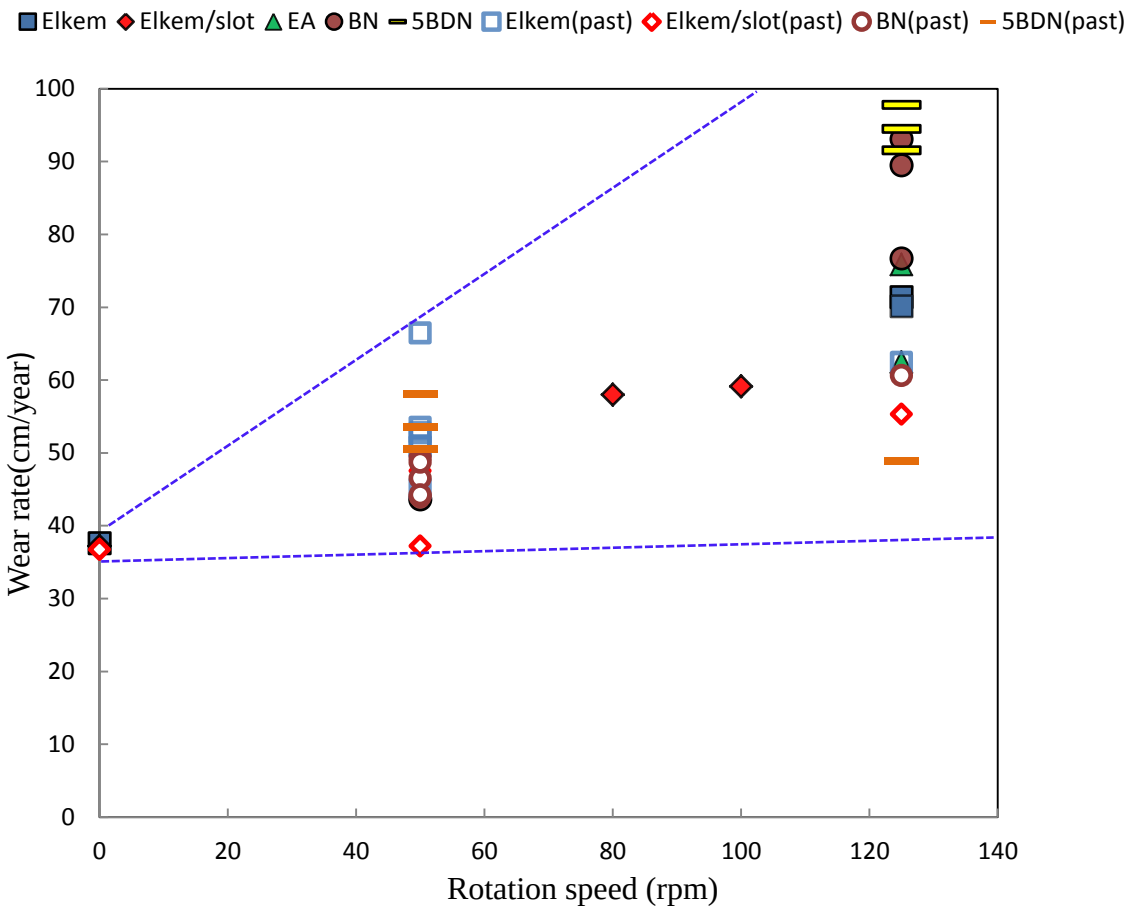

Figure 4.12. The cathode wear rate as a function of rotation speed for current work and previous study. The area between dotted lines shows how the results are distributed at different rotation speeds due to the geometry effect.

With respect to the results, the most likely hypothesis is the decrease of cryolite ratio at the cathode surface with increasing the rotation speed. Based on this assumption, the decrease in cryolite ratio continues until the cryolite ratio at the cathode surface reaches to the bulk composition, with maximum acidity. From this certain point it is expected to obtain constant wear rate with increasing rotation speed. But the results imply to the wear rate that still increases by increasing the rotation speed. It seems, when the cryolite ratio reaches to the bulk composition, the other wear mechanism is dominant in the system. The extra wear at high rotation speed may happen due to the mixing effect. During the electrolysis, the CO_2 gas is

produced at the anode surface. At the stagnant state or low rotation speeds the CO_2 bubbles leave the bath, slowly. When the cathode starts to fast rotation, the molten cryolite is stirred well, than the slow speeds. In this situation, the direction of CO_2 bubbles is not only upward and close to the anode wall. Indeed, during the stirring by cathode, the CO_2 bubbles move in different directions. Hence, the mixing creates an opportunity for CO_2 bubbles to approach toward cathode. The CO_2 gas at the cathode surface can react with carbon via the Boudouard reaction to produce CO gas. This reaction leads to further carbon consumption at high rotation speeds. This is an assumption for increased wear rate at high speeds, where cryolite ratio at the cathode surface is approximately equal to the bulk composition. Therefore at the fast rotation speeds, the wear mechanism may switches to the reaction between carbon cathode and CO_2 bubbles to make CO gas. The result of this reaction is increase in carbon consumption and wear rate.

4.4 The effect of current density

In addition of hydrodynamic condition and cathode material, the current density has a significant effect on the cathode wear rate. Most laboratory studies prove that the wear rate increases with increasing the current density. The laboratory studies correlate well with industrial observations [2]. The worn cathodes from industry show that the highest wear is occurred at the periphery of the cell, where the higher current density is expected. Figure 4.13 illustrates the results of two series of experiments that have been done before the present study. These experiments were performed with the aim of study about correlation between wear rate and current density. The rotation speed and the experiment time were constant for all tests. Both trends are in good agreement so that, some of the results are completely matched. The results show a direct relation between current density and wear rate, where the wear rate is increased by increasing the current density. Therefore the current density as a key factor has an extremely important effect on the cathode wear rate. Even if not directly influencing the cathode wear, increased current density gives rise to other wear enhancing factors, e.g. increased convection due to electromagnetic forces [2].

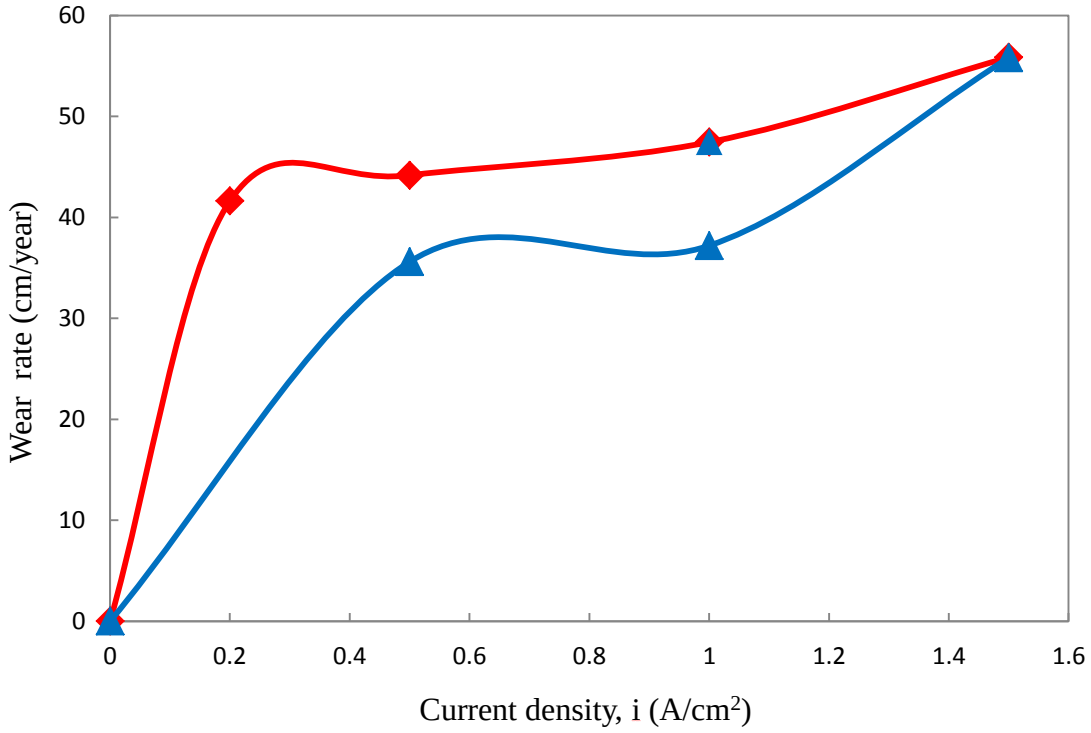

Figure 4.13. The cathode wear rate as a function of current density. The results of two studies show the similar trend.

The samples with slots have been designed for study about the wear mechanism and the effect of current density on the cathode wear rate. Figure 4.14 shows the cross sectional view of the worn cathode after experiment. It is evident in the Figure 4.14 that the outer surface of the cylindrical cathode is worn to a larger extent than the bottom of the slots. Besides the 2-mm slots seem to be more worn at the bottom and walls compared to the 5-mm slots. This experiment was performed at zero rotation speed, thus the resulting wear is similar on both walls of the slots. For the experiments with rotation, a systematic preferred wear is occurred at the upper part of side 1 of each slot. Figure 4.15 presents a cross section of the worn cathode, where the rotation speed was 50 rpm [9]. By comparing Figures 4.14 and 4.15 it can be observed that, the rotation speed caused a more severe wear at the side of the slot that faces the rotation direction.

Figure 4.14. Image of the scanned polished cross section of the worn cathode specimen, run at 0 rpm and 1 A/cm^2.

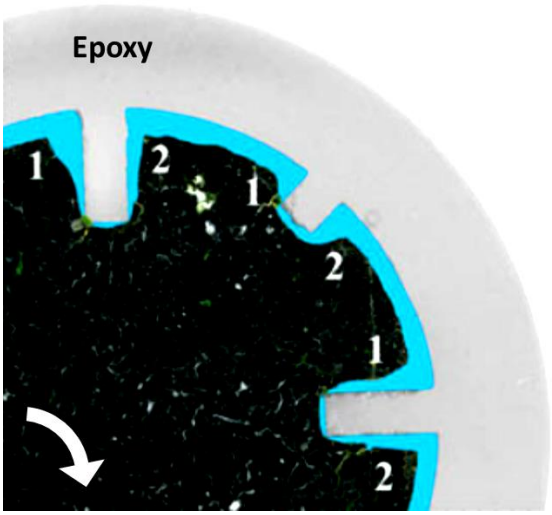

Figure 4.15. Superimposed image of the scanned polished cross section of the cathode specimen, run at 50 rpm and 1 A/cm^2. The blue color represents the worn area. The white arrow shows the direction of rotation [9].

The importance of polarization is revealed when the experiment is run without initial molten aluminium and at zero current. In this situation no wear is observed. Figures 4.16 and 4.17 display two different cross sections that were examined with EPMA to identify the depth of bath penetration at different experimental conditions. The measurement was performed from outer surface toward the center of the cathode sample. The first experiment was performed with polarization and without aluminium at the bottom of the crucible. After the electrolysis, the cathode wear was observed as it was expected. The second experiment was carried out without polarization and without aluminium. The result of this test shows that in the absence of the current, no wear happened for the sample. The scanned areas via the EPMA confirm that for the first experiment (with polarization) the bath components penetrate into the cathode during the experiment. Contrary, for the second experiment (without polarization), the measurement indicates the bath does not penetrate into the cathode. Figures 4.16 and 4.17 show the scanned area only at the surface and at the center of the samples. The measured elements are Na, F, Ca, Mg, Al, Si and O.

When the experiment is run without polarization and with initial molten aluminium, the result is completely different. In this case however the cathode was infiltrated with bath components, no wear was detected. As generally agreed, the main wear mechanism is formation and dissolution of aluminium carbide at the surface of cathode. It can be concluded that an electrochemical reaction is needed to cause the formation of aluminium carbide at the surface exposed to the electrolyte, at least under the condition that no aluminium layer is available in the direct vicinity of the cathode surface [9]. It is known that the molten aluminium can not wet the carbon cathode. On the other hand in industrial cells the open porosities of the cathode block is filled with bath components after a short time in operation. It brings up that the presence of sodium at the aluminium–bath interface changes the wettability of the carbon cathode. Thus sodium promotes the infiltration of bath into the cathode [3]. In this experimental set up there is a pool of aluminium at the bottom of crucible. This aluminium allows the formation of dissolved sodium in the melt according to reaction (2.12). This is explained why the cathode is fully infiltrated even in the absence of electric field [9]. A comparison between above experimental condition, normal set up (with polarization and with aluminium) and virgin sample is shown in Figure 4.18.

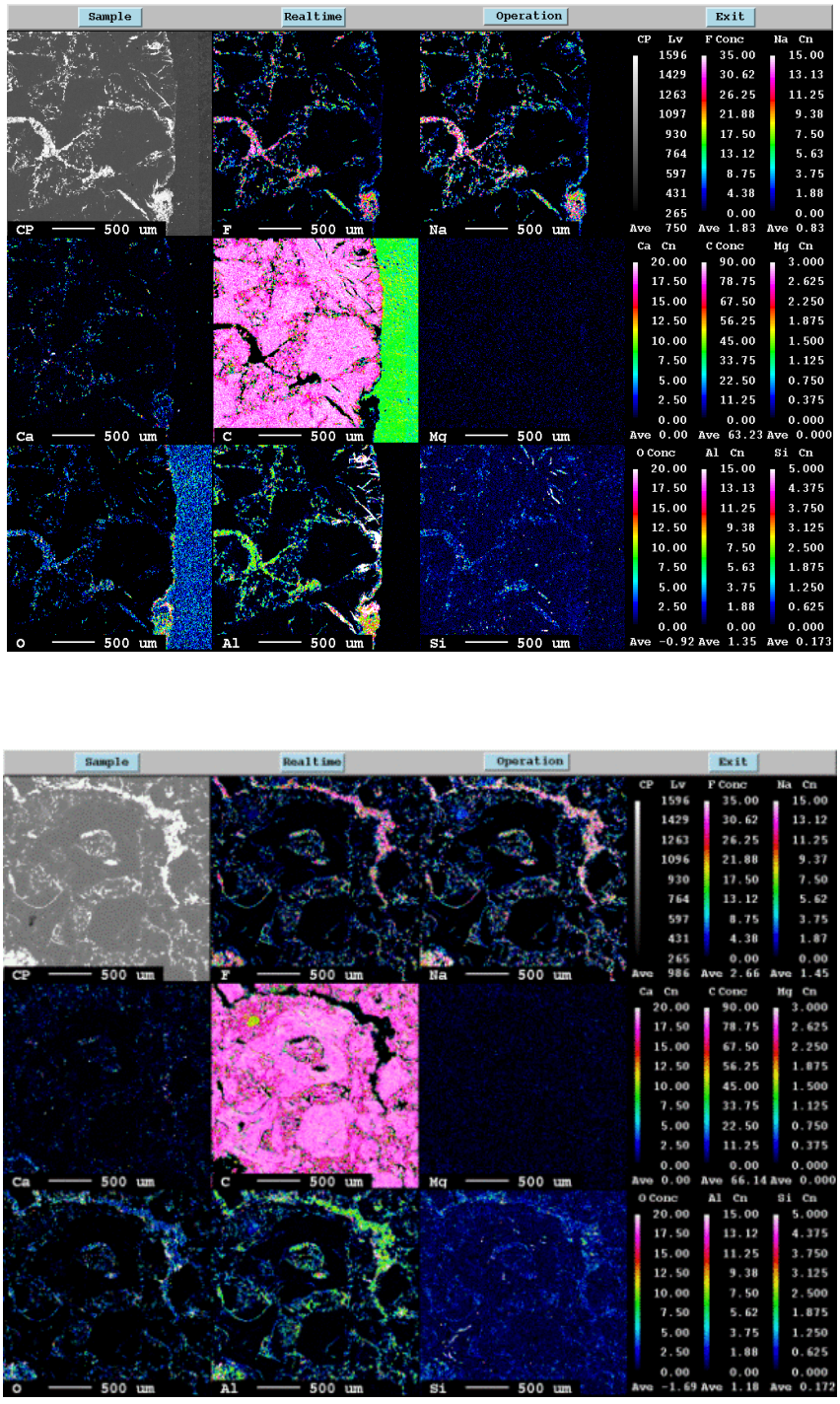

Figure 4.16. Micrograph and element distributions of Na, F, Ca, Mg, Al, Si and O at the surface (top) and the center (down) for the 24 h wear test duration with polarization and without aluminium.

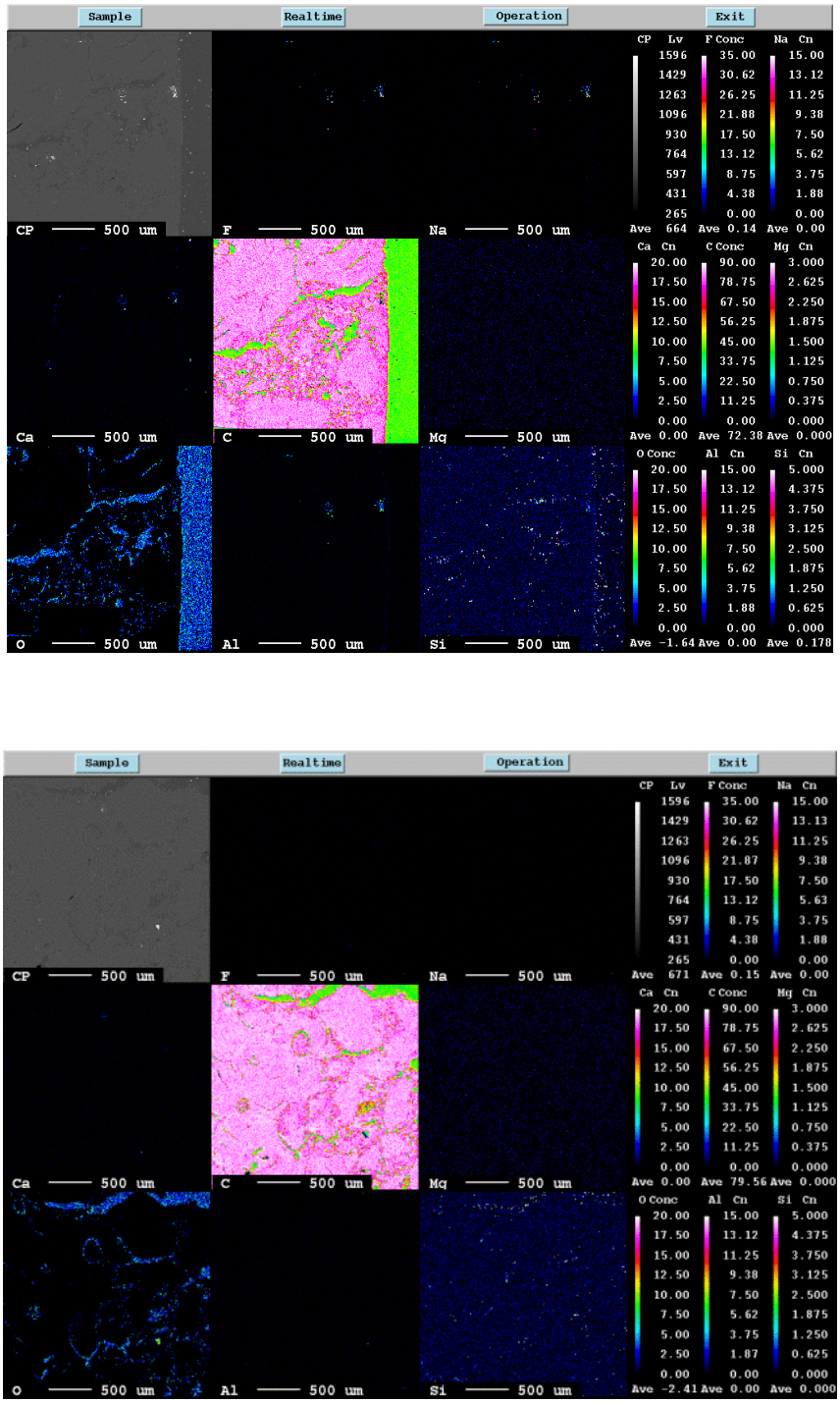

Figure 4.17. Micrograph and element distributions of Na, F, Ca, Mg, Al, Si and O at the surface (top) and the center (down) for the 24 h wear test duration without polarization and without aluminium.

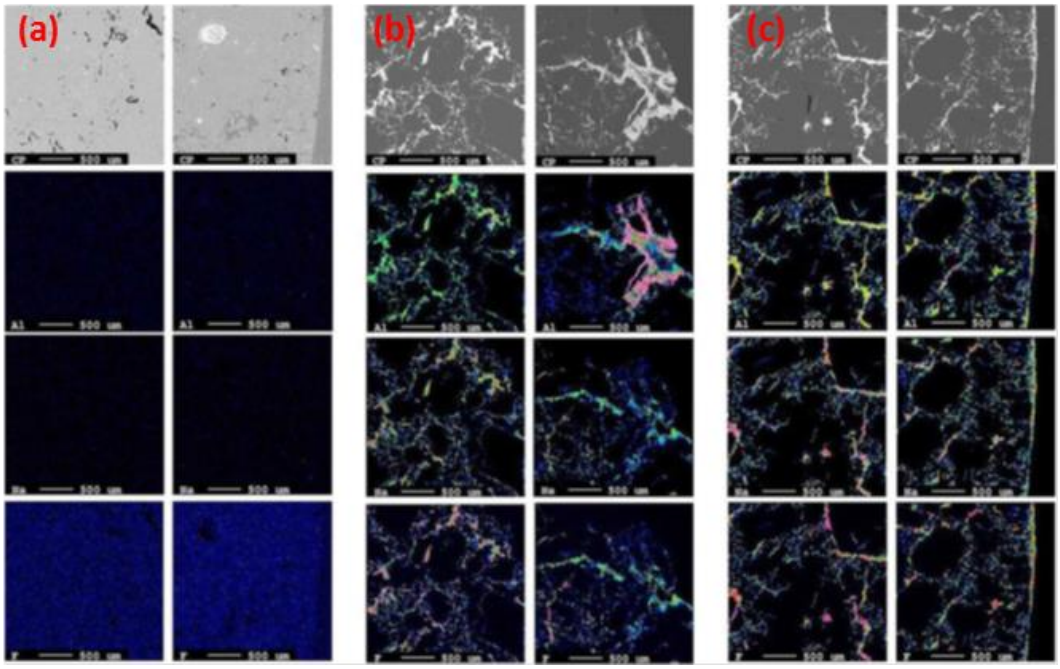

Figure 4.18. Micrograph and element distributions of Al, Na and F at the surface (right) and the center (left). (a) Virgin sample, (b) 24 h wear test duration with polarization and with aluminium, (c) 24 h wear test duration without polarization and with aluminium [9].

In order to obtain data about bath penetration rate, in a past study, the experiment times gradually were decreased. The wear test durations were 24 h, 1 h, 10 min and 2 min, where all the experiments were performed with polarization and in presence of initial molten aluminium. The cross sections related to four different experiments were examined with EPMA. The results indicate that even after a wear test time of only 2 minutes, the entire cathode was penetrated with bath [5]. Figure 4.19 indicates the micrograph and element distributions of Na and F which is representing the bath components. For the experiment with an electrolysis time of 24 hours, the sample was infiltrated with bath. It was in good agreement with expectation. Decreasing the exposure time to two minutes showed that the sodium penetrates into the cathode material very fast and persuades the bath penetration since, no concentration gradients could be identified. This is an emphasis on the key role of sodium to change the wettability of carbon cathode. The effect of polarization and initial molten aluminium on the cathode wear, as well on the bath penetration into the cathode is shown in Table 4.2.

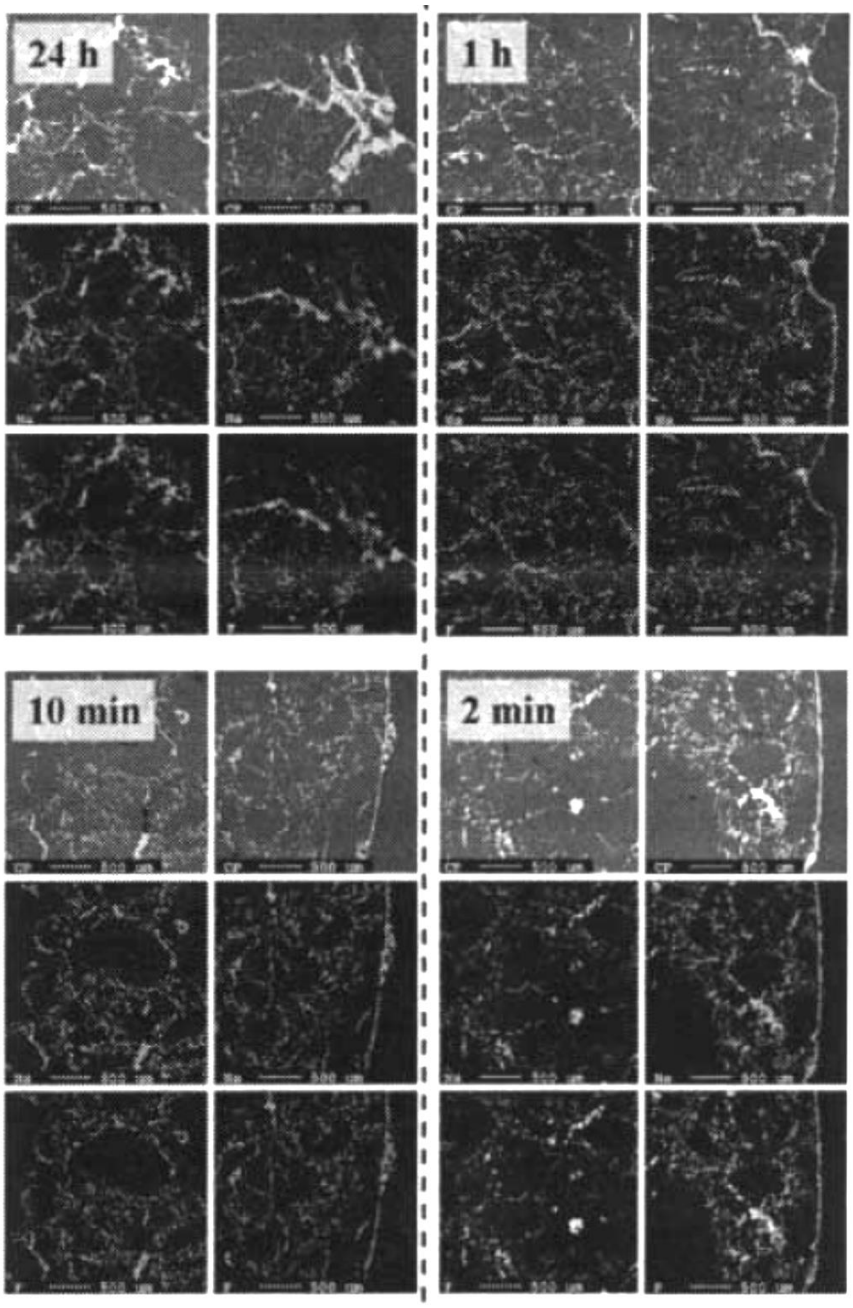

Figure 4.19. Micrograph and element distributions of Na and F for the 24 h, 1 h, 10 min and 2 min wear test duration at 1 A/cm^2 and presence of aluminium. (Right) surface, (left) center [5].

Table 4.2. The effect of polarization and aluminium on the cathode wear and bath penetration into the cathode.

	Polarization Aluminium	Polarization No Aluminium	No Polarization Aluminium	No Polarization No Aluminium
Cathode wear	**Yes**	**Yes**	**No**	**No**
Penetration	**Yes**	**Yes**	**Yes**	**No**

4.5 X-ray Computed Tomography: Bath penetration

As mentioned earlier, one of the important parts of this study was the examination of samples via the x-ray computed tomography (CT) technique. CT is a nondestructive testing for visualizing interior futures within solid objects. Actually the CT method was chosen for obtain more data about what is happened inside the samples after experiment and comparison the samples before and after the experiment. Hence, the CT allows a macroscopic observation on the porosities, bath penetration, grain size and grain distribution. For each category of cathode material one sample was sent for tomography, before and after the experiment. The results indicate the depth of bath penetration into the cathodes. Moreover, the size of porosities, grain size and grain distribution is clearly observable. The tomograms show a significant different in depth of penetration between anthracite based and graphitized cathodes. The graphitized cathode after the electrolysis had been penetrated completely by bath components. Contrary, in the anthracite based material most of the pores, especially in the central parts of the sample were not penetrated. Based on theory and previous studies it was not expected to observe such a result for the anthracitic cathode. Since, for ensuring about repeatability of the result, the tomography was performed for two more anthracitic samples. The new tomograms confirmed the first experiment, so that all three anthracitic cathodes were not fully infiltrated. Figures 4.20-4.27 display the tomograms from EI, EA, BN and 5BDN materials, before and after the experiment. The tomograms corresponding to different cross sections of 5BDN samples are given in Appendix C.

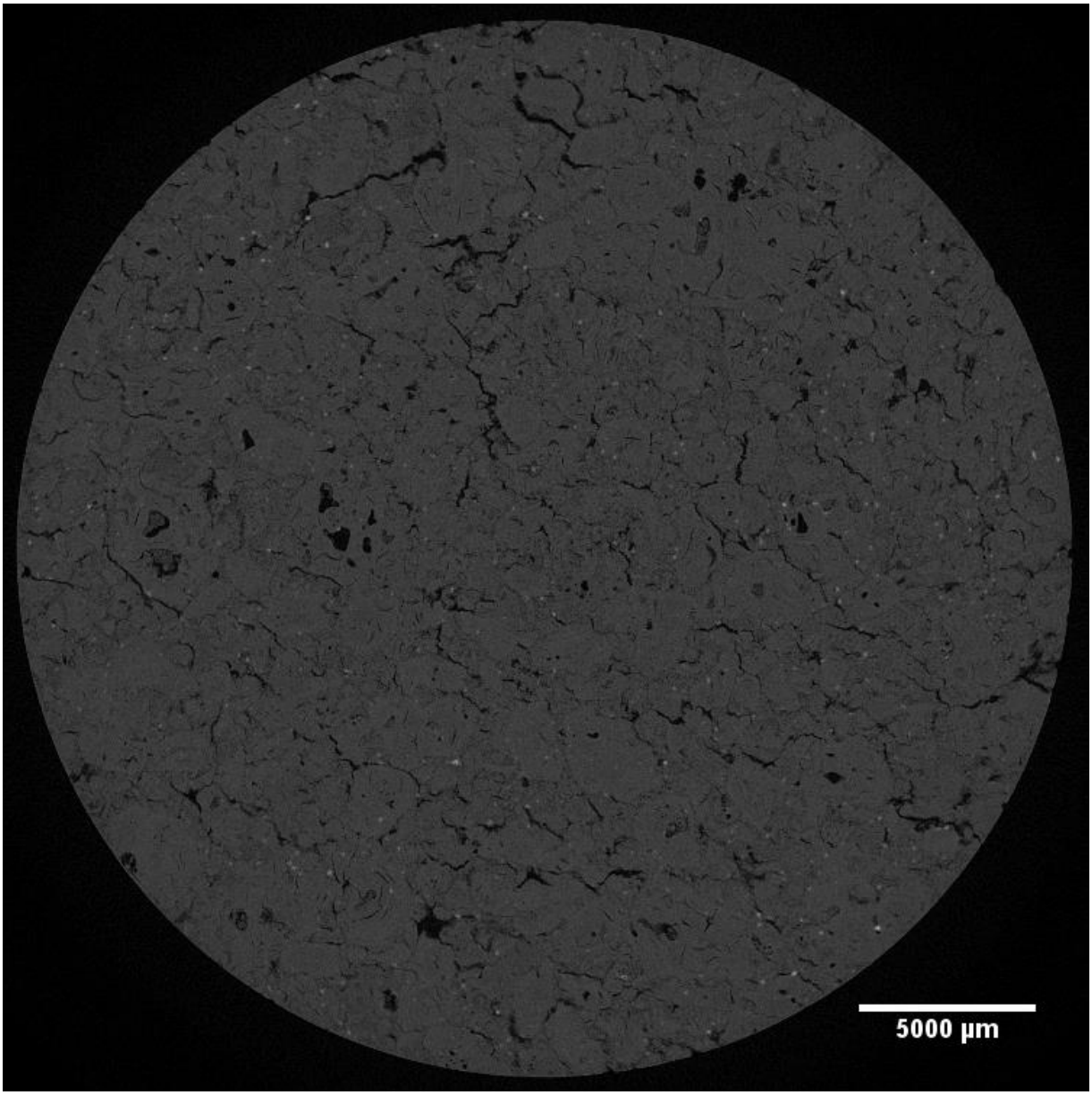

Figure 4.20. The tomogram of virgin cathode from Elkem graphitized carbon, EI. The resolution of tomogram: 40.66 µm/pixel.

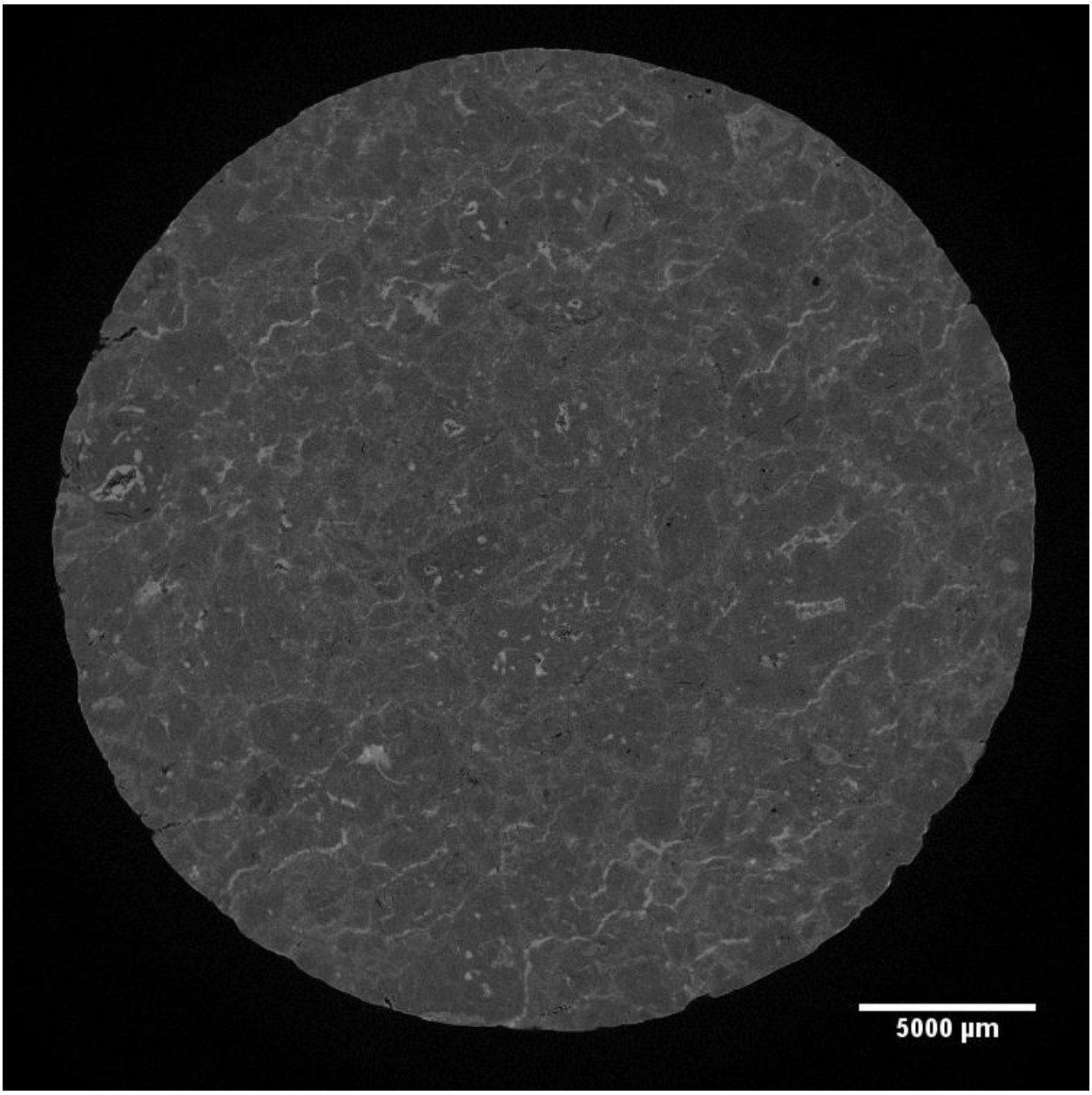

Figure 4.21. The tomogram of worn cathode from Elkem graphitized carbon, EI31. The resolution of tomogram: 40.66 µm/pixel.

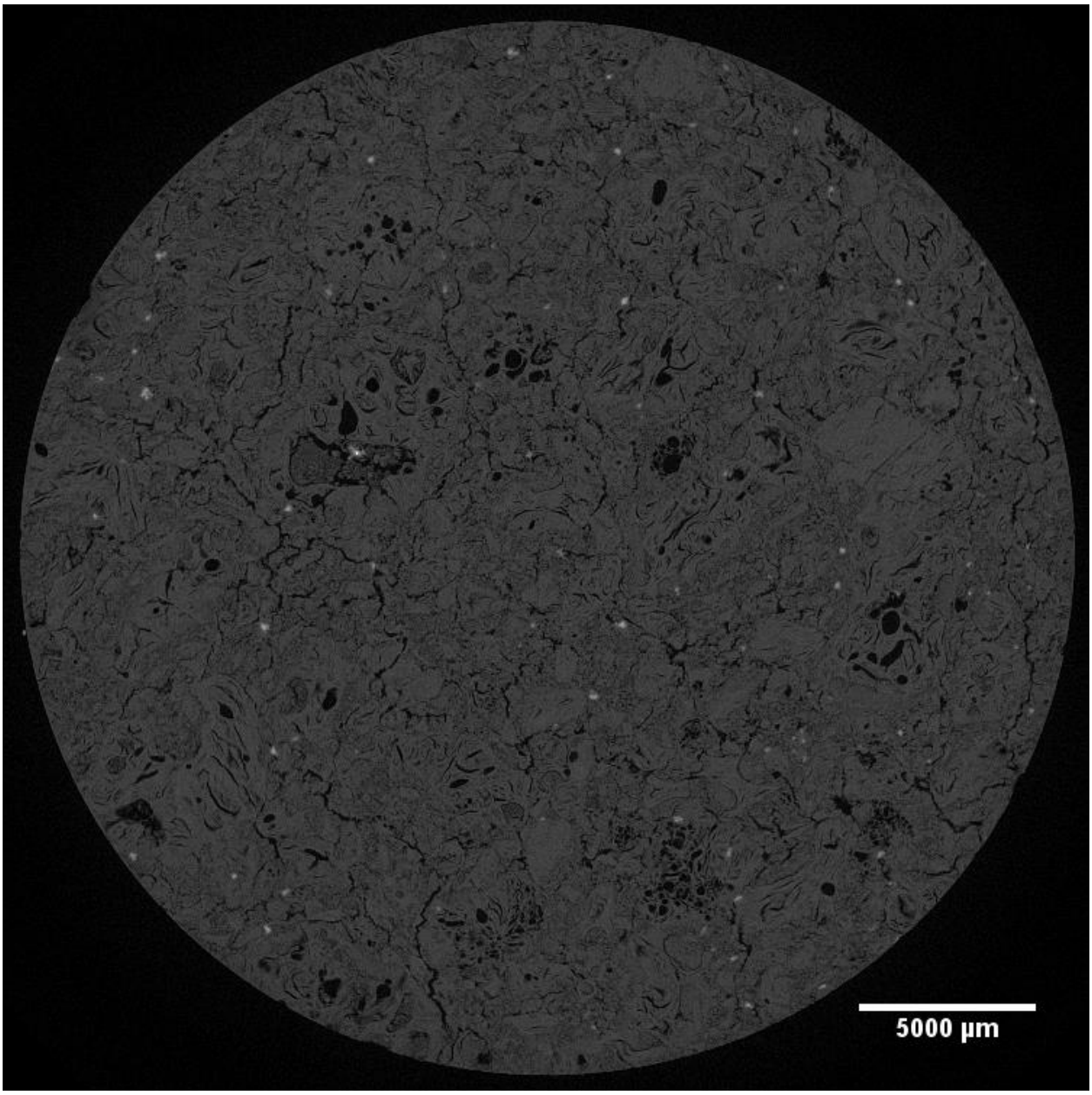

Figure 4.22. The tomogram of virgin cathode from Elkem graphitized carbon, EA. The resolution of tomogram: 40.66 µm/pixel.

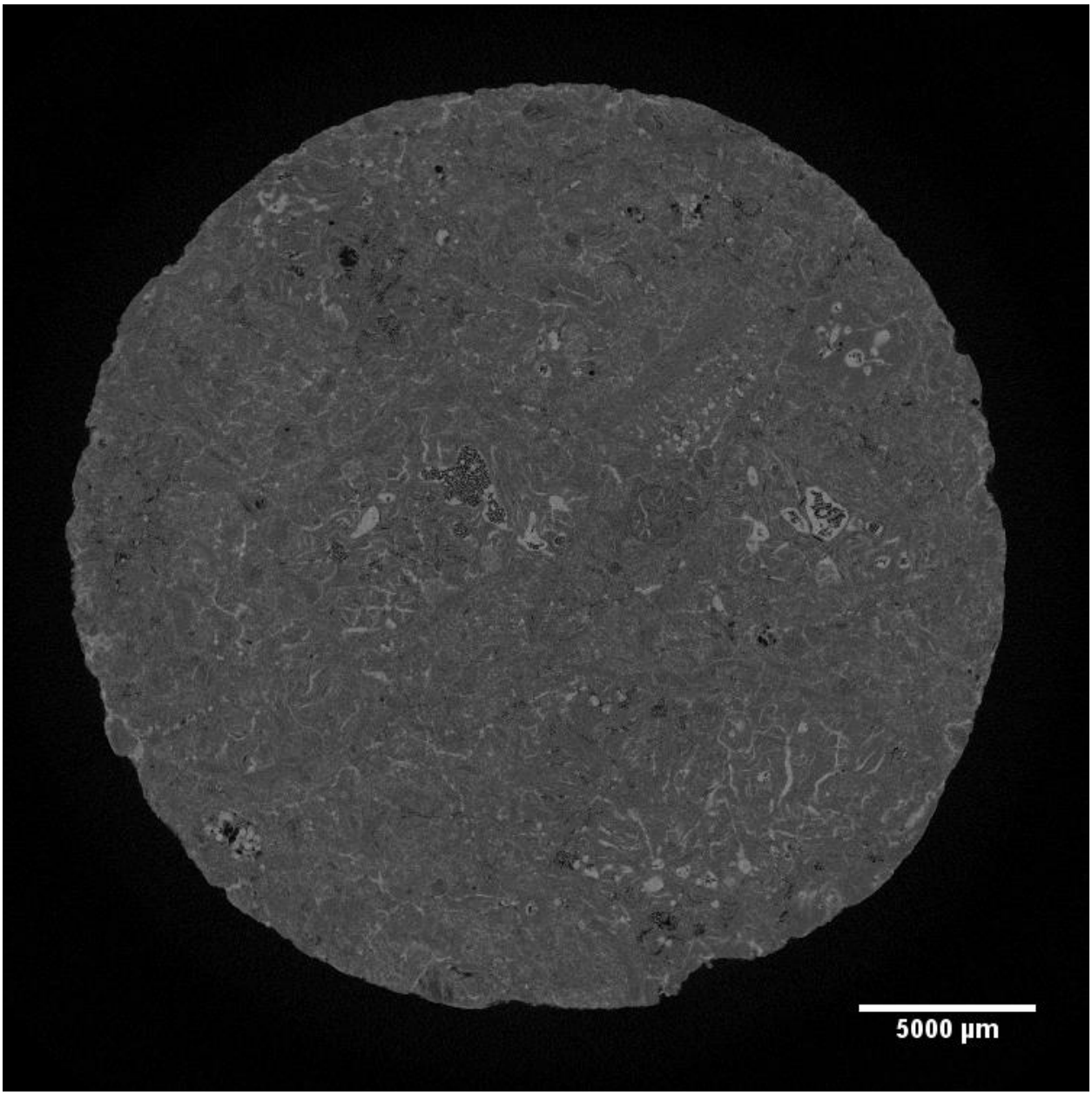

Figure 4.23. The tomogram of worn cathode from Elkem graphitized carbon, EA1. The resolution of tomogram: 40.66 µm/pixel.

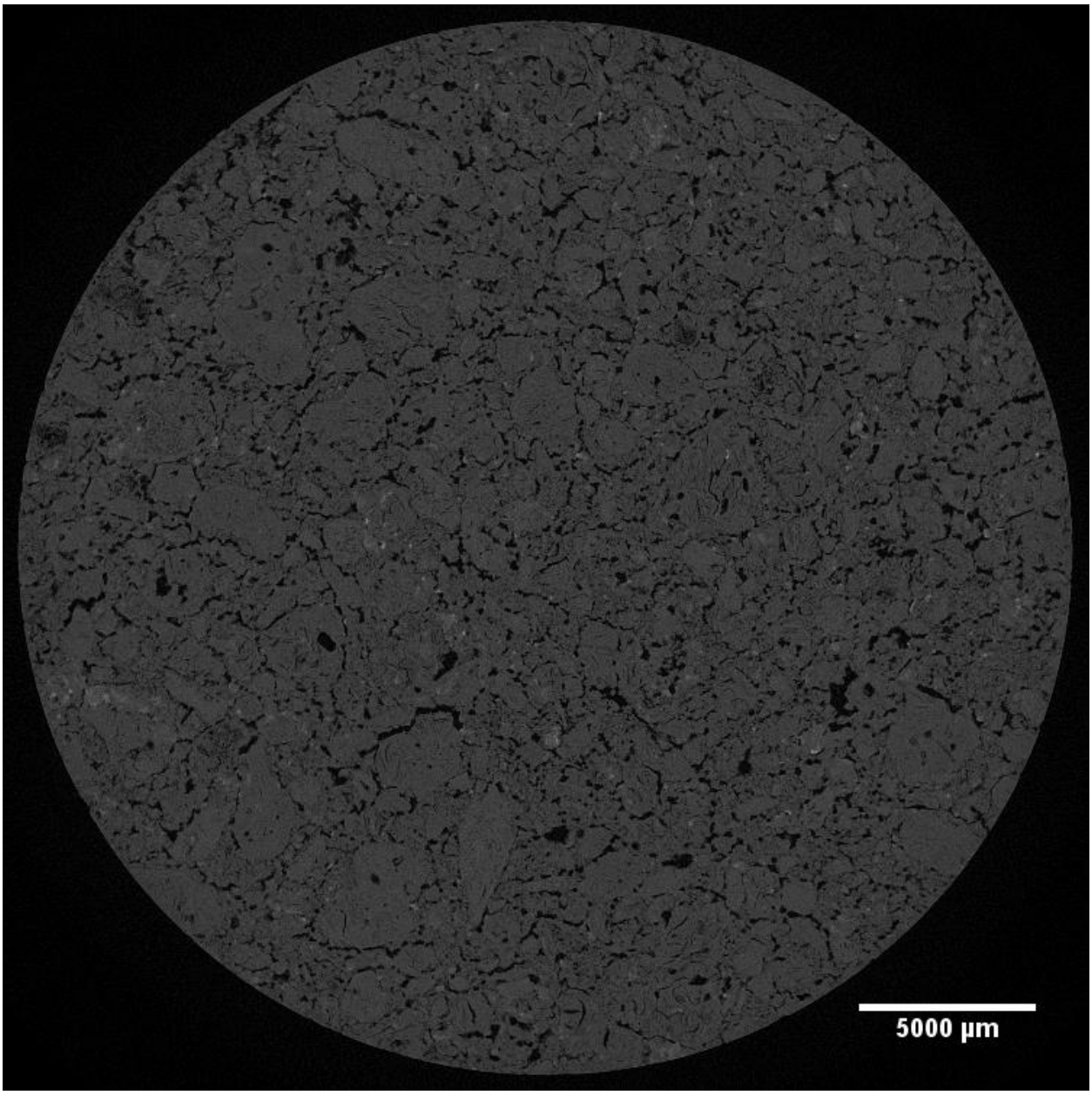

Figure 4.24. The tomogram of virgin cathode from graphitized carbon, BN. The resolution of tomogram: 40.66 µm/pixel.

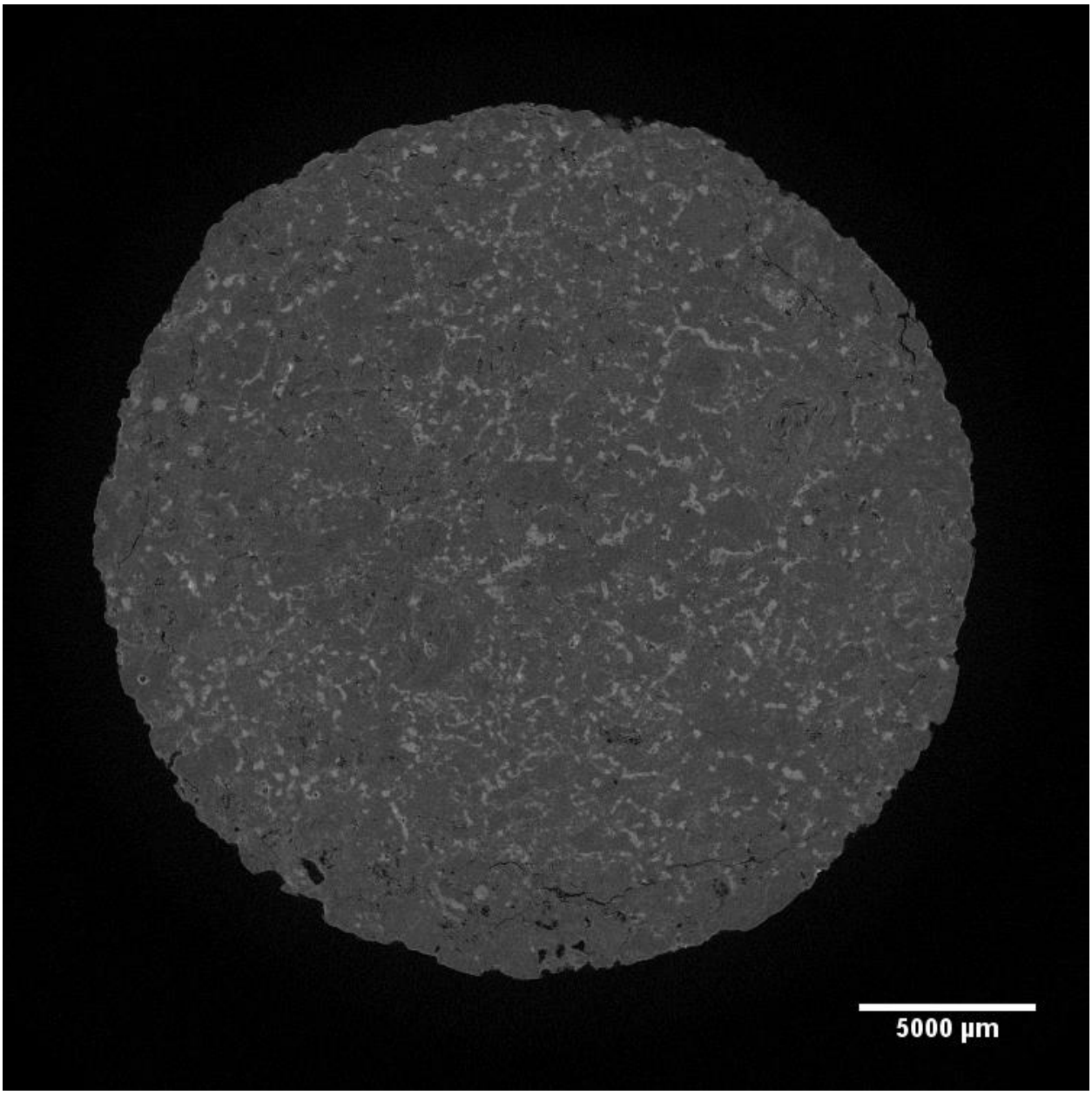

Figure 4.25. The tomogram of worn cathode from graphitized carbon, BN10. The resolution of tomogram: 40.66 µm/pixel.

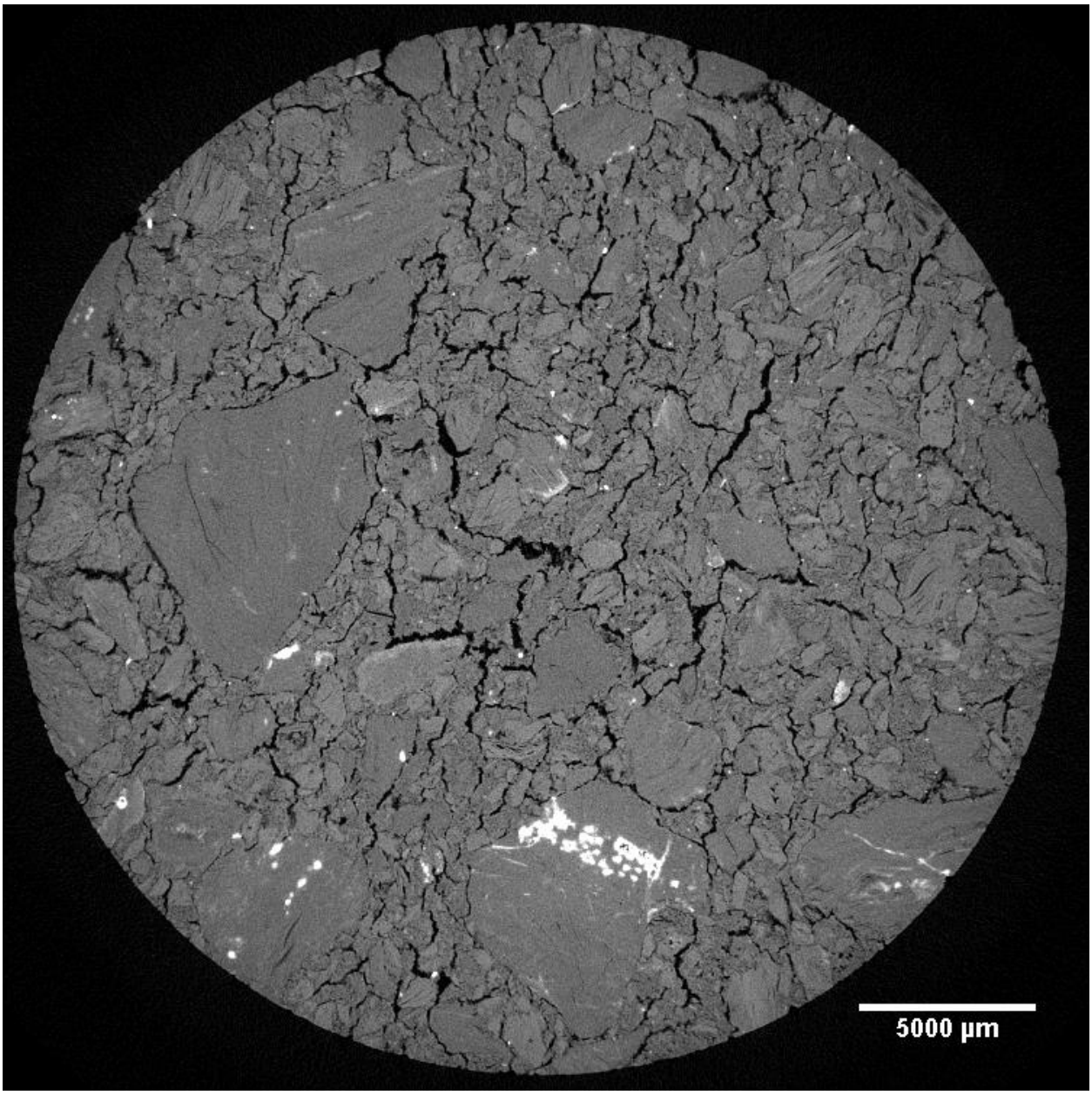

Figure 4.26. The tomogram of virgin cathode from anthracite based carbon, 5BDN. The resolution of tomogram: 40.66 µm/pixel.

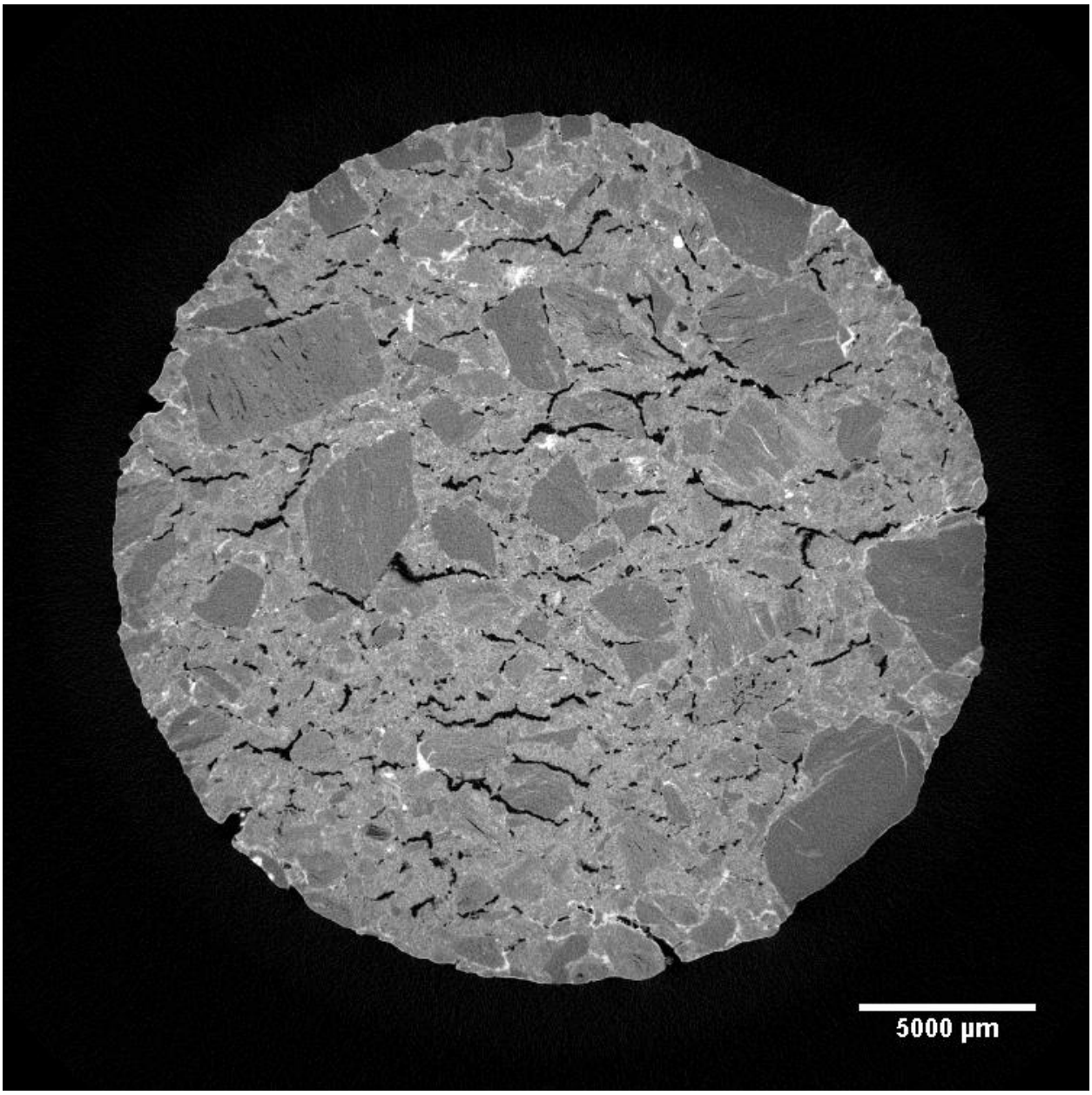

Figure 4.27. The tomogram of worn cathode from anthracite based carbon, 5BDN20. The resolution of tomogram: 40.66 µm/pixel.

Infiltration of bath components into the cathode is correlated to the wettability of carbon materials. Basically, carbon poorly wetted by the cryolitic bath (fluoride melts) [22,1]. Therefore, it is expected that the carbon materials is impervious to the penetration. Although, after a certain period of time the carbon block will be fully penetrated by bath.

Sodium is the reason of bath penetration. Sodium activity and sodium chemical potential are key parameters for wetting of carbon cathode by cryolite. Sodium is produced due to the direct reduction at the cathode surface, according to the reaction (2.14). As well, the primary deposition of aluminium is taken place through the reaction (2.13). By putting on the current, the electrochemical reaction starts which leads to producing sodium. Thus, by apply the current, the sodium chemical potential increases. In other words, the wettability is increased by starting the electrochemical reactions. However, what is happening in atomic level is still unknown. The other way to make sodium is reaction between cryolite and aluminium. If the experiment setup has aluminium and cryolite together, aluminium is dissolved into the cryolite which forming sodium metal. It is known that sodium is formed at the interface between the liquid aluminium and molten cryolite, by reduction of Na^+ which is the main free cation present in the cryolite-aluminium mixture, according to the chemical reaction (2.12). It means that the sodium activity increases. Sodium absorption in the cathode block enhances the wetting properties of the carbon and allows cryolite to penetrate into the cathode [1]. It seems if the type of cathode material changes, it is expected to observe the influence of sodium on penetration, either slower or takes longer time. This is an important new result that penetration of bath into the anthracitic material is stopped or becomes slower. The properties and behavior of carbon materials in terms of sodium handling are complex and highly dependent on the crystallographic structure [22]. In less ordered carbons (amorphous carbon) the sodium is absorbed between the graphene layers and in microporosities [6]. The sodium uptake in less ordered forms of carbon is higher than in graphite. In addition, the absorption decreases with increasing graphitization grade and temperature. In brief, well-graphitized carbons always more resistant to sodium attack than other forms of carbon [22]. The sodium diffusion coefficient increases with current density and temperature. If current density, temperature and cryolite ratio are kept constant, the sodium diffusivity is scaled by graphitization grade. Therefore it increases according to the following sequence [22,1].

graphitized > graphitic > semigraphitized > semigraphitic > amorphous

Based on literature which briefly mentioned above, the tomography results corresponding to anthracitic cathodes is in contradiction with previous findings. According to the former studies, it was expected the anthracitic sample fully penetrated, while the most of pores are empty. The tomograms of anthracitic samples show that the size of unfilled pores is very larger than the filled pores. The proper wettability of carbon cathode for bath penetration is a key factor. In fact, the wetting property is dependent on cohesive forces, surface tension and adhesive forces. These three main variables determine the extent of wettability. Cohesive force is the intermolecular bonding of a substance, whereas adhesive force is the attraction force between unlike molecules. The surface tension occurs as a result of like molecules (cohesive forces) banding together to

form a somewhat impenetrable surface on the body of liquid phase. The transportation of molten cryolitic bath into the pores happens due to the underlying principles of cohesion and transportation. This scientific phenomenon is called capillary action. Capillary action is the rise of liquid through slim tube, cylinder or permeable substance due to adhesive and cohesive forces interacting between the liquid and the surface. Capillary phenomenon only occurs when the adhesive forces are stronger than the cohesive forces, which invariably becomes surface tension, in the liquid. Therefore, when intermolecular bonding of a liquid itself is considerably lower than the substance's surface it is interacting, capillary action occurs. In capillary phenomenon the diameter of tube is determined the height of raised liquid. By increasing the diameter of tube the height of liquid is decreased. Figures 4.28 and 4.29 are respectively shown the function of cohesive and adhesive forces and the influence of diameter on the height of the liquid in the tube. The decrease in the height of liquid continues by increasing the diameter of the tube until a certain diameter. The capillary action stops at this particular size. For each system there is a critical diameter, so that for the channels with the diameters larger than the critical size, the penetration of liquid in the channel is stopped and capillary action does not work.

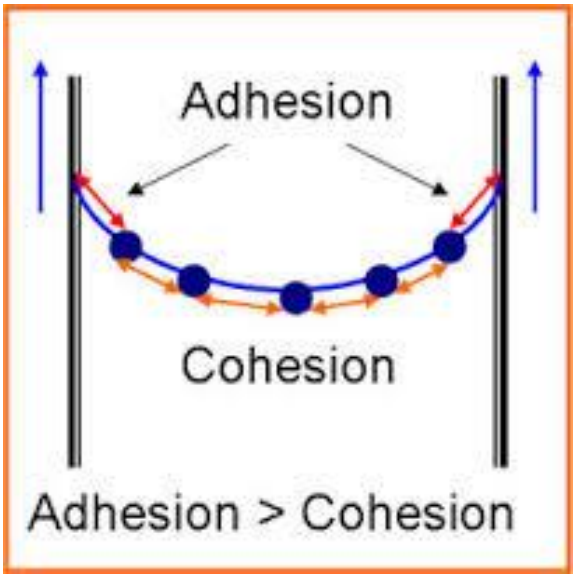

Figure 4.28. The function of cohesive and adhesive forces in the capillary tube to raise the liquid in the tube.

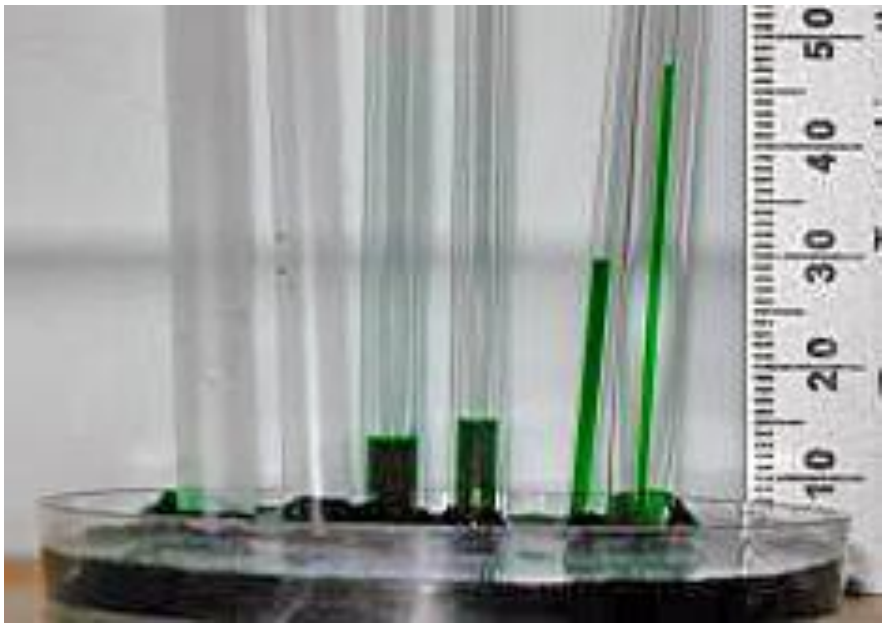

Figure 4.29. The inverse proportion between the diameter of the tube and the height of the liquid, in capillary phenomenon.

The molten bath at the experiment temperature, 970 °C, has a very low viscosity (close to the water viscosity). Thus, it can penetrate into the carbon pores in a short time via the capillary phenomenon. Among the experimented carbon materials, the anthracitic cathode has the biggest pores than the others. It seems that the diameter of the large pores (unfilled pores) in anthracitic carbon is equal or over the critical size. It is confirmed when in the graphitized cathodes, even the farthest areas from the surface, were fully penetrated by the bath. All the examined samples via the tomography were tested at 125 rpm, except the graphitized sample, EI31, that was experimented at 0 rpm. All three graphitized samples, BN10 (125 rpm), EA1 (125 rpm) and EI31 (0 rpm) are fully infiltrated. Hence, the rotation speed cannot be a determining factor on the depth of penetration. Therefore, for all the examined samples by the tomography, the only variable was carbon material. It can be concluded that the most likely scenario that happens for the anthracite based cathodes is the oversized pores which leads to stop the capillary phenomenon and consequently lack of the penetration of bath into the big pores.

5. Conclusion

The inverted test cell was successfully used to identify the influence of carbon material, rotation speed and current density on the wear rate. The rotation speed beside the other factors effects on the cathode wear rate. Totally fifteen cathodes were experimented to observe the effect of hydrodynamic conditions. The results indicate a remarkable increase in wear rate by increasing the rotation speed, where the other parameters were kept constant. As generally agreed the main wear mechanism is related to the formation and dissolution of aluminium carbide at the cathode surface. The mass transport occurs through the diffusion layer. The thickness of diffusion layer is a determining factor on the quantity of wear rate. It is influenced by the rotation speed. Faster rotation speed gives thinner diffusion layer which leads to higher wear rate. It seems by changing the thickness of diffusion layer, the cryolite ratio changes at the cathode surface. Based on evidence, when the cryolite ratio for several experiments is constant, the higher rotation speed gives lower cryolite ratio at the surface (more acidity) which results to higher wear rate. The cathodic current density has an important role on the wear rate. The importance of current density was demonstrated, where the wear rate is increased by increasing the current density. The experiment without current and without initial molten aluminium showed no wear and no bath penetration into the cathode. The other experiment without polarization and with aluminium revealed no carbon consumption detected, however the sample was penetrated. In presence of current and aluminium, the molten bath penetrates into the cathode within a very short time (2 min).

The x-ray computed tomography (CT) was performed for each category of carbon materials. Except the anthracite based cathodes, the other carbon materials (graphitized cathodes) were fully infiltrated by bath. The tomograms display that the size of pores in anthracite based cathodes is very larger than the other carbon materials. The capillary phenomenon helps to penetrate of bath into the cathode. Hence, likely the oversized pores in anthracitic material act as a barrier against the capillary action and the penetration of bath.

6. Future work

It is explained in previous chapter that the most likely hypothesis for increased wear rate at high rotation speeds is mixing effect. At high speed the cryolite ratio at the cathode surface is approximately close to the bulk concentration. So it is expected to obtain constant wear rate by increasing speed. But the results show an increase wear rate by increasing speed. Whether the mixing effect at high speeds is the dominant mechanism for increased wear rate or not need more studies. It is evident that CO_2 gas invariably is produced at the anode surface and leaves the bath from top of the crucible. Based on the mixing effect hypothesis, the CO_2 bubbles at high speeds come close to the cathode surface. Then the CO_2 bubbles can react with cathode carbon to produce CO gas via the Boudouard reaction, which leads to extra carbon consumption and more wear rate. Aim of the new experiment is prevention of collision between CO_2 bubbles and cathode. The suggested experimental setup consists of a porous tube (cylindrical membrane) inside the graphitic crucible as a separator between anode and cathode. The membrane should be open for ionic transport. In this situation there is less chance for CO_2 bubbles to react with cathode. If the new setup results to stop in wear rate increasing, the mixing effect could be one of the wear mechanisms at high rotation speeds.

It is known that the lower cryolite ratio (more acidity) gives higher wear rate. It seems by increasing the rotation speed, the cryolite ratio at the cathode surface will decrease (the second scenario, Figure 8). To realize how the cryolite ratio changes by the rotation speed, a series of experiments should be perform. The acidic cryolite ratio (CR_A) is lower than the basic cryolite ratio (CR_B). Thus at zero rotation speed the CR_A gives higher wear rate than the CR_B.

$CR_A < CR_B \rightarrow$ wear rate (CR_A) > wear rate (CR_B) (at the identical rotation speed)

Then the basic cryolite ratio should be experiment in different rotation speeds. The rotation speed for each experiment is higher than the previous one. By increasing the rotation speed wear rate is increased. The increasing wear rate continues until the rotation speed reaches a particular speed. At the mentioned specific speed the obtained wear rate (for CR_B) becomes equal to the wear rate of acidic cryolite ratio (CR_A) at zero rotation speed. It can prove that the cryolite ratio at the cathode surface is inversely proportional to the rotation speed at a given current density.

References

1. K. Vasshaug, “The influence of the formation and dissolution of aluminium carbide on the cathode wear in aluminium electrolysis cells”, PhD Thesis, Norwegian University of Science and Technology, Trondheim, Norway 2008.
2. Ø. Østrem, “Cathode wear in Hall-Héroult cells”, PhD Thesis, Norwegian University of Science and Technology, Trondheim, Norway 2013.
3. M. Sørlie and H.A. Øye, “Cathodes in Aluminum Electrolysis”, 2nd edition, Aluminum-Verlag, Düsseldorf, Germany 1994.
4. E. Skybakmoen, S. Rørvik, A. Solheim, K.R. Holm, P. Tiefenbach and Ø. Østrem, “Measurement of cathode surface wear profiles by laser scanning”, Light Metals, 1061-1066 (2011).
5. K. Tschöpe, A. Støre, S. Rørvik, and et al., “Investigation of the cathode wear mechanism in a laboratory test cell”, Light Metals, 1349-1354 (2012).
6. J.G. Hop, “Sodium expansion and creep of cathode carbon”, PhD Thesis, Norwegian University of Science and Technology, Trondheim, Norway 2003.
7. K. Grjotheim and H. Kvande, “Introduction to aluminium electrolysis” Aluminium-Verlag, Düsseldorf, Germany 1993.
8. J. Thonstad, P. Fellner, G.M. Haaberg, J. Híveš, H. Kvande and Å. Sterten, “Aluminium Electrolysis”, 2nd edition, Aluminium-Verlag, Düsseldorf, Germany 2001.
9. K. Tschöpe, A. Støre, A. Solheim, and *et al*., “Electrochemical wear of carbon cathodes in electrowinning of aluminum”, JOM vol. 65, 1403-1410 (2013).
10. B. Novàk, “On the chemical and electrochemical formation of aluminum carbide in aluminum electrolysis” PhD Thesis, Norwegian University of Science and Technology, Trondheim, Norway 2013.
11. A. Solheim, “Some hypothesis concerning cathode wear in aluminium electrolysis cells”,
12. R. Fourcault and B. Samanos, 2nd Australian Aluminium Smelter Technology Course, Sydney, 1987.
13. R.C. Dorward, “Reaction between aluminum and graphite in the presence of cryolite”, Metallurgical Transactions, 4 386-388 (1973).
14. S. Toda and T. Wakasa, “Improvement of abrasion resistance of graphitized cathode block for aluminium reduction cells, Light Metals 647-653 (2003).
15. B. Novàk, K. Tschöpe, A.P. Ratvik and T. Grande, “Fundamental of aluminium carbide formation” Light Metals 1343-1348 (2012).

16. H. Kvande, Q. Zhuxian, Y. Kwantsung and K. Grjotheim “”Penetration of bath into the cathode lining of aluminium reduction cells” Light Metals, 161-167 (1989).
17. P. Rafiei, F. Hiltmann, M. Hyland, B. James and B. Welch, “Electrolytic degradation within cathode materials”, Light Metals, 747-752 (2001).
18. S. Wilkening and P. Reny, “Erosion rate testing of graphite cathode materials”, Light Metals, 597-602 (2004).
19. E. Skybakmoen, A. Solheim, and Å. Sterten, “Alumina solubility in molten salt systems of interest for aluminium electrolysis and related phase diagram data”, Metallurgical and Materials Transactions 28B, 81-86 (1997).
20. R. Ødegard, Å. Sterten, J. and Thonstad, “On the solubility of aluminium carbide in cryolitic melts-Influence on cell performance”, Light Metals, 295- (2006).
21. Z. Wang, J. Rutlin and T. Grande, “Sodium diffusion in cathode lining in aluminum electrolysis cells”, Light Metals 841-847 (2010).
22. K. Tschöpe, “Degradation of cathode lining in Hall-Héroult cells, Autopsies and FEM simulations” PhD Thesis, Norwegian University of Science and Technology, Trondheim, Norway 2010.
23. A.V. Frolov, A.O. Gausev, N.I. Shurov and *et al.*, “Wetting and cryolite bath penetration in graphitized cathode materials”, Light Metals 645-649 (2006).
24. K.I. Popov, P.M. Živković and N.D. Nikolić, “A mathematical model of the current density distribution in electrochemical cells”, Journal of the Serbian Chemical Society, 805-521 (2011).
25. D. Landolt, “Electrochemical and materials science aspects of alloy deposition”, Electrochimica Acta vol. 39 1075-1089 (1994).
26. A.W. Bolt, “Mass Transport”, Current Separations vol 14, 104-109 (1996).
27. J. Thonstad and S. Rolseth, “On the cathodic overvoltage on aluminium in the NaF-AlF_3-Al_2O_3 melts – I, Electrochimica Acta vol. 23, 233-241 (1978).
28. C. Madore, D. Landolt, C. Haßenflug and J.A: Hermann, “Application of the rotating cylinder Hull cell to the measurement of throwing power and the monitoring of copper plating baths” Plating and Surface Finishing, 36-41 (1995).

Appendix A: Apparent density and open porosity of virgin cathode samples

Table 1: Experimental data for all samples

Sample name	Immersed weight (g)				Weight in air (g)				Dried weight (g)				Density (g/cm^3)	Porosity (%)
				Average				Average				Average		
S-30	37.908	37.901	37.900	37.903	82.735	82.693	82.668	82.699	77.219	77.219	77.219	77.219	1.724	12.23
S-31	37.836	37.838	37.837	37.837	82.620	82.624	82.560	82.601	77.106	77.106	77.106	77.106	1.722	12.28
E-30	38.349	38.348	38.350	38.349	83.576	83.495	83.466	83.512	77.924	77.924	77.924	77.924	1.725	12.37
E-31	38.586	38.585	38.584	38.585	83.966	84.002	83.992	83.987	78.369	78.369	78.369	78.369	1.726	12.37
5BDN-20	33.691	33.690	33.686	33.689	78.923	78.909	78.940	78.924	72.054	72.055	72.055	72.055	1.593	15.19
5BDN-21	33.300	33.309	33.310	33.306	78.021	78.049	78.010	78.027	71.331	71.331	71.331	71.331	1.595	14.97
BN-21	35.916	35.917	35.917	35.917	80.637	80.759	80.737	80.711	72.918	72.918	72.918	72.918	1.628	17.4
BN-22	36.143	36.143	36.138	36.141	81.039	81.120	81.044	81.068	73.446	73.446	73.446	73.446	1.635	16.93
EA-1	37.890	37.893	37.895	37.893	83.296	83.297	83.277	83.290	72.832	72.832	72.832	72.832	1.604	23.04
EA-2	37.460	37.457	37.459	37.459	82.843	82.796	82.740	82.793	72.187	72.187	72.187	72.187	1.592	23.4
E-14	39.081	39.073	39.075	39076.33	84.164	84.153	84.146	84154.33	78.088	78.089	78.088	78088.33	1.73	13.46
BN-9	37.108	37.108	37.105	37107	82.104	82.096	82.083	82094.33	74.482	74.482	74.483	74482.33	1.66	16.92
BN-10	36.823	36.827	36.828	36826	81.782	81.773	81.766	81773.67	73.848	73.849	73.849	73848.67	1.64	17.63
5BDN-12	34.087	34.087	34.084	34086	78.985	78.974	78.963	78974	72.244	72.244	72.244	72244	1.61	15

Appendix B: The diameter of cathode samples before and after the wear test

Table 2: Cathode diameter for sample SI-13 before and after the experiment

Diameter (mm); before		
Position 1	Position 2	Position 3
29.58	29.63	29.64
29.63	29.65	29.67
29.66	29.65	29.68
29.62	29.66	29.68
29.62	29.65	29.67
29.63	29.66	29.66
29.62	29.65	29.67
29.58	29.65	29.68
29.64	29.66	29.69
29.67	29.66	29.67
Average diameter (mm)		
29.649		

Diameter (mm); after		
Position 1	Position 2	Position 3
27.41	26.98	27.38
27.34	27.32	27.39
27.55	27.48	27.4
27.47	27.55	27.39
27.61	27.58	27.61
27.59	27.62	27.65
27.68	27.49	27.72
27.63	27.58	27.67
27.62	27.54	27.71
27.55	27.54	27.61
Average diameter (mm)		
27.522		

Table 3: Cathode diameter for sample SI-30 before and after the experiment

Diameter (mm); before		
Position 1	Position 2	Position 3
29.68	29.47	29.68
29.67	29.5	29.67
29.68	29.47	29.67
29.66	29.48	29.66
29.59	29.53	29.6
29.55	29.51	29.59
29.62	29.54	29.6
29.61	29.56	29.59
29.63	29.58	29.63
29.64	29.61	29.63
Average diameter (mm)		
29.597		

Diameter (mm); after		
Position 1	Position 2	Position 3
25.94	25.37	25.58
26.17	25.54	26.24
26.26	25.91	26.34
26.35	26.17	26.47
26.48	26.28	26.46
26.52	26.38	26.53
26.57	26.37	26.66
26.57	26.42	26.48
26.5	26.41	26.42
26.24	26.22	26.05
Average diameter (mm)		
26.263		

Table 4: Cathode diameter for sample SI-31 before and after the experiment

Diameter (mm); before		
Position 1	Position 2	Position 3
29.57	29.52	29.57
29.57	29.5	29.59
29.64	29.59	29.63
29.65	29.62	29.62
29.64	29.64	29.65
29.63	29.63	29.63
29.63	29.64	29.63
29.64	29.64	29.66
29.62	29.63	29.63
29.63	29.62	29.64
Average diameter (mm)		
29.616		

Diameter (mm); after		
Position 1	Position 2	Position 3
25.57	25.87	25.88
25.9	26.08	26.1
26.06	25.84	26.08
26.27	26.07	25.75
26.36	26.26	25.96
26.58	26.43	26.18
26.76	26.51	26.55
26.81	26.57	26.56
26.36	26.27	26.59
26.2	25.76	26.1
Average diameter (mm)		
26.209		

Table 5: Cathode diameter for sample EI-14 before and after the experiment

Diameter (mm); before		
Position 1	Position 2	Position 3
29.64	29.6	29.61
29.67	29.6	29.62
29.64	29.64	29.65
29.63	29.61	29.65
29.63	29.6	29.65
29.64	29.61	29.65
29.67	29.63	29.66
29.65	29.65	29.67
29.67	29.66	29.68
29.66	29.67	29.68
Average diameter (mm)		
29.643		

Diameter (mm); after		
Position 1	Position 2	Position 3
25.81	25.37	25.69
25.88	25.58	25.83
25.98	25.71	25.7
26.12	25.54	25.82
26.08	25.78	25.72
26.09	25.78	25.75
26.09	25.67	25.65
26.12	25.75	25.72
25.97	25.68	25.64
25.68	25.63	25.34
Average diameter (mm)		
25.8		

Table 6: Cathode diameter for sample EI-30 before and after the experiment

Diameter (mm); before		
Position 1	Position 2	Position 3
29.66	29.65	29.65
29.65	29.66	29.66
29.66	29.66	29.66
29.68	29.68	29.66
29.69	29.69	29.68
29.68	29.68	29.68
29.69	29.69	29.69
29.69	29.7	29.69
29.69	29.71	29.7
29.7	29.71	29.7
Average diameter (mm)		
29.68		

Diameter (mm); after		
Position 1	Position 2	Position 3
25.87	25.18	25.34
26.08	25.71	25.68
26.16	25.83	25.53
26.38	25.8	25.77
26.23	26.09	25.84
26.23	26.07	25.76
26.21	25.7	25.66
26.1	25.55	25.51
25.75	25.53	25.47
25.67	25.38	25
Average diameter (mm)		
25.769		

Table 7: Cathode diameter for sample BN-9 before and after the experiment

Diameter (mm); before		
Position 1	Position 2	Position 3
29.62	29.65	29.64
29.66	29.68	29.66
29.66	29.69	29.64
29.64	29.64	29.64
29.65	29.67	29.64
29.66	29.69	29.68
29.65	29.69	29.65
29.66	29.66	29.67
29.64	29.66	29.63
29.61	29.63	29.64
Average diameter (mm)		
29.653		

Diameter (mm); after		
Position 1	Position 2	Position 3
24.68	24.53	24.43
24.82	24.6	24.82
24.95	24.74	24.94
25.08	24.76	24.77
25.37	24.86	24.7
24.75	24.79	24.71
24.82	24.95	24.91
24.73	24.93	24.76
24.63	24.77	24.45
24.46	24.57	24.26
Average diameter (mm)		
24.751		

Table 8: Cathode diameter for sample BN-10 before and after the experiment

Diameter (mm); before		
Position 1	Position 2	Position 3
29.63	29.61	29.64
29.64	29.64	29.66
29.63	29.65	29.66
29.64	29.66	29.66
29.66	29.64	29.69
29.62	29.6	29.66
29.61	29.61	29.63
29.62	29.63	29.66
29.64	29.62	29.62
29.65	29.6	29.59
Average diameter (mm)		
29.636		

Diameter (mm); after		
Position 1	Position 2	Position 3
24.56	23.86	24.45
24.55	24.24	24.71
24.57	24.48	24.91
24.7	24.53	24.92
24.64	24.57	24.9
24.52	24.61	25
24.57	24.68	24.8
24.38	24.56	24.63
24.44	24.66	24.43
23.98	24.09	24.12
Average diameter (mm)		
24.535		

Table 9: Cathode diameter for sample 5BDN-12 before and after the experiment

Diameter (mm); before		
Position 1	Position 2	Position 3
29.58	29.56	29.58
29.61	29.56	29.61
29.62	29.62	29.61
29.6	29.61	29.62
29.6	29.61	29.61
29.61	29.61	29.59
29.6	29.6	29.58
29.61	29.57	29.59
29.59	29.51	29.57
29.61	29.53	29.55
Average diameter (mm)		
29.591		

Diameter (mm); after		
Position 1	Position 2	Position 3
24.25	24.32	24.3
24.69	24.46	24.56
24.33	24.3	24.62
24.69	24.06	24.76
24.55	24.05	24.67
24.91	24.16	24.53
24.7	24.01	24.66
24.46	23.96	23.42
24.21	23.26	23.55
23.96	23.19	23.47
Average diameter (mm)		
24.235		

Table 10: Cathode diameter for sample 5BDN-20 before and after the experiment

Diameter (mm); before		
Position 1	Position 2	Position 3
29.54	29.55	29.55
29.52	29.56	29.55
29.53	29.57	29.56
29.57	29.57	29.57
29.57	29.58	29.58
29.58	29.57	29.57
29.56	29.54	29.55
29.54	29.57	29.55
29.54	29.65	29.54
29.66	29.62	29.57
Average diameter (mm)		
29.566		

Diameter (mm); after		
Position 1	Position 2	Position 3
24.12	23.55	23.59
24.38	24.54	24.23
24.82	24.57	24.28
24.45	24.26	24.62
25.19	23.95	24.49
25.66	24.44	24.51
24.6	24.61	24.37
24.57	24.43	24.57
24.53	24.43	24.27
24.27	23.85	23.59
Average diameter (mm)		
24.391		

Table 11: Cathode diameter for sample EI-31 before and after the experiment

Diameter (mm); before		
Position 1	Position 2	Position 3
29.6	29.61	29.62
29.62	29.6	29.61
29.62	29.63	29.64
29.61	29.62	29.63
29.6	29.61	29.63
29.62	29.63	29.64
29.61	29.62	29.63
29.6	29.61	29.61
29.61	29.61	29.61
29.63	29.62	29.64
Average diameter (mm)		
29.618		

Diameter (mm); after		
Position 1	Position 2	Position 3
27.44	27.37	27.38
27.63	27.52	27.55
27.69	27.69	27.68
27.74	27.74	27.72
27.71	27.7	27.73
27.54	27.62	27.55
27.64	27.6	27.56
27.51	27.46	27.63
27.47	27.54	27.46
27.33	27.37	27.22
Average diameter (mm)		
27.56		

Table 12: Cathode diameter for sample BN-21 before and after the experiment

Diameter (mm); before		
Position 1	Position 2	Position 3
29.61	29.6	29.59
29.6	29.59	29.58
29.63	29.63	29.62
29.63	29.62	29.61
29.63	29.62	29.6
29.63	29.6	29.6
29.6	29.61	29.61
29.6	29.62	29.58
29.59	29.6	29.56
29.59	29.6	29.58
Average diameter (mm)		
29.604		

Diameter (mm); after		
Position 1	Position 2	Position 3
24.8	24.29	23.99
24.55	24.66	24.09
24.63	24.9	24.4
25.17	25.09	24.4
25.25	25.05	25.01
25.48	25.55	25.49
25.58	25.6	25.65
25.38	25.69	25.89
25.24	25.47	25.55
25.12	24.98	25.25
Average diameter (mm)		
25.073		

Table 13: Cathode diameter for sample 5BDN-21 before and after the experiment

Diameter (mm); before		
Position 1	Position 2	Position 3
29.56	29.6	29.56
29.58	29.6	29.57
29.58	29.61	29.56
29.57	29.59	29.51
29.57	29.56	29.51
29.55	29.56	29.5
29.56	29.58	29.57
29.57	29.58	29.59
29.56	29.58	29.57
29.58	29.57	29.58
Average diameter (mm)		
29.568		

Diameter (mm); after		
Position 1	Position 2	Position 3
23.55	23.14	22.41
23.58	23.89	23.83
23.77	24.39	23.94
23.72	23.98	23.39
24.78	24.69	24.39
24.61	25.07	24.95
24.93	25.31	24.87
24.77	25.04	25.04
24.52	24.85	24.94
24.15	24.53	24.32
Average diameter (mm)		
24.312		

Table 14: Cathode diameter for sample BN-22 before and after the experiment

Diameter (mm); before		
Position 1	Position 2	Position 3
29.63	29.64	29.64
29.64	29.63	29.64
29.64	29.63	29.64
29.64	29.64	29.63
29.65	29.64	29.63
29.63	29.61	29.63
29.63	29.64	29.65
29.64	29.64	29.64
29.65	29.63	29.64
29.64	29.63	29.63
Average diameter (mm)		
29.636		

Diameter (mm); after		
Position 1	Position 2	Position 3
26.42	26.45	25.51
26.7	26.81	26.78
26.84	27.14	26.62
26.99	27.39	27.27
27.15	27.37	27.43
27.24	27.48	27.51
27.2	27.45	27.53
27.08	27.31	27.43
27.07	27.11	27.31
26.7	26.97	27.1
Average diameter (mm)		
27.045		

Table 15: Cathode diameter for sample EA-1 before and after the experiment

Diameter (mm); before		
Position 1	Position 2	Position 3
29.63	29.62	29.62
29.62	29.62	29.62
29.63	29.62	29.62
29.64	29.63	29.62
29.63	29.63	29.62
29.63	29.62	29.62
29.63	29.63	29.61
29.63	29.63	29.63
29.63	29.62	29.61
29.62	29.62	29.61
Average diameter (mm)		
29.624		

Diameter (mm); after		
Position 1	Position 2	Position 3
25.99	25.97	25.78
26.1	26.21	26.15
26.36	26.49	26.26
26.41	26.03	26.32
26.44	26.21	26.3
26.4	26.77	26.08
26.28	26.39	26.18
26.27	26.31	26.28
26.06	26.12	26.32
25.73	26.06	25.75
Average diameter (mm)		
26.201		

Table 16: Cathode diameter for sample EA-2 before and after the experiment

Diameter (mm); before		
Position 1	Position 2	Position 3
29.65	29.62	29.62
29.64	29.61	29.62
29.64	29.62	29.62
29.64	29.63	29.63
29.63	29.63	29.63
29.63	29.62	29.64
29.64	29.62	29.64
29.63	29.64	29.63
29.63	29.63	29.63
29.63	29.62	29.63
Average diameter (mm)		
29.629		

Diameter (mm); after		
Position 1	Position 2	Position 3
25.67	24.89	25.33
25.7	25.12	25.42
26.01	25.59	25.23
26.18	25.55	25.02
26.2	25.66	25.23
25.86	25.43	25.47
26.33	25.46	25.37
25.84	25.04	25.17
25.42	25.16	25.12
25.53	25.08	25.17
Average diameter (mm)		
25.475		

Appendix C: The tomograms of different cross sections from anthracite based cathodes after the wear test

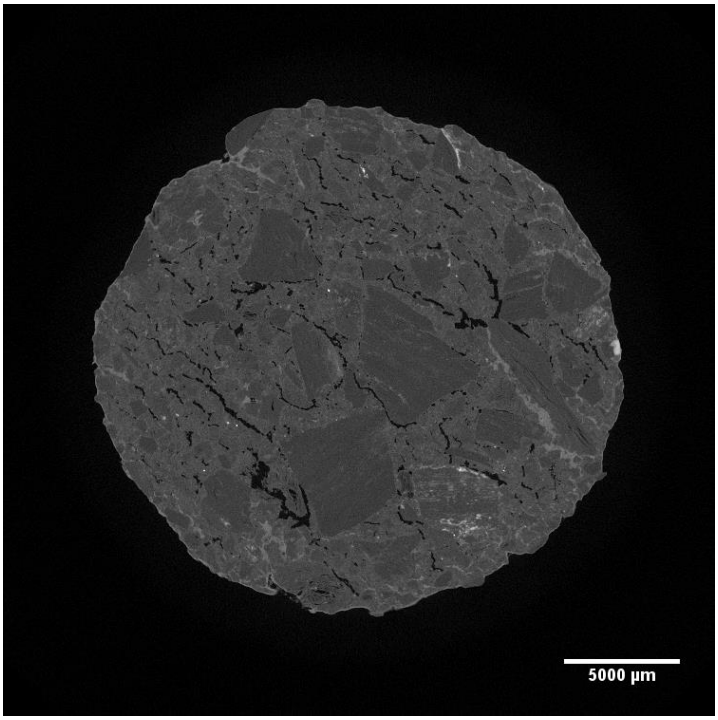

Figure 1: 5BDN 12, cross section 1; Resolution: 40.66 µm/pixel

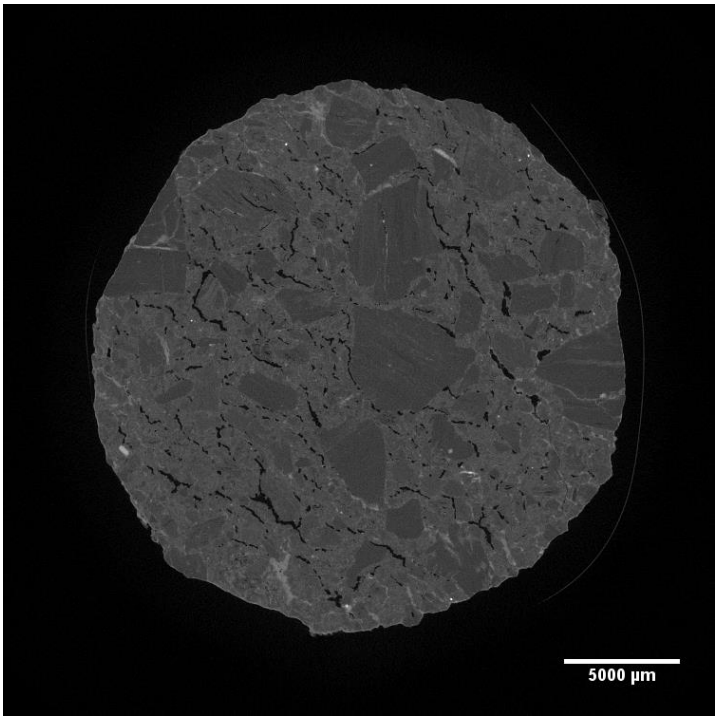

Figure 2: 5BDN 12, cross section 2; Resolution: 40.66 µm/pixel

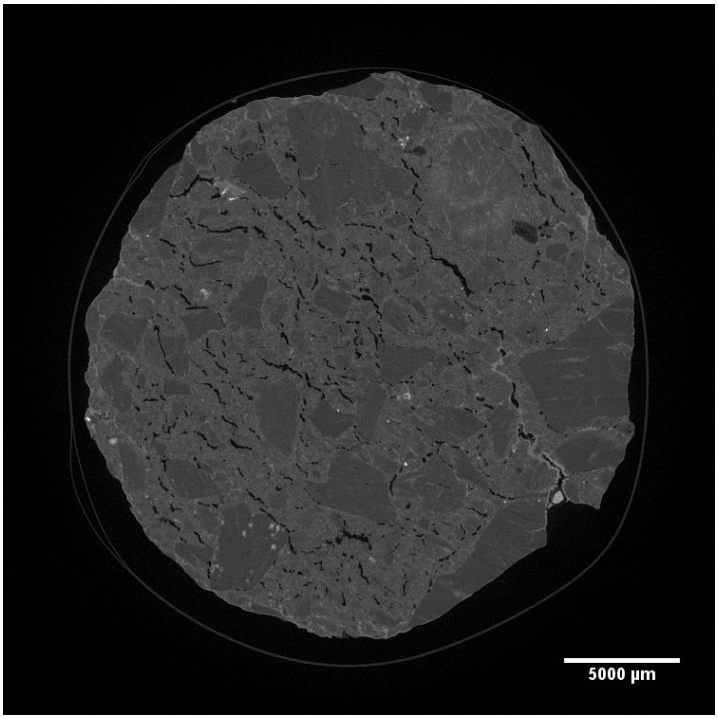

Figure 3: 5BDN 12, cross section 3; Resolution: 40.66 µm/pixel

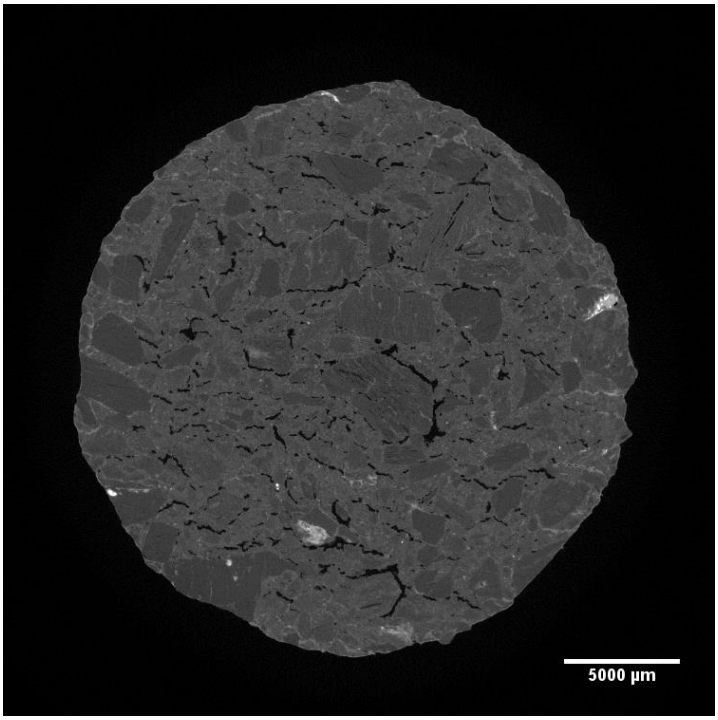

Figure 4: 5BDN 12, cross section 4; Resolution: 40.66 µm/pixel

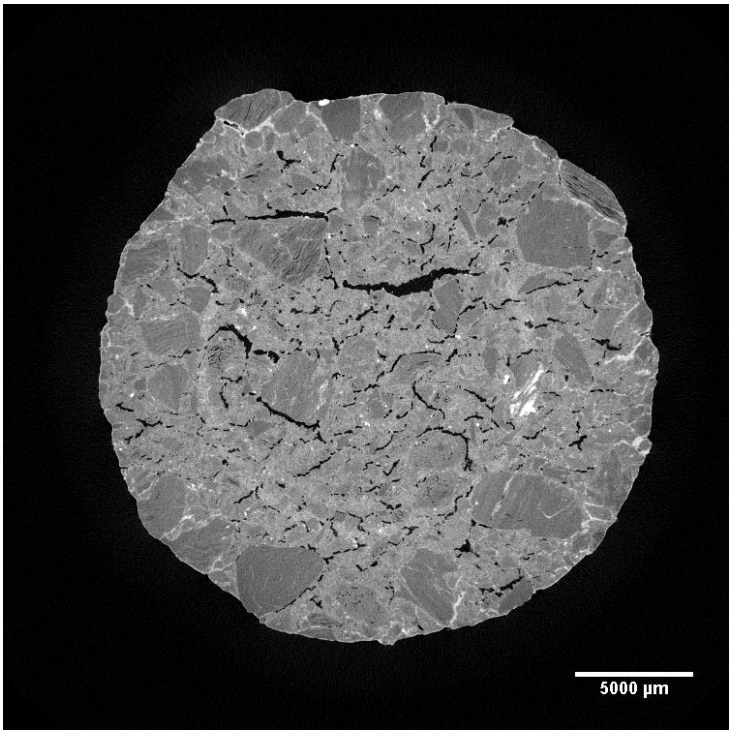

Figure 5: 5BDN20, cross section 1; Resolution: 40.66 µm/pixel

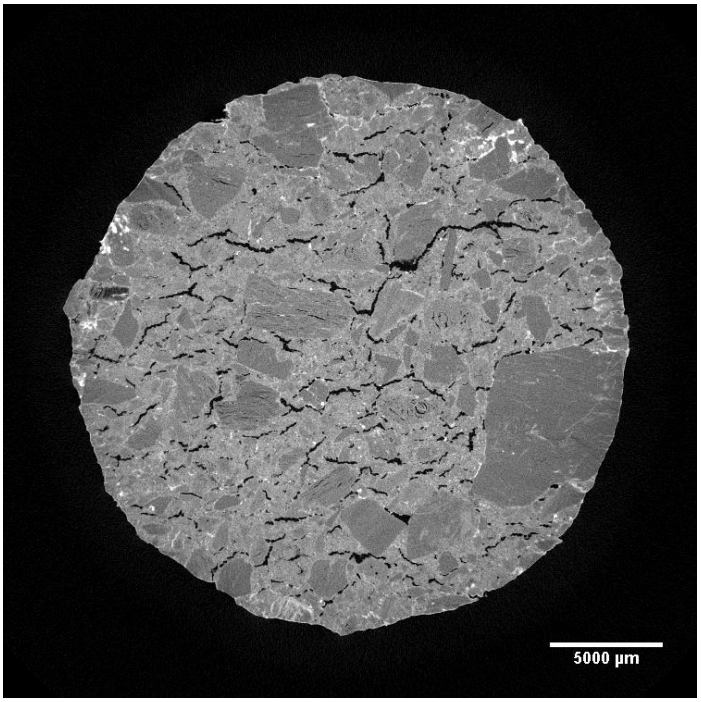

Figure 6: 5BDN20, cross section 2; Resolution: 40.66 µm/pixel

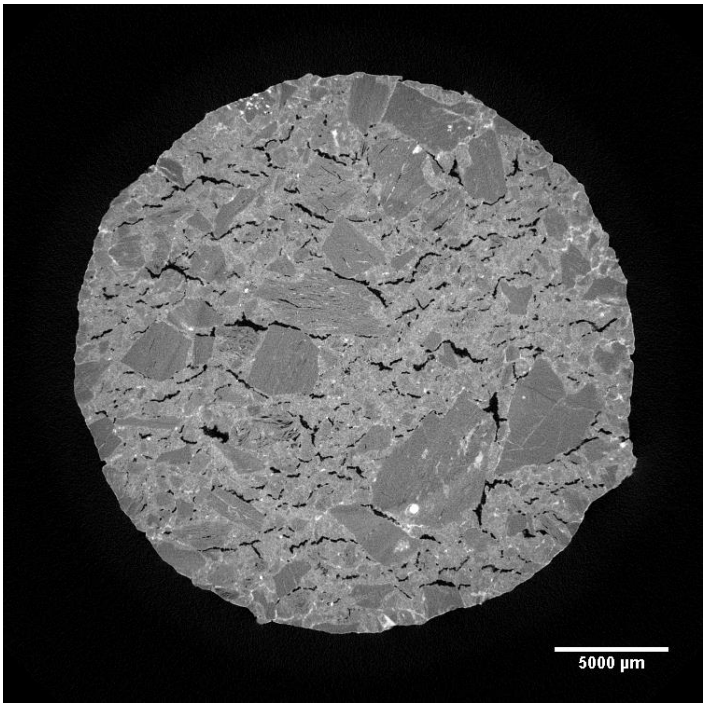

Figure 7: 5BDN20, cross section 3; Resolution: 40.66 µm/pixel

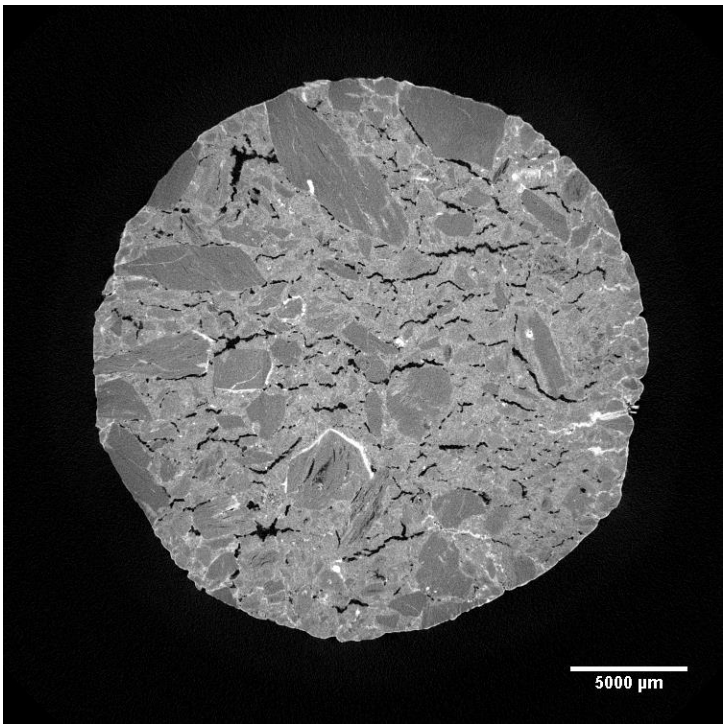

Figure 8: 5BDN20, cross section 4; Resolution: 40.66 µm/pixel

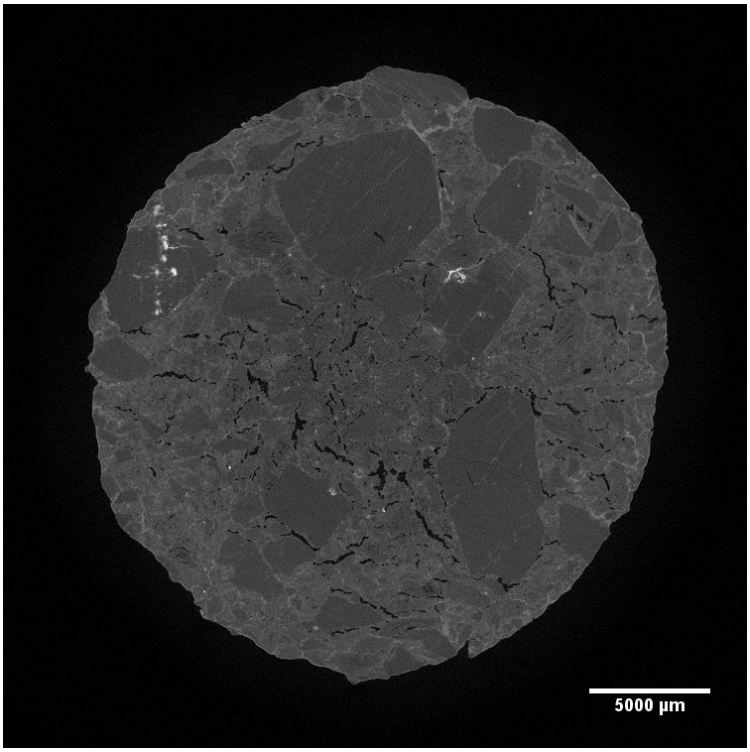

Figure 9: 5BDN21, cross section 1; Resolution: 40.66 µm/pixel

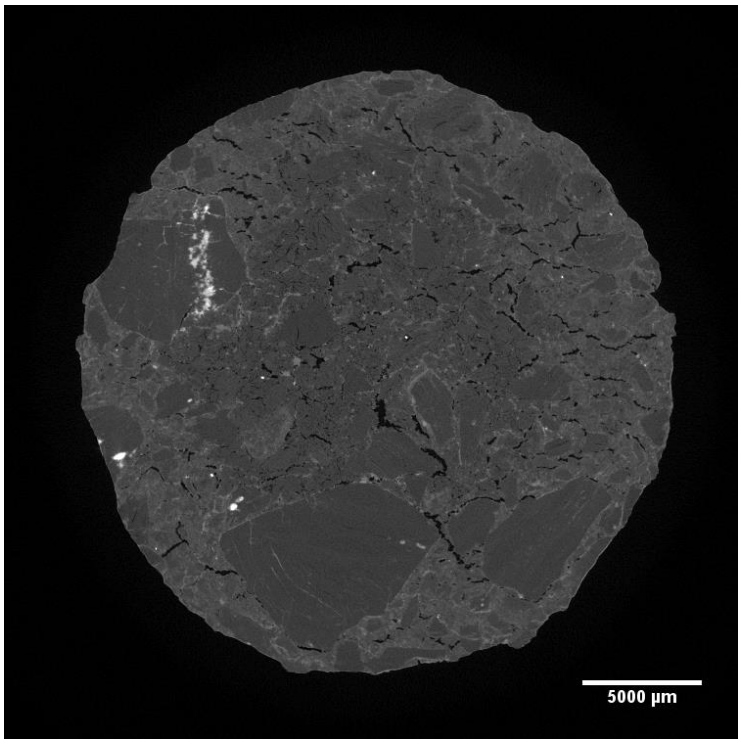

Figure 10: 5BDN21, cross section 2; Resolution: 40.66 µm/pixel

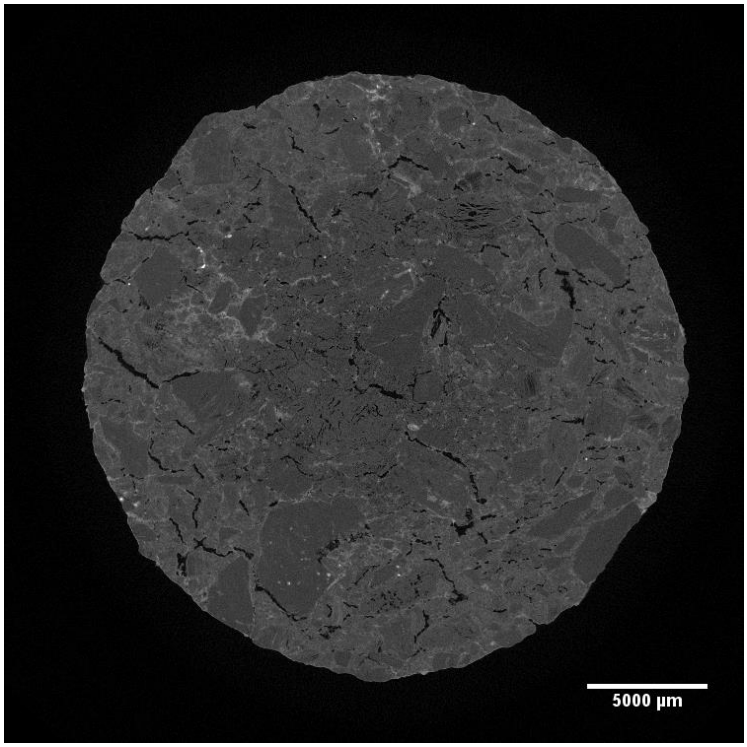

Figure 11: 5BDN21, cross section 3; Resolution: 40.66 µm/pixel

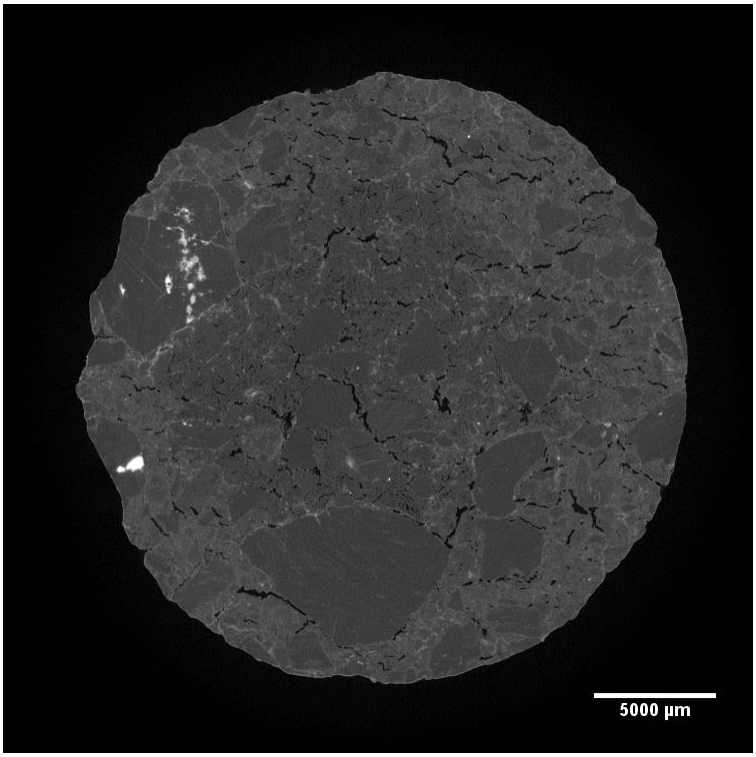

Figure 12: 5BDN21, cross section 4; Resolution: 40.66 µm/pixel